

DECELERATION OF A RELATIVISTIC, PHOTON-RICH SHELL: END OF PREACCELERATION, DAMPING OF MHD TURBULENCE, AND THE EMISSION MECHANISM OF GAMMA-RAY BURSTS

CHRISTOPHER THOMPSON
CITA, 60 St. George St., Toronto, ON M5S 3H8, Canada
Accepted by the Astrophysical Journal, 18 April 2006

ABSTRACT

We consider the interaction of a relativistically-moving shell, composed of thermal photons, a reversing magnetic field and a small admixture of charged particles, with a dense Wolf-Rayet wind. A thin outer layer of Wolf-Rayet material is entrained by the jet head; it cools and becomes Rayleigh-Taylor unstable, thereby providing an additional source of inertia and variability. The gamma-rays emitted by the shell load the ambient medium with electron-positron pairs and, close to the engine, force this medium to move at nearly the same speed as the shell. We show that this pre-acceleration of the wind material defines a characteristic radiative compactness at the point where the reverse shock has completed its passage back through the shell. We argue that the prompt gamma-ray emission is triggered by this external braking, at an optical depth ~ 1 to electron scattering. Torsional waves, excited by the forced reconnection of the reversing magnetic field, carry a fluctuating current, and are damped at high frequencies by the electrostatic acceleration of electrons and positrons. We show that inverse Compton radiation by the accelerated charges is stronger than their synchrotron emission, and is beamed along the magnetic field. Thermal radiation that is advected out from the base of the jet cools the particles. The observed relation between peak energy and isotropic luminosity – both its amplitude and scaling – is reproduced if the blackbody seeds are generated in a relativistic jet core that is subject to Kelvin-Helmholtz instabilities with the Wolf-Rayet envelope. This relation is predicted to soften to $E_{\text{peak}} \sim L_{\text{iso}}^{1/4}$ below an isotropic luminosity $L_{\text{iso}} \sim 3 \times 10^{50}$ ergs s^{-1} . Spectrally harder bursts will arise in outflows which encounter no dense stellar envelope. The duration of spikes in the inverse-Compton emission is narrower at higher frequencies, in agreement with the observed relation. The transition from prompt gamma-ray emission to afterglow can be explained by the termination of the thermal X-ray seed and the onset of synchrotron-self-Compton emission. GLAST will probe the mechanism of particle heating at the reverse shock by measuring the inverse-Compton scattering of the seed photons.

Subject headings: gamma rays: bursts; supernovae: general; turbulence; radiation mechanisms: non-thermal

1. INTRODUCTION

Models of gamma-ray burst (GRB) outflows have long been plagued by uncertainties in the mechanism by which gamma-rays are emitted, including the underlying instability that triggers the rapid variability, the mechanism by which particles are energized, and the location of the gamma-ray emitting region. These uncertainties are closely interlocked. Because there is no shortage of plausible mechanisms which could, in principle, generate gamma-rays in a relativistic outflow, the lack of convergence on one issue has tended to impede progress on all the others.

The data offer some important clues which have not yet been fully exploited by theoretical models. For example, individual GRB light curves show only weak changes in the pattern of variability from the beginning to the end of the burst (Beloborodov, Stern, & Svensson 1998; Ramirez-Ruiz & Fenimore 2000). This, in spite of the basic requirement – based on simple considerations of gamma-ray opacity (Cavallo & Rees 1978) – that the non-thermal gamma-rays must be emitted in a region that is vastly larger than the central engine – by some 6-8 orders of magnitude. One deduces that this dissipative zone must be concentrated within a fairly narrow range of radius, in spite of the large distance that the outflow must travel. In addition, a well-defined correlation has emerged between the peak energy of gamma-ray bursts and their isotropic luminosity, in a sample of BeppoSAX and HETE-II bursts with measured redshifts (Amati et al. 2002; Ghirlanda et al. 2004; Lamb, Donaghy, & Graziani 2005). A third clue is that the short gamma-ray bursts have systematically harder spectra than the long bursts.

The recent burst GRB 050509b had an isotropic luminosity of $\sim 3 \times 10^{49}$ ergs s^{-1} at a redshift of $z = 0.2$, but a much harder spectrum than the Amati relation would imply (Bloom et al. 2005). This observation has interesting implications for the location of the dissipative zones in a GRB outflow.

Strong circumstantial evidence has emerged that long GRBs involve the ejection of relativistically moving material from $\sim 2-3M_{\odot}$ black holes, which are formed in the collapse of massive stars (Woosley 1993; Paczyński 1998). The gamma-ray burst 030329 coincided with the energetic Type Ic supernova 2003dh (Stanek et al. 2003). The optical spectrum of this supernova was similar to that of the energetic Type Ic SN 1998bw (Galama et al. 1998). This previous supernova coincided with a gamma-ray burst (GRB 980425) of a much smaller isotropic luminosity, which may therefore have involved a buried jet. The progenitors of the long GRBs are apparently Wolf-Rayet stars surrounded by fast and dense winds. The origin of the short gamma-ray bursts is more uncertain, and may involve a mix of sources including binary neutron star systems (Eichler et al. 1989) and extragalactic Soft Gamma Repeaters (Duncan 2001).

The Wolf-Rayet/jet model offers two specific locations where the physics of gamma-ray emission can be well constrained: first, where the collimated relativistic outflow breaks out of the Wolf-Rayet star; and, second, where it begins to be decelerated substantially by its interaction with the external medium (including the outermost thin layer of stellar material that is entrained during the breakout of the relativistic jet). Our first goal in this paper is to define how the deceleration phase is modified by pair creation in the Wolf-Rayet wind, and the as-

sociated radiative acceleration of the pair-loaded wind material. Previous treatments of this process (Thompson & Madau 2000; Mészáros, Ramirez-Ruiz, & Rees 2001; Beloborodov 2002) assume a given pattern of gamma-ray emission, and do not examine its feedback on the forward and reverse shocks at the very earliest stage where the prompt burst is generated. One finds that the relativistic ejecta have a characteristic *compactness* at the point where the reverse shock wave completes its passage through the ejecta shell, because the process of pre-acceleration shuts off below a critical value of the fluence of the gamma-rays flowing across the forward shock. Rapid deceleration of the relativistic ejecta follows once this threshold is reached. The compactness is, in fact, regulated to a value somewhat larger than unity, and the optical depth through the swept-up e^+e^- pairs has a similar value. One therefore obtains a direct feedback between the physical conditions in the dissipative zone, and the radiative mechanism.

The gamma-ray emission depends on the presence of some irregularities in the outflow. These irregularities could be caused by stochastic flips in the sign of a dynamo-generated magnetic field that is swept into the outflow (Thompson 1994); or, alternatively, they could involve fluctuations in momentum and energy flux that manifest themselves as internal shock waves in a relativistic particle outflow (Rees & Mészáros 1994).

The seed irregularities are, in both of these models, imprinted into the outflow near its base. Nonetheless, the models are distinguished by the *isotropy* of the emission in the bulk frame. The synchrotron or inverse-Compton radiation of shock-accelerated particles is nearly isotropic in the rest frame of the shocked fluid. The observation of fast variability in many gamma-ray bursts then requires that the gamma-rays be emitted far inside the radius at which the bulk motion begins to be reduced significantly (Sari & Piran 1997). The basic disadvantage of this approach is that the location of the dissipative zone depends sensitively on the frequency and amplitude of the seed irregularities. Calculating the pattern of these irregularities from first principals requires a detailed theoretical understanding of almost every aspect of the central engine and its outflow. In spite of recent herculean efforts to simulate jet outflows (McKinney & Gammie 2004; de Villiers, Staff, & Ouyed 2005; McKinney 2005a,b), the model retains considerable freedom in practice.

A hybrid model of jet dissipation is suggested by considering the influence of jet breakout on the subsequent motion of the reverse shock wave. A thin outer layer of the Wolf-Rayet star accumulates energy from the relativistic beam emerging from below, and is pushed outward to higher speeds. Existing calculations of this ‘breakout shell’ are limited to a one-dimensional approximation (Waxman & Mészáros 2003). We calculate the column density of this shell, and the growth of its Lorentz factor, by taking into account the slippage of the swept-up matter to the side of the beam. Rayleigh-Taylor instabilities allow the relativistic fluid to emerge through the breakout shell in isolated spots, which can radiate independently.

Our second goal in this paper is to establish a realistic mechanism by which the gamma-ray emission may be triggered directly by the deceleration off the ‘breakout’ shell and the external wind medium. Calculations of prompt high-energy emission from the forward shock (Mészáros & Rees 1993; Mészáros, Rees, & Paphanassiou 1994; Chiang & Dermer 1999; Sari & Esin 2001) have neglected the effects of pre-acceleration of the ambient medium, have assumed that the

radiating particles are shock-accelerated, and therefore cannot easily account for fast variability in the emission. This forces us to focus on an alternative source of energy in the outflow – in particular, a strong non-radial magnetic field, which is independently motivated by considerations of the launching of the relativistic outflow. The magnetic field provides a characteristic direction for particle acceleration, and provides plausible instabilities which cause impulsive and localized injections of energy.

The relative proportions of energy carried by Poynting flux and by ions are still very uncertain in observed extragalactic jet sources (e.g. Sikora et al. 2005). Basic conservation laws limit the transfer of energy from the magnetic field to the particles through internal instabilities, if the inner boundary conditions of the outflow are time-invariant. Magnetic flux, in particular, is not easily eliminated from a fast-moving astrophysical fluid with a very high magnetic Reynolds number. The ion luminosity can increase by a logarithmic factor with respect to the Poynting luminosity in a smooth outflow (Begelman & Li 1994). The magnetic field will, nonetheless, have a strong softening effect on internal shock waves if the ordered Poynting luminosity L_P comprises 10 percent of the outflow luminosity (Kennel & Coroniti 1984; Zhang & Kobayashi 2005); and will contribute substantially to the post-shock pressure if the Poynting luminosity is somewhat smaller than this. Recent jet simulations suggest an approximate equipartition between kinetic and magnetic energy at a distance of $\sim 10^{10}$ cm from a stellar-mass black hole (McKinney 2005a,b).

The particle luminosity could also be increased by reconnection of a reversing magnetic field. This process is much more effective when the field is being pushed into the external medium, at a large distance from the engine where the sound-crossing time of the shell is smaller than the flow time (Thompson 1994; see Lyubarsky & Kirk 2001 for a more detailed discussion in the context of pulsar wind termination shocks). Tangling of the magnetic field allows a reverse shock wave to form even when the fast mode speed is higher than the speed of the outflow relative to the contact discontinuity.

Radiation that is advected out from the base of the outflow has a characteristic energy of ~ 1 MeV (Goodman 1986). Seed black body photons will be present in combination with a magnetic field in many models of the central engine, and therefore can play an important role as a source of inverse-Compton seeds at a large radius, and help to define the spectral peak of the gamma-ray emission (Thompson 1994). Our third goal in this paper is to investigate this effect in more detail, in light of more recent ideas that the propagation of a relativistic jet through the envelope of a Wolf-Rayet star (Zhang, MacFadyen, & Woosley 2003; Matzner 2003) can create a lower-energy thermal component in the jet cocoon (Ramirez-Ruiz, MacFadyen, & Lazzati 2002). We find that the observed relation between peak energy and isotropic luminosity in BeppoSAX and HETE-II bursts (Amati et al. 2002; Lamb et al. 2005) arises directly – without free parameters – from dissipation in a *relativistically-moving jet core* that is heated but not fully decelerated by Kelvin-Helmholtz instabilities with the jet cocoon. (The cocoon acquires a similar temperature, but its specific entropy is not realistically high enough to seed the gamma-ray emission proper.) Instead the portion of the jet material that acquires a high entropy within the Wolf-Rayet star is preferentially accelerated to high Lorentz factors after breaking out of the stellar photosphere. One can therefore establish a direct connection

between the presence of a fireball component at the base of the jet, and the observability of that portion of the jet as a gamma-ray burst.

It has also previously been suggested that the outflow can dissipate over a much wider range of radii, thereby creating a low-energy blackbody excess in gamma-ray burst spectra (Mészáros et al. 2002), or possibly a harder blackbody component just inside the photosphere which could help to regulate the peak energy in the observed manner (Mészáros & Rees 2000; Rees & Mészáros 2005). If the jet is magnetically dominated but very cold at its base, then continuing dissipation would be required to push it to a large Lorentz factor (Drenkhahn & Spruit 2002). However, it is difficult to establish clear predictions when the dissipation is driven by instabilities in the freely expanding portion of the outflow, given the number of physical effects which influence the growth of these instabilities.

The energy density of a gamma-ray burst outflow is orders of magnitude higher than that of the Solar corona, and the ambient radiation field has a much stronger influence on the cooling of charged particles. In fact, the conditions in the GRB outflow are much closer to those expected in the magnetic corona of an accretion disk around a stellar-mass black hole. This suggests that, when drawing lessons from Solar physics, we should focus on those physical processes which appear to be *energetically dominant* in the Sun’s atmosphere, and not only those which are directly responsible for the hard X-ray emission that emerges from that much more dilute environment. In the largest Solar flares, the output in thermal (~ 1 keV) X-rays is smaller than the kinetic energy of the ejected plasma by an order of magnitude; and the output in hard X-rays and gamma-rays is smaller yet by six orders of magnitude (e.g. Somov 1992). Processes very similar to those which heat the Sun’s chromosphere and thermal corona will, in the more extreme environment of a gamma-ray burst, create a much harder photon spectrum.

A non-potential magnetic field transfers energy to particles through various channels. Energetically important channels include the damping of large-scale magnetohydrodynamic motions (through the formation of high-frequency spectrum of MHD waves); and a sudden change in the topology of magnetic field lines through reconnection. In a GRB outflow, charged particles are created at a sufficient rate by photon collisions ($\gamma + \gamma \rightarrow e^+ + e^-$) to ensure that the MHD condition applies on large scales. For this reason, we have previously suggested that the main role of reconnection in GRB outflows is not to cancel off the toroidal magnetic field (as in the Coroniti 1990 model of the Crab pulsar wind), but instead to facilitate a tangling up of the field through a change in topology.

Damping of MHD turbulence is expected to be a ubiquitous process in any relativistic outflow containing a magnetic field. In this paper, we examine, in more detail than previously (Thompson & Blaes 1998; Lyutikov & Thompson 2005), the regime in which the magnetic energy density is at least comparable to the rest-energy density of the entrained charged particles. The wave energy is transferred to the light charges (electrons and positrons) primarily through electrostatic acceleration along the magnetic field. As a result, the radiation is beamed along the local direction of the magnetic field. This means that inverse-Compton cooling will dominate synchrotron cooling even if the magnetic energy is larger than the energy density of the ambient radiation field. Bulk relativistic motion of the magnetofluid provides another avenue for beamed emission (Lyutikov & Blandford 2003), but it is not required.

An overarching goal of this paper is to identify the key components of the outflow which *must* be included for a proper description of GRB emission. We find that it is essential to include a thermal radiation field as well as a strong magnetic field, these two components being in approximate equipartition at the base of the outflow. A small admixture of baryons is probably present, which can carry a significant portion of the luminosity in some parts of the jet; but the baryons actually play a less essential role in the emission physics. For the purposes of investigating the prompt gamma-ray emission, the bulk of the outflow can be assumed to expand freely in between the photosphere of the Wolf-Rayet star and the dissipation zone. Closer to the central engine, the outflow probably is magnetically dominated and is susceptible to global MHD instabilities (Lyutikov & Blandford 2003; Giannios & Spruit 2006). The field lines are then entrained in the heated outflow, and stretched back into a non-radial configuration outside the Wolf-Rayet envelope. The fast motion of the jet implies strict limits on the factor by which the field energy can be reduced this close to the engine.

1.1. Plan of the Paper

The plan of this paper is as follows. We begin in §2 by defining the inner boundary conditions of the relativistic outflow, and how they are influenced by the interaction between jet and Wolf-Rayet envelope. Basic constraints on the tangling of the jet magnetic field interior to the stellar photosphere are outlined in §2.1. The fundamental relation between black-body temperature and isotropic luminosity is worked out in §2.2. The baryons and the magnetic field are tightly coupled, and are accelerated together by the flux of thermal photons outside the baryonic photosphere (§2.3). Next we examine the interaction between the relativistic shell and the Wolf-Rayet wind (§3.1), with a particular focus on the radiative compactness in the deceleration zone (§3.2) and optical depth in electron-positron behind the forward shock (§3.3). These calculations are repeated in §4 in the case where the fragmenting ‘breakout’ shell is the dominant source of inertia.

The evolution of the magnetic field near the contact discontinuity is the subject of §5. We consider whether a reverse shock will form, and how its structure is modified by small-scale structure in the magnetic field (§5.1). We note that magnetic reconnection across a neutral sheet can be facilitated by rapid synchrotron cooling in some circumstances (§5.3). The Rayleigh-Taylor instability of the contact discontinuity is analyzed in §5.4. The instability is weak except when a dense breakout shell is present.

We argue in §6 that the damping of torsional MHD waves in a background radiation field provides a promising approach to the non-thermal and strongly variable emission of gamma-ray bursts. The section begins (§6.1) by reviewing the fact that electrons and positrons will be electrostatically accelerated along the background magnetic field by high-frequency waves near the inner scale of the turbulent spectrum (Thompson & Blaes 1998; Lyutikov & Thompson 2005). It is argued that electrostatic heating occurs primarily through many small impulses, at a scale somewhat larger than the scale at which the torsional waves become charge-starved. The beaming of the inverse-Compton radiation of the heated charges is calculated in §6.3. When the Kolmogorov energy flux is above a critical value, the electrostatic heating cannot be balanced instantaneously by Compton cooling (§6.4).

The beaming of the inverse-Compton emission provides a

nice explanation for the rapid variability of the gamma-ray flux at higher energies. The correlation between variability timescale and photon energy is analyzed in §7.1. The effect of inverse-Compton scattering on pair creation in the relativistic ejecta is considered in §7.2, and it is noted that strong anisotropy in the gamma-ray emission can cause a significant increase in the pair creation rate.

The paper concludes in §8 with a critical summary of how the model fares in explaining the non-thermal spectra of gamma-ray bursts. We show in §8.1 that an inhomogeneous distribution of particle energies will naturally arise behind the reverse shock wave, and can explain the presence of a high-energy continuum above the peak energy in the spectrum of a typical GRB. The pairs swept up by the forward shock during the deceleration phase leave a radiative signature in the form of inverse-Compton photons peaking at an energy $\sim 10^2 - 10^3$ times the peak burst energy (§8.2). High-energy spectral measurements will therefore provide a direct diagnostic of the process of pair-loading and pre-acceleration. The implications of weak optical emission in the prompt GRB for the mechanism of particle heating are drawn in §8.4, the transition from prompt GRB emission to afterglow is addressed in §8.5 and, finally, the ‘peculiar’ burst 941017 is discussed in light of these results in §8.6.

A summary list of our results is provided in §9.

2. GEOMETRY AND INNER BOUNDARY CONDITIONS OF THE RELATIVISTIC OUTFLOW

Our approach to the gamma-ray emission problem starts with a basic simplification: the relativistic outflow that powers the GRB suffers only a negligible dissipation between the central engine and the non-thermal emission zone at $\sim 10^{14} - 10^{15}$ cm. The base of this freely expanding outflow coincides with the photosphere of the progenitor star. The temperature in the outflow is already small enough that thermal pairs have annihilated (Goodman 1986; Shemi & Piran 1990), and the entrained baryons and electrons provide the main scattering opacity. We now discuss the relative partitioning of energy between the thermal photons, magnetic field, and baryons.

In this paper we focus on a Wolf-Rayet progenitor, with a radius of $\sim 2 \times 10^{10}$ cm. The star is a source of a strong stellar wind, $\dot{M}_w \sim 0.5 \times 10^{-5} - 10^{-4} M_\odot \text{ yr}^{-1}$ (Nugis & Lamers 2000) that provides an effective stopping agent for the relativistic ejecta. The central engine is a $\sim 2 - 3 M_\odot$ black hole that is surrounded by a neutronized torus (Woosley 1993). This torus is fed by the collapse of the inner core of the Wolf-Rayet star. Accretion and the emission of a Poynting-dominated jet continues until the star explodes as the result of the energy deposited in it by the jet (Paczyński 1998). The duration of the outflow is not lengthened compared with the period of activity Δt of the central engine, and so we leave Δt as a free parameter, normalized to the observed durations of long GRBs, $\Delta t \sim 10$ s in the cosmological rest frame.

It should be noted that careful studies of the X-ray/optical/radio afterglow radiation of GRBs have called into question the presence of a dense Wolf-Rayet wind environment in several burst events. A lower mass-loss rate is, indeed, expected from Wolf-Rayet stars of lower metallicity (Chevalier, Li, & Fransson 2004); but the mass-loss rates from luminous WC stars are also often inferred to be higher than $\sim 10^{-5} M_\odot \text{ yr}^{-1}$. Observations of strong radio emission at ~ 1 month post-burst can place interesting constraints on the wind density (e.g. Chevalier et al. 2004), but under some assumptions, e.g. that

the magnetic field energy fraction ε_B is constant between the early and later synchrotron-emitting phases. (The wind density derived for GRB 020405 scales as $\dot{M} \sim (\varepsilon_{B,1 \text{ month}}/\varepsilon_{B,1 \text{ day}})^2$: see eqs.[1] and [2] of Chevalier et al. 2004.)

The sharpness of the break in the optical light curve provides a valuable probe of the density profile surrounding the burst source (Panaitescu & Kumar 2000, 2001, 2002). In the case of a jet with non-radial structure, it is difficult to reproduce the sharpness of the break in about 1/2 of events, if the energy flux but not the Lorentz factor is allowed to vary as a power-law about the jet axis (Panaitescu 2005). On the other hand, the Lorentz factor Γ_{rel} of the jet material is expected also to vary about the jet axis. Some calculations have included a strong angular gradient in Γ_{rel} (Kumar & Granot 2003), but more general distributions of Γ_{rel} have not been explored. Recently Swift has made available simultaneous X-ray and optical light curves which have revealed different break patterns in these bands. GRB 050525a provides an example of an afterglow showing a much sharper break in the optical band than in the X-ray band $\sim 10^4$ s post-burst (Blustin et al. 2006). The implications for the density profile from jet break phenomenology therefore appear to us to be somewhat ambiguous (see also Yost et al. 2003). Given these caveats, we will focus solely on a r^{-2} density profile in this paper and generally normalize \dot{M} to a value $\sim 10^{-5} M_\odot \text{ yr}^{-1}$. The implications of more dilute winds for the dissipation of the magnetized fireball are examined briefly in §8.5.

The simplest relativistic jet expands ballistically into a fixed solid angle. A linear increase of Lorentz factor with radius can be a good approximation to the actual situation even if the magnetic field is dynamically dominant close to the central engine. The transfer one half of the magnetic energy to thermal radiation allows the outflow to continue to accelerate by pressure gradient forces inside its photosphere (Drenkhahn & Spruit 2002). We argue here that this process can be effective even when the thermalization is localized at some small radius, and that the acceleration can continue outside the outflow photosphere if the matter loading is very small. One then has

$$\Gamma(r) = \Gamma(R_*) \left(\frac{r}{R_*} \right), \quad (1)$$

up to some maximum Lorentz factor Γ_{max} that depends on the thermalization radius. It is $\Gamma_{\text{max}} \sim 10^2$ for a jet emerging from a Wolf-Rayet envelope. The remaining irregularities in the magnetic field are then frozen in, and fall out of causal contact either because Γ saturates, or because the fluid passes through the reverse shock wave (Thompson 1994; Lyubarsky & Kirk 2001).

2.1. Tangling of a Dynamo-Generated Magnetic Field

The most plausible mechanism for generating a baryon-poor outflow invokes a large-scale ordered magnetic field threading the black hole (Blandford & Znajek 1977), but such a Poynting-dominated outflow can undergo global current-driven instabilities as it propagates through the envelope of the Wolf-Rayet star. In our approach to the burst emission problem, these instabilities are not the direct source of the gamma-ray emission (as suggested by Lyutikov & Blandford 2003), but they will facilitate a tangling up of the magnetic field inside the Wolf-Rayet photosphere. The limitations of causality prevent the ordered Poynting flux from decreasing to a small fraction of the total energy flux during the propagation of the jet through the Wolf-Rayet envelope. The field can be smoothed over a length-scale $\Delta r'_B$ (in the bulk frame) only if the Alfvén crossing time

$\Delta r'_B/V'_A$ is shorter than the flow time t' . In a cold medium, the Alfvén speed can be normalized to the speed of light through the fraction ε'_B of the energy density carried by the magnetic field: $V'_A/c \simeq (2\varepsilon'_B)^{1/2}/(1+2\varepsilon'_B)^{1/2}$. The duration of a flow that expands with Lorentz factor Γ is $t' \sim r/c\Gamma$, and so one obtains a lower bound $\varepsilon'_B \gtrsim (\Delta r'_B/ct')^2 \sim (\Gamma\Delta r'_B/r)^2$ on the magnetic energy density. If the field starts out with a reversal scale $\Delta r'_{B0}$ and $\varepsilon_{B0} \sim 1$, and if its reversals are random, then conservation of magnetic flux implies that $\varepsilon'_B \sim \Delta r'_{B0}/\Delta r'_B$. Combining these expressions gives

$$\varepsilon'_B \gtrsim \left(\frac{\Delta r'_{B0}}{r/\Gamma} \right)^{2/3}. \quad (2)$$

The magnetic field that is carried outward by the relativistic outflow is ultimately generated by a dynamo process within the central engine. The fluid shear in the neutron torus surrounding a $2-3M_\odot$ black hole with a modest spin has a characteristic timescale of $t_{\text{dyn}} \sim 10^{-3}$ s. The convection motions inside a nascent neutron star have a similar duration. The sign of the magnetic field that is advected into the outflow will vary with the sign of the dynamo generated field (Thompson 1994). The timescale for field reversals must be longer than the flow time $r/c \sim 10^{-4}$ s at the base of the outflow; but simulations of the MRI instability also suggest that it will be much shorter than the total duration $\Delta t \sim 10$ s of the inflow to the black hole from the collapsing core of the progenitor star (Woosley 1993; Paczyński 1998). This means that the characteristic radial scale Δr_B for toroidal field reversals in the outflow will not be much smaller than the radius R_* of the Wolf-Rayet star. Taking $\Delta r_{B0}/c \sim 0.1$ s (before untangling) and $R_* = 2 \times 10^{10}$ cm gives $\Delta r_{B0}/R_* \sim 0.15$ and

$$\varepsilon'_B \gtrsim 0.3\Gamma^{4/3} \left(\frac{\Delta r_{B0}/c}{0.1 \text{ s}} \right)^{2/3} \quad (3)$$

from eq. (2). This lower bound is large enough that the field will have a significant effect on internal shocks farther out (§5.1).

2.2. Seed Blackbody Photons and the $E_{\text{peak}}-L_{\text{iso}}\Delta t$ Relation

A nearly black body photon gas is generated by the damping of turbulent motions in the jet. This seed radiation field can carry a significant fraction ε_{bb} of the outflow luminosity L . At the stellar photosphere, $r = R_*$, the rest-frame temperature T'_{bb} of the photons is given by

$$\begin{aligned} \frac{4}{3}\Gamma^2 a T'_{\text{bb}}{}^4 &= \varepsilon_{\text{bb}} \frac{L}{\Delta\Omega R_*^2 c} = \varepsilon_{\text{bb}} \frac{L_{\text{iso}}}{4\pi R_*^2 c}; \\ k_B T'_{\text{bb}} &= 46 \frac{(\varepsilon_{\text{bb}} L_{50})^{1/4}}{\Gamma(R_*)^{1/2}} \left(\frac{\Delta\Omega}{10^{-2}} \right)^{-1/4} \text{ keV}. \end{aligned} \quad (4)$$

Here $L_{\text{iso}} = L(4\pi/\Delta\Omega)$ is the isotropic luminosity of a two-sided jet flowing through a solid angle $\Delta\Omega = 2 \times \pi\theta^2$. Note that when the Lorentz boost of the jet material is taken into account, the temperature of the blackbody component could be as large as $\frac{4}{3}\Gamma(R_*)T'_{\text{bb}} \sim 100$ keV. It therefore provides a useful seed for the prompt gamma-ray emission.

As we now argue, the jet material that develops a high entropy inside the Wolf-Rayet star is favored as an observable source of rapidly variable GRB emission for two reasons. First, one obtains a simple relation between isotropic luminosity L_{iso}

and the mean energy per photon carried by the thermal component of the outflow. This agrees closely with the relation between E_{peak} and isotropic burst energy $L_{\text{iso}}\Delta t$ that was obtained by Amati et al. (2002) from a sample of BeppoSAX bursts with measured redshifts, and confirmed by HETE-II burst localizations (Lamb et al. 2005). Second, the strong momentum flux of the black body photons allows this material to be accelerated to a higher Lorentz factor outside the Wolf-Rayet photosphere. The limiting Lorentz factor and the maximum tolerable matter loading are considered in the following section 2.3.

Jet material moving at a Lorentz factor $\Gamma \gg \theta^{-1}$, where θ is the angle from the axis of the jet, will sustain only a small velocity shear in the fluid rest frame, and will remain cold. Material that is decelerated to $\Gamma \ll \theta^{-1}$ mixes easily with the much heavier cocoon material and decelerates to $\Gamma \sim 1$. At an angle θ , there is therefore a characteristic Lorentz factor $\Gamma \sim 1/\sqrt{3}\theta$ above which a Kelvin-Helmholtz mode will not have time to grow on a lengthscale $\sim \theta R_*$ (in the bulk frame). (Here we have equated the sound-crossing time $\theta R_*/c_s = \sqrt{3}\theta R_*/c$ with the flow time $R_*/\Gamma c$ in the bulk frame.)

If the entire jet fluid were to decelerate to $\Gamma \sim 1$ within the stellar envelope, then the relation between temperature and (isotropic) luminosity would follow the usual blackbody relation, $T_{\text{bb}} \sim L_{\text{iso}}^{1/4}$. The temperature-luminosity relation becomes harder with Γ at the above critical value. Observations of GRB afterglows suggest that the total energy E carried by the jet is roughly independent of opening angle (Frail et al. 2001; Bloom et al. 2003). In that case, one has

$$L_{\text{iso}}\Delta t \left(\frac{\Delta\Omega}{4\pi} \right) = L_{\text{iso}}\Delta t \left(\frac{\theta^2}{2} \right) = 5 \times 10^{50} \text{ ergs}. \quad (5)$$

The corresponding Lorentz factor is then

$$\Gamma(R_*) = \frac{1}{\sqrt{3}\theta} = 1.8 L_{\text{iso}51}^{1/2} \Delta t_1^{1/2}. \quad (6)$$

Combining eqs. (4) and (5) gives

$$k_B T'_{\text{bb}} = 10 \varepsilon_{\text{bb}}^{1/4} \Delta t_1^{-1/4} \left(\frac{R_*}{2 \times 10^{10} \text{ cm}} \right)^{-1/2} \text{ keV}. \quad (7)$$

This temperature is low enough that the thermal creation of electron-positron pairs can be neglected. The relation between Lorentz-boosted temperature and isotropic luminosity can then be expressed in terms of the mean energy per black-body photon,

$$\begin{aligned} 2.7 k_B T_{\text{bb}} &= 2.7 \left[\frac{4}{3} \Gamma(R_*) \right] k_B T'_{\text{bb}} \\ &= 70 \frac{\varepsilon_{\text{bb}}^{1/4}}{\Delta t_1^{1/4}} \left(\frac{L_{\text{iso}}\Delta t}{10^{52} \text{ ergs}} \right)^{1/2} \left(\frac{R_*}{2 \times 10^{10} \text{ cm}} \right)^{-1/2} \text{ keV}. \end{aligned} \quad (8)$$

If one substitutes $\varepsilon_{\text{bb}} \sim \frac{1}{2}$ and takes into account that the isotropic luminosities of long GRBs appear to have a much broader distribution than do their durations¹, then one very nearly reproduces the observed relation (Amati et al. 2002; Lamb et al. 2005). The normalization is $\sim 60\%$ of the measured value, but an additional $\sim \frac{1}{2}$ of the outflow energy must be carried by a separate component, whose dissipation generates the high-energy, non-thermal tail to the gamma-ray burst spectrum. We emphasize that this relation depends on only one

¹ The observed T_{90} distribution covers the range 4–40 s at half maximum (Paciesas et al. 1999), which of course includes the broadening effects of a distribution of source redshifts.

free parameter, the radius of the Wolf-Rayet star, which is of course constrained independently.

The inferred width of the burst energy distribution depends on the details of the beaming correction that is employed. The most detailed effort, by Ghirlanda et al. (2004), indicates a spread of ~ 1 order of magnitude in the case of a r^{-2} circumburst density profile. However, Swift has observed additional time-structure in the afterglow light curves at times intermediate between the burst duration $\Delta t \sim 10 - 10^2$ s, and the later achromatic breaks that were used by Ghirlanda et al. (2004) to normalize the jet opening angle (Tagliaferri et al. 2005). There remains, therefore, some ambiguity in the mapping between the prompt gamma-ray emission and the later phases of the afterglow.

The distribution of burst energies also depends on the mechanism by which the jet is collimated. The beaming-corrected burst energies are remarkably similar to the typical kinetic energy of a core-collapse supernova (Frail et al. 2001). They are also similar to the gravitational binding energies of the cores of 20-30 M_\odot evolved stars (typically $E_B \sim 1 - 2 \times 10^{51}$ ergs; see Figs. 5 and 6 of Woosley & Weaver 1995). Current modelling of Blandford-Znajek jets from black holes suggests that strong collimation requires the presence of a geometrically thick torus around the hole (e.g. McKinney & Gammie 2004). The extent to which this condition is satisfied in hyper-accreting tori (accretion rates $\dot{M} \sim 2M_\odot/10 \text{ s} = 0.2M_\odot \text{ s}^{-1}$) depends on the density profile in the outer atmosphere of the torus, which in turn is sensitive to the dissipative processes operating there. A geometrically thin, neutrino-cooled disk can form self-consistently at this accretion rate (e.g. Narayan, Piran, & Kumar 2001). When the outflow is broad close to the engine, strong collimation is possible only if the outflow energy is comparable to E_B : if the outflow energy is smaller, it will be swept back by the accretion flow, and if it is substantially larger it will trigger a quasi-spherical blast wave. These considerations provide a physical motivation for our assumption of a relatively narrow distribution of burst energies, compared with current beaming corrections (Ghirlanda et al. 2004).

Rees & Mészáros (2005) have outlined a related approach to the $E_{\text{peak}} - L_{\text{iso}} \Delta t$ relation, starting with the idea that the peak energy is regulated by dissipation and thermalization just inside the photosphere of the outflow. The radius of the photosphere is determined self-consistently by the luminosity and composition of the outflow, the scaling of Γ with radius, and the particular radiative processes occurring in the outflow. As a result, definite predictions for the slope of the relation, or its normalization, are not easily obtained. Note also that the causal relation $\Gamma \sim 1/\sqrt{3}\theta$ is more difficult to satisfy this far out in the outflow. For all of these reasons, we conclude that the Amati et al. (2002) relation arises more naturally at a *fixed* radius, during jet breakout from the Wolf-Rayet star. The prompt gamma-ray emission is, in this picture, reprocessed ‘fireball’ radiation, with the position of the fireball displaced outward from the radius of the black hole accelerator ($\sim 10^7$ cm) to its surrounding stellar envelope ($\sim 10^{10}$ cm).

We expect that the relation (8) between T_{bb} and $L_{\text{iso}} \Delta t$ will be modified at low luminosities, because its derivation depends on Γ being larger than unity. One sees from eq. (6) that this assumption must break down below a luminosity $L_{\text{iso}} \sim 3 \times 10^{50} \Delta t^{-1}$ ergs s^{-1} . At lower luminosities, the relation is predicted to soften to $T_{\text{bb}} \sim L_{\text{iso}}^{1/4}$ when the jet material moves transrelativistically [$\Gamma(R_\star) \simeq 1$].

An apparent inconsistency between the Amati et al. (2002) relation and the BATSE burst sample has been uncovered by Nakar & Piran (2005). These authors find that $\sim \frac{1}{2}$ of the BATSE bursts are harder spectrally than the $E_{\text{peak}} - L_{\text{iso}} \Delta t$ relation would imply, no matter where each burst source is placed in redshift space. Note that the BATSE sample has a lower flux threshold than the BeppoSAX sample, so that the bulk of the BATSE bursts need not sit in the $E_{\text{peak}} \propto L_{\text{iso}}^{1/2}$ portion of the color-luminosity relation. Our predicted modification of the Amati et al. (2002) relation, at energies lower than $E_{\text{iso}} \sim 3 \times 10^{51}$ ergs, could therefore resolve this apparent contradiction without recourse to beaming or orientation effects.

The $T_{\text{bb}} - L_{\text{iso}}$ relation that we have derived is also consistent with a ‘structured’ jet, but we note that a range of Lorentz factors within the jet core is required. The published structured-jet models generally assume a distribution of energy flux across the jet, but a constant Lorentz factor. In practice, there is no reason to expect that Γ varies much more weakly than L_{iso} . The kinematic model considered here implies that $\Gamma \propto L_{\text{iso}}^{1/2} \Delta t^{1/2}$ at the boundary of the Wolf-Rayet star. The asymptotic Lorentz factor of the freely-expanding jet material scales as $\Gamma \propto L_{\text{iso}}^{3/8} \Delta t^{1/8}$ (see eq. [12] below).

2.3. Baryon Contamination and Terminal Lorentz Factor

Effective thermalization of the radiation field at a temperature (7) requires the presence of a small baryon component, since the temperature (7) is too small to excite pairs thermally. The mass in baryons depends, in turn, on the details of the launching of the jet, and can be expected to vary from burst to burst (depending especially on the viewing angle if additional material is mixed from the envelope). The baryon loading of the outflow is represented by the parameter

$$\Gamma_b = \frac{L}{\dot{M}_b c^2}. \quad (9)$$

The associated electrons provide a scattering depth

$$\tau_{\text{T},b} = \frac{\sigma_{\text{T}} Y_e L_{\text{iso}}}{8\pi \Gamma_b \Gamma^2(R_\star) m_p R_\star c^3} \left(\frac{r}{R_\star} \right)^{-3}. \quad (10)$$

Here $Y_e \sim \frac{1}{2}$ is the ratio of the number of protons to total nucleons that are bound up in charged ions. (The role of free neutrons is briefly addressed below.)

A substantial optical depth at radius R_\star is needed if the photon distribution function is to relax to a black body. The jet material is still optically thin to free-free absorption at the temperature (7), and so effective thermalization requires a Compton parameter $y_{\text{C}} = 4(k_{\text{B}} T'_{\text{bb}} / m_e c^2) \tau_{\text{T},b} \gtrsim 5$. Thermalization is therefore possible only if the baryon loading is larger than

$$\Gamma_b \lesssim 7 \times 10^4 \varepsilon_{\text{bb}}^{1/4} \Delta t_1^{-5/4} \quad (11)$$

at $r = R_\star = 2 \times 10^{10}$ cm. The large scattering depth for thermalization means that the blackbody photons must be created within the jet. More generally, unless Γ_b is extremely large and the jet is extremely clean, the jet core will not see the soft thermal photons that are created in the surrounding cocoon (cf. Ghisellini et al. 2000).

Above a critical baryon density, the Lorentz-boosted photon temperature $\frac{4}{3} \Gamma T'_{\text{bb}}$ will be cooled by adiabatic expansion before the photons and matter decouple. To avoid this, one requires that the scattering depth (10) drop below unity before Γ reaches Γ_b . Combining eqs. (1), (6), and (10) gives the required

lower bound on Γ_b ,

$$\begin{aligned}\Gamma_b > \Gamma_{b \text{ crit}} &= \left[\frac{\sigma_T Y_e \varepsilon_{\text{bb}} L_{\text{iso}} \Gamma(R_*)}{8\pi m_p c^3 R_*} \right]^{1/4} \\ &= 85 L_{\text{iso}51}^{3/8} \Delta t_1^{1/8} (Y_e \varepsilon_{\text{bb}})^{1/4} \left(\frac{R_*}{2 \times 10^{10} \text{ cm}} \right)^{-1/4}.\end{aligned}\quad (12)$$

The key point here is that $\Gamma_{b \text{ crit}}$ depends on the launching radius of the freely expanding jet. Increasing R_* from $\sim 10^6 - 10^7$ cm (the physical size of the central engine) to $R_* \sim 10^{10}$ cm has the effect of reducing $\Gamma_{b \text{ crit}}$ by an order of magnitude.

The magnetic field carries inertia, which can limit the bulk motion of the outflow if it is cold at its base. The role of thermal pressure in accelerating the outflow has been examined by Drenkhahn & Spruit (2002). At a large optical depth, the radiation field is advected with the other components of the flow, and a pressure-gradient force is responsible for pushing the flow to a higher Lorentz factor. Although some acceleration is possible by this mechanism in the optically thin region of the flow, we focus here on the force imparted by the radiation field to the magnetofluid. This effect is already familiar from studies of particle-dominated fireballs, and is especially important if the outflow undergoes strong heating near its base. It is straightforward to see that the limiting Lorentz factor (12) is not modified significantly by the magnetic field as long as the particle Lorentz factor Γ is much larger than² $(B^2/8\pi\rho c^2)^{1/3}$. In a steady state, both the Poynting flux $S = (B^2/8\pi)v_r$ and the momentum flux $P = (B^2/8\pi)(1+v_r^2/c^2)$ carried by the non-radial magnetic field B receive (negative) corrections $\Delta S/S \simeq \Delta P/P \simeq -\Delta\Gamma/\Gamma^3$ in response to a change $\Delta\Gamma$ that is driven by Compton scattering. When Γ satisfies the above inequality, both ΔS and ΔP are negligible compared with the increase $\rho c^3 \Delta\Gamma$ in the particle kinetic energy flux. Further out in the flow, the inertia of electron-positron pairs can dominate the inertia of the baryons, and some of the energy carried by the magnetic field is converted to non-thermal photons.

It is possible to set an upper bound to the baryon kinetic luminosity, and to the terminal Lorentz factor of outflow. Outside the photosphere of the Wolf-Rayet star, the baryons will continue to accelerate off the flux of thermal photons. The collimation of the photons grows with radius, $\Gamma_\gamma(r) \simeq \Gamma(R_*)(r/R_*)$. The baryons maintain a Lorentz factor $\Gamma \simeq \Gamma_\gamma$ as long as

$$\Gamma_\gamma \lesssim \frac{1}{2} \ell_\gamma = \frac{Y_e \sigma_T (\varepsilon_{\text{bb}} L_{\text{iso}})}{8\pi r^2 m_p c^2} \left(\frac{r}{2\Gamma_\gamma^2 c} \right). \quad (13)$$

This leads to a maximum Lorentz factor essentially equal to eq. (12) (e.g. Shemi & Piran 1990). When $\Gamma_b > \Gamma_{b \text{ crit}}$, the Lorentz factor saturates at a value

$$\Gamma \simeq \Gamma_{b \text{ crit}} \quad (\Gamma_b \gg \Gamma_{b \text{ crit}}), \quad (14)$$

and the baryons carry only a fraction $\varepsilon_b \simeq \Gamma_{b \text{ crit}}/\Gamma_b$ of the total energy of the outflow. The proportions of the energy flux carried by thermal photons, baryons, and magnetic field must of course sum to unity,

$$\varepsilon_{\text{bb}} + \varepsilon_b + \varepsilon_B = 1. \quad (15)$$

In a cold flow, ε_B is related to the rest-frame magnetic energy density ε'_B by $\varepsilon_B \simeq 2\varepsilon'_B$.

An important feature of this acceleration mechanism is the correlation between the presence of a strong thermal photon

flux at the base of the jet, and the development of a large terminal Lorentz factor outside the Wolf-Rayet envelope. Portions of the jet which dissipate less inside the Wolf-Rayet star may attain a lower terminal Lorentz factor, and their deceleration will be pushed to a larger radius.

Neutrons play a limited role in this jet model. Advected outward from the central engine, they are entrained by the protons and alpha particles at the Wolf-Rayet photosphere, and decouple from them somewhat inside the baryonic scattering photosphere. The neutron mass flux \dot{M}_n can be much larger than the proton mass flux, due to the effects of neutronization in the central engine (e.g. Beloborodov 2003). We take a (representative) ratio $\dot{M}_n/\dot{M}_p = 8$, which corresponds to $\dot{M}_n/\dot{M}_\alpha = 4.5$ if all of the protons have combined into alpha particles. The neutrons then decouple from the alpha particles just after the combined neutron-ion fluid (temporarily) reaches the limiting Lorentz factor

$$\begin{aligned}\Gamma_n &= \frac{L_{\text{iso}}}{(\dot{M}_n + \dot{M}_\alpha)c^2} \\ &= 13 L_{\text{iso}51}^{3/8} \Delta t_1^{1/8} \varepsilon_{\text{bb}}^{1/4} \left(\frac{R_*}{2 \times 10^{10} \text{ cm}} \right)^{-1/4} \left(\frac{\Gamma_b}{\Gamma_{b \text{ crit}}} \right).\end{aligned}\quad (16)$$

The neutrons fall behind the outer half of the ejecta shell at a radius $\Gamma_n^2 c \Delta t = 5 \times 10^{13} L_{\text{iso}51}^{3/4} \Delta t_1^{1/4} \varepsilon_{\text{bb}}^{1/2} (R_*/2 \times 10^{10} \text{ cm})^{-1/2} (\Gamma_b/\Gamma_{b \text{ crit}})^2$ cm. At this radius, a fraction $\ln 2 \Gamma_n \Delta t / t_{1/2} = 0.1 L_{\text{iso}51}^{3/8} \Delta t_1^{9/8} (R_*/2 \times 10^{10} \text{ cm})^{-1/4}$ of the neutrons have decayed. The effective inertia of the decayed neutrons (mass ΔM_n) is larger than the inertia of the alpha particles, $(\Gamma_{b \text{ crit}}/\Gamma_n) \Delta M_n > M_\alpha$, when $L_{\text{iso}} \gtrsim 10^{51}$ erg/s. Even in this case, the neutron decay will have a modest effect on the dynamics of the contact discontinuity, which at this point has a significantly smaller Lorentz factor than that of the relativistic outflow (§4). The effect of the neutrons is also limited when Γ_b is larger than $\Gamma_{b \text{ crit}}$ and the inertia of the outflow is dominated by an advected magnetic field.

3. DECELERATION OF THE RELATIVISTIC OUTFLOW

We now consider the interaction between the relativistic ejecta and the Wolf-Rayet wind. The ejecta form a flattened shell outside a distance $c\Delta t$ from the star. A thin layer of shocked wind material collects in front of the ejecta shell, and is preceded by a forward shock wave. We focus first on the idealized, one-dimensional treatment of this problem, and defer consideration of Rayleigh-Taylor instabilities to §4 and §5.4.

There is an extensive treatment of the dynamics of the reverse shock wave in the literature, assuming ideal shock jump conditions (Sari & Piran 1995; Mészáros & Rees 1997; Sari & Piran 1999; Nakar & Piran 2004), and taking into account the effects of magnetic pressure in that approximation (Zhang & Kobayashi 2005). Our goal here is to include i) the effects of pair loading and preacceleration of the medium ahead of the forward shock; and ii) the possibility of strong dissipation of the non-radial magnetic field behind the reverse shock. The first effect is an inevitable consequence of the observed gamma-ray emission if it occurs inside $\sim 10^{16}$ cm; and the second is necessary if the emission is triggered by the interaction of the ejecta with the external medium (cf. §8.5). The relativistic outflow will also interact with the thin shell of material that is collected by the jet head following breakout. We defer a discussion of the

² Here ρ is the rest energy density of the entrained charges in the frame of the engine.

associated effects to §4, after we have analyzed the interaction with the expanding Wolf-Rayet wind material.

We distinguish between the luminosity L_{rel} carried by the particles and magnetic field; and the total isotropic luminosity L_{iso} , which also has a contribution from the seed thermal photons. They are related by

$$L_{\text{rel}} = (1 - \varepsilon_{\text{bb}})L_{\text{iso}}. \quad (17)$$

The mass profile in the Wolf-Rayet wind is

$$\rho_w(r) = \frac{\dot{M}_w}{4\pi r^2 V_w} \quad (18)$$

when the mass loss rate $\dot{M}_w = \dot{M}_{w-5} \times 10^{-5} M_{\odot} \text{ yr}^{-1}$ and wind speed $V_w = V_{w8} \times 10^8 \text{ cm s}^{-1}$ are constant over the emission region. The mass swept up from the wind inside a radius r is

$$M_w(r) = \frac{\dot{M}_w r}{V_w}. \quad (19)$$

A relativistic jet emerging from the photosphere of a Wolf-Rayet star will also collect a thin shell of matter from the stellar envelope, which can exceed $M_w(r)$ for sufficiently small r (§4).

3.1. Dynamics of the Contact Discontinuity

Pair creation by gamma-rays streaming into the external medium has a strong influence on the propagation of the forward shock (Thompson & Madau 2000; Mészáros, Ramirez-Ruiz, & Rees 2001; Beloborodov 2002). What has not been examined is the feedback of the pre-acceleration of the pair-loaded Wolf-Rayet wind on the dissipative processes occurring in the relativistic outflow. We show here that the bulk of the dissipation is delayed to a radius where the relativistic motion of the ambient medium has nearly, but not completely, decayed away. As a result, the compactness of the radiation emitted behind the forward shock is regulated to a characteristic value that depends weakly on L_{rel} .

The structure of the flow near the contact is displayed in Fig. 1. If the wind material were held static before passing through the forward shock, then Γ_c would be obtained by moving to the rest frame of the contact and balancing the momentum flux on both sides,³

$$\Gamma_c^2 \rho_w c^2 = \Gamma_c^2 (1 - \beta_{\text{rel}} \beta_c)^2 \left(\frac{L_{\text{rel}}}{4\pi r^2} \right) \simeq \frac{1}{\Gamma_c^2 (1 + \beta_c)^2} \left(\frac{L_{\text{rel}}}{4\pi r^2} \right). \quad (20)$$

We will separate our treatment of the deceleration of the contact from the acceleration of the relativistic outflow closer to the engine, and focus on the regime $\Gamma_{\text{rel}} = (1 - \beta_{\text{rel}}^2)^{-1/2} \gg \Gamma_c$. It should be kept in mind that, in the specific case of a breakout jet from a Wolf-Rayet star, the seed thermal photons are able to push the baryons and entrained magnetic field to a limiting Lorentz factor (12) that is close to the values of Γ_c derived below. Continuing dissipation of the magnetic field combined with pair creation could push the particles to yet higher speeds (e.g. Drenkhahn & Spruit 2002); but the observed correlation between peak energy and isotropic gamma-ray burst energy (Amati et al. 2002; Lamb et al. 2005) suggests that this dissipation is not energetically important in between the photosphere of the Wolf-Rayet star and the gamma-ray photosphere at $\sim 10^{14} \text{ cm}$ (eq. [48]). We therefore approximate

³ This expression holds if the relativistic outflow and the ambient medium are both cold and particle-dominated in their respective rest frames. This condition will be approximately satisfied in the ambient medium even after it is loaded with electron-positron pairs and pre-accelerated (Beloborodov 2002). The momentum balance at the reverse shock also remains similar when the relativistic outflow is magnetically dominated, as long as the Poynting flux is converted efficiently to radiation. This is plausible if the magnetic field reverses sign on a small scale (e.g. Thompson 1994; Drenkhahn & Spruit 2002).

$\Gamma_{\text{rel}} \gg \Gamma_c \gg 1$ in eq. (20), which gives the equilibrium solution

$$\Gamma_c = \Gamma_{\text{eq}} = \left(\frac{L_{\text{rel}} V_w}{4\dot{M}_w c^3} \right)^{1/4} = 35 L_{\text{rel}51}^{1/4} V_{w8}^{1/4} \dot{M}_{w-5}^{-1/4}. \quad (21)$$

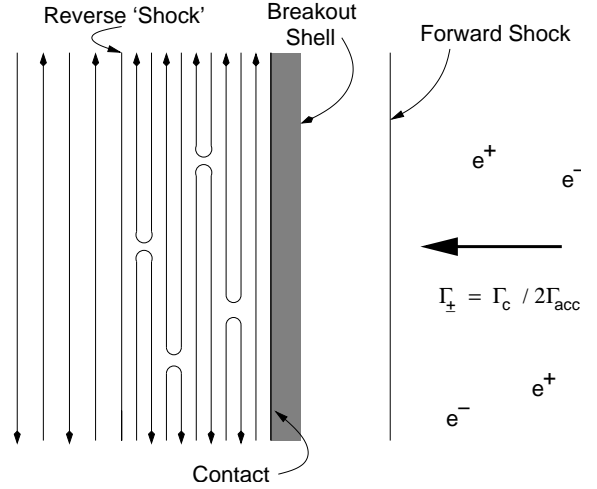


FIG. 1.— Structure of the relativistic outflow between the forward and reverse shock waves. The ambient medium is loaded with electron-positron pairs that are created by side-scattering of the gamma-ray photons. These pairs and the ions from the Wolf-Rayet wind collect in a shell behind the forward shock. In the idealized one-dimensional flow problem, this shell is separated from the shocked shell of relativistic eject by a contact discontinuity. The magnetic field that is advected across the reverse shock wave undergoes forced reconnection and tangles up. The reverse shock is, in fact, not a true shock but has a finite thickness (§5.1). The breakout shell is a thin layer of material from the Wolf-Rayet star that is advected out by the jet head, and becomes transparent at a radius $\sim 10^{14} \text{ cm}$ (§4).

This result is modified when the effects of pair loading and pre-acceleration of the Wolf-Rayet wind material are taken into account. We are interested in the regime where the wind material reaches a Lorentz factor $\Gamma_{\text{amb}} \gg 1$ (but still less than the Lorentz factor Γ_c of the contact). The Wolf-Rayet wind material is then swept up by the forward shock at a radius close to where it was sitting at the moment of the explosion. Each shell of mass ΔM_b passing through the forward shock now deposits a momentum $\Gamma_c \Gamma_{\text{amb}} (\beta_{\text{amb}} - \beta_c) (\mathcal{M}_{\pm} \Delta M_b) c \simeq -(\Gamma_c / 2\Gamma_{\text{amb}}) (\mathcal{M}_{\pm} \Delta M_b) c$ in the frame of the contact. The left-hand side of eq. (20) is therefore replaced by $(\Gamma_c^2 / 2\Gamma_{\text{amb}}) \mathcal{M}_{\pm} \rho_w c^2$, where

$$\mathcal{M}_{\pm}(\rho, n_{e^+}) = \frac{2m_e n_{e^+}}{\rho} + 1 \quad (22)$$

corrects for the inertia of the electron positron pairs (density n_{e^+}) that have been created in the ambient medium (Thompson & Madau 2000; Beloborodov 2002). The shell Lorentz factor becomes

$$\Gamma_c = (2\Gamma_{\text{amb}})^{1/4} \Gamma_{\text{eq}}. \quad (23)$$

When pre-acceleration is efficient, $\Gamma_{\text{amb}} \sim \Gamma_c / 2$, one has

$$\Gamma_c \sim \mathcal{M}_{\pm}^{-1/3} \Gamma_{\text{eq}}^{4/3} = \mathcal{M}_{\pm}^{-1/3} \left(\frac{L_{\text{rel}} V_w}{4\dot{M}_w c^3} \right)^{1/3}. \quad (24)$$

It turns out that $\mathcal{M}_{\pm} \sim 1$ except very near the beginning of the deceleration phase, and so we define a reference Lorentz factor

$$\tilde{\Gamma}_{\text{eq}} = \Gamma_{\text{eq}}^{4/3} = 1.1 \times 10^2 L_{\text{rel}51}^{1/3} V_{w8}^{1/3} \dot{M}_{w-5}^{-1/3}. \quad (25)$$

with the dependence on \mathcal{M}_\pm removed.

The baryons provide a useful set of markers for the flow: after pre-acceleration their number density is

$$n_b = \frac{\rho_w/m_p}{1-\beta_{\text{amb}}} \simeq 2\Gamma_{\text{amb}}^2 \frac{\rho_w}{m_p} \quad (\Gamma_{\text{amb}} \gg 1). \quad (26)$$

In the frame of the contact one has

$$n'_b = \Gamma_c \frac{\rho_w}{m_p} \quad (\Gamma_{\text{amb}} \gg 1). \quad (27)$$

The rate at which baryons are swept up by the contact does not depend on the speed of the ambient medium, as long as the ambient material moves only a modest distance from its starting point at the moment of the explosion. (Pre-acceleration does still alter the value of Γ_c itself and the ram pressure of the oncoming flow.)

The outflow that powers the gamma-ray emission in a long burst is concentrated⁴ within a time interval $\Delta t \sim 10$ s and therefore carries a limited energy $E_{\text{rel}} = L_{\text{rel}}\Delta t$. The energy which is swept up within a distance r from the central engine is

$$\Delta E_{\text{rel}}(r) = L_{\text{rel}} \left(\frac{r}{2\Gamma_{\text{eq}}^2 c} \right) = 2\Gamma_{\text{eq}}^2 M_w(r) c^2, \quad (28)$$

with nearly equal proportions being dissipated behind the forward and reverse shocks. We are interested in the dynamics of the outflow close enough to the engine that electrons and positrons cool rapidly. Nonetheless, the ions carry the bulk of the energy flux across the forward shock in the latter part of the prompt deceleration phase (§3.3), and do not cool effectively by simple incoherent processes. About $\frac{1}{2}$ of the outflow energy is therefore converted to radiation, and a fraction $\varepsilon_+ \sim \frac{1}{4}$ is transported by radiation across the forward shock,

$$\Delta E_+ = \varepsilon_+ \Delta E_{\text{rel}}. \quad (29)$$

Above a critical value of the compactness

$$\ell_+ = \frac{\sigma_T \Delta E_+}{4\pi r^2 m_e c^2} = \left(\frac{\varepsilon_+}{2\Gamma_c^2} \right) \frac{\sigma_T L_{\text{rel}}}{4\pi r m_e c^3}, \quad (30)$$

the exterior medium is loaded with electron positron pairs and accelerated to a high Lorentz factor comparable to Γ_{eq} (Thompson & Madau 2000). This critical compactness is $\ell_{\text{crit}} \sim 100$ when the gamma-ray spectrum has a high energy tail that extends well above ~ 1 MeV (Beloborodov 2002). A Lorentz factor $\Gamma_{\text{amb}} \sim 10^2$ is attained at $\ell_+ \sim 10^3$. We make use of the approximate scaling

$$\Gamma_{\text{amb}} \simeq \left(\frac{\ell_+}{\ell_{\text{crit}}} \right)^2 \quad (10^2 \lesssim \ell \lesssim 10^3), \quad (31)$$

which agrees at the $\sim 20\%$ level with the results obtained by Beloborodov (2002) for incident spectra with photon energy indices -1.5 to -2 .

One can obtain the equilibrium Lorentz factor (24) in a simple way by comparing the energy ΔE_+ of the gamma-rays passing across the forward shock, with the inertia of the ambient medium. This implies a maximum Lorentz factor

$$\Gamma_{\text{amb}}(\text{max}) = \frac{\Delta E_+}{\mathcal{M}_\pm M_w(r) c^2}, \quad (32)$$

or equivalently,

$$\frac{\Gamma_{\text{amb}}(\text{max})}{\tilde{\Gamma}_{\text{eq}}} = \left(\frac{\varepsilon_+}{2\mathcal{M}_\pm} \right) \frac{L_{\text{rel}} V_w}{\Gamma_c^2 \tilde{\Gamma}_{\text{eq}} M_w c^3} = \frac{2\varepsilon_+}{\mathcal{M}_\pm} \left(\frac{\Gamma_c}{\tilde{\Gamma}_{\text{eq}}} \right)^{-2}. \quad (33)$$

⁴ We suggest in §8.5 that the end of the prompt gamma-ray burst coincides with the termination of the thermal photon pulse, due to the explosion of the Wolf-Rayet star. A broader relativistic wind may, therefore, continue to flow from the central engine after the GRB ends, but at a diminishing rate due to the decreasing mass flux onto the central black hole.

Substituting this into eq. (23), one sees that $\Gamma_c \sim \tilde{\Gamma}_{\text{eq}}$ is the largest Lorentz factor which can be maintained by a balance between momentum deposition on the two sides of the contact.

The first phase of deceleration corresponds to the passage of the reverse shock through the shell. We now show that this occurs before pre-acceleration becomes ineffective. The prompt emission of gamma rays is therefore directly tied to the end of pair loading of the ambient medium.

The beginning of deceleration can be identified with the radius $R_{\text{decel-}}$ at which the ambient medium can no longer be pushed to a Lorentz factor $\Gamma_{\text{amb}} = \frac{1}{2}\tilde{\Gamma}_{\text{eq}}$ before hitting the forward shock. The corresponding compactness is (eq. [31])

$$\ell_+(R_{\text{decel-}}) \simeq \left(\frac{\tilde{\Gamma}_{\text{eq}}}{2} \right)^{1/2} \ell_{\text{crit}}. \quad (34)$$

Expressing ℓ_+ in terms of $\tilde{\Gamma}_{\text{eq}}$ using eq. (30) gives

$$R_{\text{decel-}} = 1.1 \times 10^{14} \varepsilon_+ L_{\text{rel}51}^{1/6} \dot{M}_{w-5}^{5/6} V_{w8}^{-5/6} \text{ cm}. \quad (35)$$

Outside this radius,

$$\Gamma_c(r) = \tilde{\Gamma}_{\text{eq}} \left(\frac{r}{R_{\text{decel-}}} \right)^{-1/4} \quad (r > R_{\text{decel-}}). \quad (36)$$

The prompt phase of deceleration is complete when $\int (2\Gamma_c^2)^{-1} dr = r/3\Gamma_c^2 = c\Delta t$, which occurs at a radius

$$\frac{R_{\text{decel+}}}{R_{\text{decel-}}} = \left(\frac{3\tilde{\Gamma}_{\text{eq}}^2 c\Delta t}{R_{\text{decel-}}} \right)^{2/3} = 20 \varepsilon_+^{-2/3} L_{\text{rel}51}^{1/3} \dot{M}_{w-5}^{-1} V_{w8} \Delta t_1^{2/3}, \quad (37)$$

or, equivalently, at

$$R_{\text{decel+}} = 2.5 \times 10^{15} \varepsilon_+^{1/3} L_{\text{rel}51}^{1/2} \dot{M}_{w-5}^{-1/6} V_{w8}^{1/6} \Delta t_1^{2/3} \text{ cm}. \quad (38)$$

Notice that $R_{\text{decel+}}$ depends more strongly on the relativistic outflow parameters (L_{rel} , Δt) than it does on the pre-burst wind parameters. At this point, the Lorentz factor of the contact has dropped to

$$\Gamma_c(R_{\text{decel+}}) = 53 \varepsilon_+^{1/6} L_{\text{rel}51}^{1/4} \dot{M}_{w-5}^{-1/12} V_{w8}^{1/12} \Delta t_1^{-1/6}, \quad (39)$$

and the Lorentz factor of the ambient material to

$$\Gamma_{\text{amb}} = 2.7 \varepsilon_+^{2/3} \dot{M}_{w-5}^{2/3} V_{w8}^{-2/3} \Delta t_1^{-2/3}. \quad (40)$$

Pre-acceleration has the smallest effect on deceleration for low values of \dot{M}_w and large burst durations Δt . One can compare eq. (38) with the deceleration radius of a relativistic shell propagating in a static external medium. Setting $c\Delta t = r/2\Gamma_{\text{eq}}^2$ gives

$$R_{\text{decel}} = \left(\frac{L_{\text{rel}} \Delta t^2 V_w}{\dot{M}_w c} \right)^{1/2} = 7 \times 10^{14} L_{\text{rel}51}^{1/2} \Delta t_1 \dot{M}_{w-5}^{-1/2} V_{w8}^{1/2} \text{ cm}. \quad (41)$$

The relativistic motion of the external medium has died away before the reverse shock completes its passage through the shell if

$$\Delta t_1 \dot{M}_{w-5}^{-1} V_{w8}^{-1} \gtrsim 12 \varepsilon_+. \quad (42)$$

(The coefficient the right side of this equation is obtained by substituting $\ell_+ = \ell_{\text{crit}}$ and $r = 2\Gamma_{\text{eq}}^2 c\Delta t$ in eq. [30].)

It has been suggested that, close enough to the central engine, collimation of the emitted gamma-ray shell (outside the emission radius) would allow the ambient medium to be accelerated to a Lorentz factor higher than Γ_c (Beloborodov 2002). This requires the compactness ℓ_+ of the photons escaping across the forward shock to exceed the minimum compactness that is needed to push the ambient medium to a Lorentz factor $\gtrsim \Gamma_c$. The further collimation of the photons outside the emitting radius would then allow the ambient material to ‘surf’ to a higher Lorentz factor, so that it detaches from the ejecta. This phenomenon can, indeed, be expected if the source is not surrounded by a dense wind and the pair-loaded medium has a small optical depth. But in the present context, the emission of gamma-rays cannot be decoupled from the pre-acceleration process: the optical depth of the pairs swept up from the Wolf-Rayet wind is larger than unity at $r \lesssim R_{\text{decel-}}$, and the gamma-ray photons escaping across the forward shock are in fact trapped in the pair cloud that they create (§3.3).

3.2. Compactness and Speed of Cooling

At this point, we can check our assumption that heat electrons and positrons will cool rapidly after passing through the forward and reverse shocks. Transforming to the frame of the contact, and taking the radiation to be isotropic in this frame, the energy radiated is $\Delta E'_{\text{rel}} = (3/4\Gamma_c)\Delta E_{\text{rel}}$. The radiation compactness is then

$$\ell'(r) = \frac{\sigma_T \Delta E'_{\text{rel}}(r)}{4\pi r^2 m_e c^2}. \quad (43)$$

It is related to the compactness ℓ_+ of the radiation field outside the forward shock by

$$\ell' = \frac{3}{4\Gamma_c \varepsilon_+} \ell_+. \quad (44)$$

when the emission is isotropic in the bulk frame. The critical value of ℓ_+ for pair loading and pre-acceleration is significantly greater than unity (Beloborodov 2002), and so one sees that ℓ' itself is not much greater than unity in the frame of the flow. After substituting for $\Delta E'_{\text{rel}}$ and then for Γ_c using eq. (36), we have

$$\begin{aligned} \ell'(r) &= 0.5 \frac{\ell_{\text{crit}}}{\varepsilon_+ \tilde{\Gamma}_{\text{eq}}^{1/2}} \left(\frac{r}{R_{\text{decel-}}} \right)^{-1/4} \\ &= 4.7 \frac{\dot{M}_{w-5}^{1/6}}{\varepsilon_+ L_{\text{rel}51}^{1/6} V_{w8}^{1/6}} \left(\frac{r}{R_{\text{decel-}}} \right)^{-1/4} \quad (r > R_{\text{decel-}}). \end{aligned} \quad (45)$$

At the final deceleration radius $R_{\text{decel+}}$, we have

$$\ell'(R_{\text{decel+}}) = 2.3 \varepsilon_+^{-5/6} L_{\text{rel}51}^{-1/4} \dot{M}_{w-5}^{5/12} V_{w8}^{-5/12} \Delta t_1^{-1/6}, \quad (46)$$

with $\varepsilon_+ \sim \frac{1}{4}$.

We see that the compactness is regulated to a characteristic value that depends weakly on the Wolf-Rayet wind luminosity and ambient density, and changes very slowly with radius. The compactness is large enough to ensure fast cooling of even mildly relativistic electrons and positrons. (The compactness is even higher in the portion the relativistic outflow that interacts with the fragmenting ‘breakout’ shell; §4.) This has important implications for the prompt gamma-ray spectrum, which we turn to in the following section.

3.3. Scattering Depth and Energy of the Swept-up Pairs

The scattering optical depth between the reverse and forward shocks receives a significant contribution from electrons and positrons that are swept up from the ambient medium. This depth $\tau_{\pm \text{amb}}$ is regulated to a value close to unity, for the same reason that the radiative compactness is regulated.

It is useful first to relate the deceleration radius to the radius $R_{\tau=1}$ at which the electrons in the pre-burst wind ($Y_e \simeq \frac{1}{2}$) provide unit scattering depth,

$$R_{\tau=1} = \frac{Y_e \sigma_T \dot{M}_w}{4\pi m_p V_w} = 1.0 \times 10^{11} \dot{M}_{w-5} V_{w8}^{-1} \text{ cm}. \quad (47)$$

When this inertia of the wind becomes dominated by electron-positron pairs, the scattering photosphere increases significantly, to

$$R_{\tau=1}^{\pm} \sim \left(\frac{m_p}{Y_e m_e} \right) R_{\tau=1} = 3.7 \times 10^{14} \dot{M}_{w-5} V_{w8}^{-1} \text{ cm} \quad (48)$$

during the first stages of deceleration. Comparing this rescaled photospheric radius with the deceleration radius, one has

$$\frac{R_{\text{decel-}}}{R_{\tau=1}^{\pm}} = 1.4 \frac{\varepsilon_+ \tilde{\Gamma}_{\text{eq}}^{1/2}}{\ell_{\text{crit}}} = 0.15 \varepsilon_+ \left(\frac{L_{\text{rel}51} V_{w8}}{\dot{M}_{w-5}} \right)^{1/6}. \quad (49)$$

One sees that the pairs swept up from the ambient wind provide $\tau_{\pm \text{amb}} \sim 3-10$ at $r \sim R_{\text{decel-}}$. The optical depth is even larger closer to the central engine. Pre-acceleration of the ambient medium is in fact suppressed inside a radius $\sim R_{\text{decel-}}$.

Further out in the flow,

$$\tau_{\pm \text{amb}}(r) = (\mathcal{M}_{\pm} - 1) \left(\frac{r}{R_{\tau=1}^{\pm}} \right)^{-1}. \quad (50)$$

Substituting for $R_{\text{decel-}}$ using eq. (47), one has

$$\tau_{\pm \text{amb}}(r) = 3.3 \frac{\mathcal{M}_{\pm} - 1}{\varepsilon_+} \left(\frac{\dot{M}_{w-5}}{L_{\text{rel}51} V_{w8}} \right)^{1/6} \left(\frac{r}{R_{\text{decel-}}} \right)^{-1}. \quad (51)$$

The further evolution of the scattering depth depends on the evolution of the pair loading factor $\mathcal{M}_{\pm} - 1$. One has (Beloborodov 2002)

$$\mathcal{M}_{\pm} - 1 \simeq 0.1 \left(\frac{\ell_+}{\ell_{\text{crit}}} \right). \quad (52)$$

The compactness is given by eq. (34) at the beginning of deceleration, which implies $\mathcal{M}_{\pm} - 1 = O(1)$. Further out in the flow one has

$$\mathcal{M}_{\pm} - 1 \simeq \left(\frac{r}{R_{\text{decel-}}} \right)^{-1/2}. \quad (53)$$

The scattering depth accumulated from the freshly swept-up pairs therefore decreases with radius as $\tau_{\pm \text{amb}} \propto r^{-3/2}$ outside $r = R_{\text{decel-}}$. It drops below unity before the end of the prompt deceleration phase, and reaches the value

$$\tau_{\pm \text{amb}}(R_{\text{decel+}}) = 0.1 L_{\text{rel}51}^{-2/3} \dot{M}_{w-5}^{5/3} V_{w8}^{-5/3} \Delta t_1^{-1}, \quad (54)$$

when the reverse shock has passed through the ejecta shell.

The optical depth that a gamma-ray photon sees ahead of the forward shock (denoted by $\tau_{\pm \text{ex}}$) is significantly smaller than $\tau_{\pm \text{amb}}$, because the ambient material advances only a small distance beyond its initial radius r_0 before being intercepted by the forward shock. The wind material accelerates as it drifts back through the photon shell. The shell of radiation moving ahead of the shock at radius $r \geq R_{\text{decel-}}$ has, from eqs. (30) and (34), a compactness

$$\frac{\ell_+}{\ell_{\text{crit}}} = \left(\frac{\tilde{\Gamma}_{\text{eq}}}{2} \right)^{1/2} \left(\frac{r}{R_{\text{decel-}}} \right)^{-1/2} \quad (55)$$

and a width $\Delta r = r/3\Gamma_c^2$. Having intercepted a radiation shell of compactness $\ell \leq \ell_+$, the Lorentz factor of the wind material is

$$\Gamma_{\text{amb}}(\ell, r) = \left(\frac{\ell}{\ell_+}\right)^2 \Gamma_{\text{amb}}(r) = \frac{1}{2} \tilde{\Gamma}_{\text{eq}} \left(\frac{\ell}{\ell_+}\right)^2 \left(\frac{r}{R_{\text{decel-}}}\right)^{-1}. \quad (56)$$

Starting at a radius r_0 , the wind material advances a distance

$$\begin{aligned} \frac{r-r_0}{r} &= \frac{\Delta r}{r} \int \frac{d\ell}{\ell_+} 2\Gamma_{\text{amb}}^2(\ell, r) \\ &= \frac{2}{15} \left(\frac{\Gamma_{\text{amb}}}{\Gamma_c}\right)^2 = \frac{1}{30} \left(\frac{r}{R_{\text{decel-}}}\right)^{-3/2}. \end{aligned} \quad (57)$$

The scattering depth seen by a gamma-ray photon moving ahead of the forward shock is, then,

$$\tau_{\pm \text{ex}} \simeq \left(\frac{r-r_0}{r}\right) \tau_{\pm \text{amb}} = 0.1 \varepsilon_+^{-1} \left(\frac{\dot{M}_w - 5}{L_{\text{rel}51} V_w 8}\right)^{1/6} \left(\frac{r}{R_{\text{decel-}}}\right)^{-3}. \quad (58)$$

One sees that the photons moving ahead of the ejecta shell are trapped inside a radius $\sim R_{\text{decel-}}$. This brings us to the regime assumed by Thompson & Madau (2000), where the mean inertia per scattering charge behind the forward shock is $\sim (0.1-1)m_e$. Since the compactness of the radiation emitted at $r > R_{\text{decel-}}$ is too small to push the ambient medium up to the speed of the contact, we conclude that there is never any detachment between the pair-loaded wind material and the ejecta shell.

Finally, let us calculate the characteristic Lorentz factor of the pairs which are swept back across the forward shock. This is

$$\Gamma_{\pm} = \frac{\Gamma_c}{2\Gamma_{\text{amb}}} = \left(\frac{\Gamma_c}{\tilde{\Gamma}_{\text{eq}}}\right)^{-3} = \left(\frac{r}{R_{\text{decel-}}}\right)^{3/4}. \quad (59)$$

During the last stages of the prompt deceleration, one has $\Gamma_{\pm} \sim 10$ (as may be seen by substituting eq. [37] into eq. [59]). The cooling time of these particles is substantially shorter than the flow time, by a factor $1/\ell'\Gamma_{\pm}$.

Additional pairs are created when gamma-ray photons are upscattered above the pair-creation threshold at the forward shock, but the effect is only modest. For example, photons of a bulk-frame energy $\sim m_e c^2$ have an optical depth ~ 1 to pair creation at radius $R_{\text{decel+}}$ (§7.2). If a power-law electron/positron tail, $dN/d\gamma_e \propto \gamma_e^{-2}$, is generated at the forward shock over the range of energies $\Gamma_{\pm} \lesssim \gamma_e \lesssim \gamma_{e \text{max}}$, then the increase in optical depth is $\Delta\tau_{\pm \text{amb}}/\tau_{\pm \text{amb}} \sim 2/\ln \gamma_{e \text{max}}$. Pairs will also be created in the region behind the contact, as a direct consequence of the gamma-ray emission. Some important subtleties which influence the pair-creation rate, associated with beaming and the inertia of the breakout shell, are addressed in §7.2.

4. BARYON SHEATH FROM JET BREAKOUT

We have, so far, treated the interaction of the relativistic outflow with the Wolf-Rayet wind under the assumption that the outflow emerges with only a minimal baryon contamination. The jet head must expand sub-relativistically deep in the envelope of the star (Matzner 2003), but a thin outer shell of stellar material can be accelerated to relativistic speeds. The existing analytic treatment of jet breakout (Waxman & Mészáros 2003) is one-dimensional and does not address the sideways slippage of the shocked stellar material at the head of the jet. We now give a simple estimate of the residual column Σ_* of stellar material that survives sideways slippage away from the jet head,

and compare this with the column of material that is swept up from the Wolf-Rayet wind (Fig. 2).

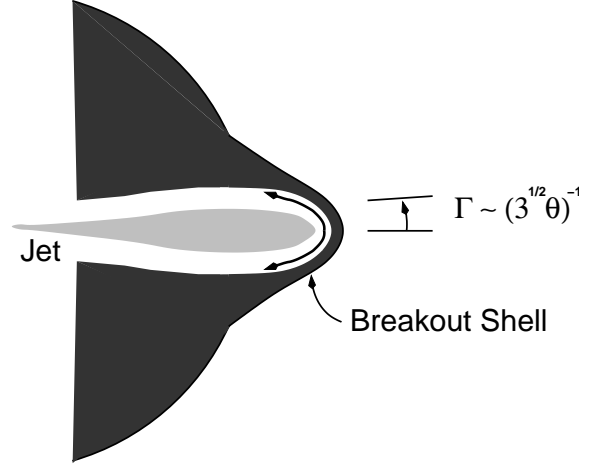


FIG. 2.— As the jet emerges from the star, the jet head accelerates to a Lorentz factor $\Gamma \gtrsim 1/\sqrt{3}\theta$. A residual shell of Wolf-Rayet envelope material becomes stuck at the jet head, and cannot flow to the side and out of the path of the relativistic outflow. This ‘breakout shell’ is optically thick close to the star, and is subject to Rayleigh-Taylor instabilities when it begins to cool at $\sim 10^{14}$ cm.

The forward shock wave accelerates close to the speed of light as it approaches the photosphere of the star (Tan, Matzner, & McKee 2001). Beyond this point, the sound speed of the shocked stellar material is $c_s \simeq c/\sqrt{3}$. The material in this shocked shell can flow a distance $\sim c_s t'$ transverse to the jet axis in the time $t' \sim r/\Gamma c$ that it takes the jet head to cross a radius r at Lorentz factor Γ . The material will therefore be lost from the jet head if $\Gamma \lesssim 1/\sqrt{3}\theta$, where θ is the opening angle. To simplify matters, we refer to the isotropic jet luminosity L_{iso} , and do not separate out the energy fluxes in thermal radiation, magnetic field, and baryons. We denote by $\Delta M_* = 4\pi R_*^2 \Sigma_*$ the equivalent spherical mass of stellar material riding at the head of the jet. This shell intercepts an energy $L_{\text{iso}}(f r/\Gamma^2 c)$ from the jet, where the coefficient f must be determined self-consistently from the dependence of Γ on radius. Neglecting radiative losses (the shell is initially optically thick) its Lorentz factor is

$$\Gamma^3 = f \frac{L_{\text{iso}} r}{\Delta M_* c^3}. \quad (60)$$

This gives $\Gamma \propto r^{1/3}$ and $f = \frac{3}{2}$. The proportion of the relativistic outflow which has been swept up by the shell grows slowly with radius; its thickness is

$$\Delta r = \frac{3}{2\Gamma^2} r. \quad (61)$$

Setting $\Gamma = 1/\sqrt{3}\theta$ at $r = R_*$, and making use of relation (6), we obtain

$$\frac{\Delta M_* c^2}{L_{\text{iso}} \Delta t} = \frac{3^{5/2} R_*}{2c \Delta t} \theta^3 = 0.016 L_{\text{iso}51}^{-3/2} \Delta t_1^{-5/2} \left(\frac{R_*}{2 \times 10^{10} \text{ cm}}\right). \quad (62)$$

The shell continues to accelerate as it intercepts further energy from the relativistic jet, so that

$$\Gamma \simeq \frac{1}{\sqrt{3}\theta} \left(\frac{r}{R_*}\right)^{1/3} = 1.8 L_{\text{iso}51}^{1/2} \Delta t_1^{1/2} \left(\frac{r}{R_*}\right)^{1/3}. \quad (63)$$

The reverse shock reaches the back of the ejecta ($\Delta r = c\Delta t$) at a radius

$$R_{\text{decel}}(\text{shell}) = 7 \times 10^{14} L_{\text{iso}51}^3 \Delta t_1^6 \left(\frac{R_*}{2 \times 10^{10} \text{ cm}} \right)^{-2} \text{ cm.} \quad (64)$$

Referring to expression (38) for $R_{\text{decel}+}$ (the deceleration radius in the absence of a breakout shell), one sees that the inertia of the shell will speed up the passage of the reverse shock through the relativistic wind. Indeed, the shell mass ΔM_* remains larger than the mass (19) of the swept-up Wolf-Rayet wind out to the radius

$$3 \times 10^{16} L_{\text{iso}51}^{-1/2} \Delta t_1^{-3/2} \dot{M}_{w-5}^{-1} V_{w8} \left(\frac{R_*}{2 \times 10^{10} \text{ cm}} \right) \text{ cm.} \quad (65)$$

It should be noted that the normalization of R_{decel} is very sensitive to the normalization of eq. (63), scaling as $R_{\text{decel}} \propto [\Gamma(R_*)]^6$. If, for example, one replaces $c_s = c/\sqrt{3}$ with c when evaluating the width of the jet, then R_{decel} grows by a factor ~ 30 .

It is clear from the above that Rayleigh-Taylor instabilities of the breakout shell can strongly modulate the gamma-ray emission at larger radii. A homogeneous shell would become transparent to photons at the radius

$$R_{\tau=1}(\text{shell}) = 8 \times 10^{13} Y_e^{1/2} L_{\text{iso}51}^{-1/4} \Delta t_1^{-3/4} \left(\frac{R_*}{2 \times 10^{10} \text{ cm}} \right)^{1/2} \text{ cm} \quad (66)$$

where $Y_e \sigma_T \Delta M_* / 4\pi r^2 m_p = 1$. Here $Y_e \simeq \frac{1}{2}$ is number of electrons per baryon in the outer layers of the Wolf-Rayet star. Before the breakout shell becomes optically thin, the particles and photons will thermalize at a low temperature. The effective temperature at the radius $R_{\tau=1}$ is given by

$$\frac{4}{3} [\Gamma(R_{\tau=1})]^2 a T_{\text{eff}}'^4 = \frac{L_{\text{iso}}}{4\pi R_{\tau=1}^2 c}. \quad (67)$$

Making use of eq. (63) to evaluate $\Gamma(R_{\tau=1})$, one finds a temperature

$$T_{\text{eff}} = \frac{4}{3} \Gamma(R_{\tau=1}) T_{\text{eff}}' = 1.8 L_{\text{iso}51}^{7/12} \Delta t_1^{1/2} \left(\frac{R_*}{2 \times 10^{10} \text{ cm}} \right)^{-1/3} \text{ keV} \quad (68)$$

in the frame of the central engine.

The pressure of the breakout shell is dominated by photons while it is optically thick. The shell therefore becomes much thinner as it expands, and it becomes subject to a corrugation instability, as we detail in §5.4. The thickness of a plume which emerges at radius r has a characteristic angular width $\delta\theta(r) \lesssim 1/\Gamma(r)$. The (isotropic) mass of baryons that is collected by such a newly formed plume is lower than ΔM_* , but only by a numerical factor ε_M . Relativistic fluid that catches up with the shell at later times will continue to flow through this opening, and the radius R_{decel} will expand by a factor ε_M^2 . This process can be expected to repeat itself on a smaller angular scale after Γ has grown by one e-folding (that is, after the breakout shell has expanded a decade or so in radius beyond the transparency radius [66]).

The last generation of Rayleigh-Taylor plumes may therefore be clean enough that the final passage of the reverse shock through the relativistic shell follows our previous analysis. The peak Lorentz factor of the contact does not, however, attain the equilibrium value $\tilde{\Gamma}_{\text{eq}}$ (eq. [24]) in this case. To find the peak

Lorentz factor of the shell, we equate expressions (36) and (63). The corresponding radius sits between $R_{\text{decel}-}$ (the beginning of deceleration assuming no breakout shell; eq. [35]) and $R_{\text{decel}+}$ (eq. [38]). One obtains

$$\Gamma_{\text{max}} = 66 L_{\text{iso}51}^{3/7} \Delta t_1^{3/14} \varepsilon_+^{1/7} \dot{M}_{w-5}^{-1/14} V_{w8}^{1/14} \left(\frac{R_*}{2 \times 10^{10} \text{ cm}} \right)^{-1/7}, \quad (69)$$

at the radius⁵

$$R_{\Gamma_{\text{max}}} = 1 \times 10^{15} \frac{\varepsilon_+^{3/7} V_{w8}^{3/14}}{L_{\text{iso}51}^{3/14} \Delta t_1^{6/7} \dot{M}_{w-5}^{3/14}} \left(\frac{R_*}{2 \times 10^{10} \text{ cm}} \right)^{4/7} \text{ cm.} \quad (70)$$

The compactness of the outflow in the bulk frame can be obtained by substituting these expressions for Γ_{max} and $R_{\Gamma_{\text{max}}}$ into eq. (43),

$$\ell'(R_{\Gamma_{\text{max}}}) = 9 L_{\text{iso}51}^{-1/14} \Delta t_1^{3/14} \varepsilon_+^{-6/7} \dot{M}_{w-5}^{3/7} V_{w8}^{-3/7} \left(\frac{R_*}{2 \times 10^{10} \text{ cm}} \right)^{-1/7}. \quad (71)$$

Note the very weak dependence of the compactness on the energy of the relativistic outflow. The compactness at smaller radii is

$$\frac{\ell'(r)}{\ell'(R_{\Gamma_{\text{max}}})} = \left(\frac{\Gamma}{\Gamma_{\text{max}}} \right)^{-3} \left(\frac{r}{R_{\Gamma_{\text{max}}}} \right)^{-1} = \left(\frac{r}{R_{\Gamma_{\text{max}}}} \right)^{-2}. \quad (72)$$

5. DYNAMICS OF THE MAGNETIC FIELD NEAR THE CONTACT DISCONTINUITY

There are several reasons to expect that the magnetic field will contribute a significant fraction of the pressure between the contact discontinuity and the reverse shock. First, most of the particle pressure behind the contact is supplied by electrons and positrons (§7.2) which lose energy rapidly to cooling. Second, simulations of relativistic jets show that magnetic and kinetic pressures remain in approximate equipartition out a large distance from the engine (McKinney 2005a,b). Third, the magnetic pressure increases by an order of magnitude across a reverse shock that is only weakly magnetized (Kennel & Coroniti 1984; Zhang & Kobayashi 2005). One caveat here is that strong pulsations in the outflow can force a reduction in σ at a large radius: after the individual pulses spread and merge, the ratio of L_P to $M_b c^2$ drops by a factor of the pulse duty cycle.

We found that the energy density in the relativistic outflow is approximately independent of its luminosity at the point where the reverse shock has completed its passage through the ejecta shell (when the inertia of the swept up material is dominated by the Wolf-Rayet wind). This result follows from the scaling $R_{\text{decel}+} \propto L_{\text{rel}}^{1/2}$ in equation (38). Setting the Poynting flux carried by a toroidal magnetic field B equal to a fraction ε_B of the wind energy flux gives

$$\frac{B^2}{4\pi} = \varepsilon_B \frac{L_{\text{rel}}}{4\pi r^2 c}. \quad (73)$$

There is a characteristic magnetic field in the outflow,

$$B = 1 \times 10^5 \frac{\varepsilon_B^{1/2} \dot{M}_{w-5}^{1/6}}{\varepsilon_+^{1/3} V_{w8}^{1/6} \Delta t_1^{2/3}} \text{ G}, \quad (74)$$

in the frame of the central engine. This field is independent of L_{rel} , and depends only weakly on \dot{M}_w and V_w . (The field in the

⁵ It should be recalled that our derivation assumes that the relativistic outflow moves at $\Gamma_{\text{rel}} \gg \Gamma_c$. In fact, Γ_{max} is close to the maximum jet Lorentz factor (12) derived previously. This approximation has the effect of reducing Γ_{max} by 10-20%.

bulk frame is weaker by a factor $\sim \Gamma_c^{-1}$.) The synchrotron energy of a relativistic electron gyrating with a Lorentz factor γ_e in the bulk frame is

$$E_{\text{sync}} \sim 0.3 \gamma_e^2 \frac{\hbar e B}{m_e c} = 3 \left(\frac{\gamma_e}{10^2} \right)^2 \frac{\varepsilon_B^{1/2} \dot{M}_{w-5}^{1/6}}{\varepsilon_+^{1/3} V_{w8}^{1/6} \Delta t_1^{2/3}} \text{ eV} \quad (75)$$

(as measured by the observer).

5.1. Reverse Shock Wave in an Outflow with a Stochastic Magnetic Field

We now examine the significant changes to the structure of the reverse shock that can result from an advected magnetic field. The fast-mode speed in the fluid upstream of the reverse shock can be approximated by the cold fluid formula,

$$\frac{V'_F}{c} = \frac{B'}{[4\pi\rho'c^2 + (B')^2]^{1/2}} = \left(1 + \frac{1}{2\sigma} \right)^{1/2}. \quad (76)$$

(The fast mode is nearly isotropic in this regime.) Here $\rho' = \rho'_i c^2 + n'_\pm m_e c^2$ is the total particle rest energy density in the bulk frame, ρ'_i is the proper rest density of ions, $n'_\pm = n'_{e^-} + n'_{e^+}$ is the proper density of electrons and positrons, and

$$\sigma = \frac{(B')^2}{8\pi\rho'c^2} = \frac{\varepsilon'_B}{1 - \varepsilon'_B}. \quad (77)$$

As previously, ε'_B is the fraction of the energy in the magnetic field in the bulk frame. Transforming to a relativistically moving frame,⁶ the ratio of Poynting flux to (cold) kinetic energy flux is 2σ .

It is possible for V'_F to exceed the speed of the relativistic outflow with respect to the contact, so that a reverse shock wave does not form (Lyutikov & Blandford 2003). The external medium will, instead, transmit momentum to the outflow through a gradual compressive disturbance. This happens if

$$\frac{\Gamma_{\text{rel}}}{2\Gamma_c} < \frac{1}{[1 - (V'_F)^2/c^2]^{1/2}} = (1 + 2\sigma)^{1/2}. \quad (78)$$

We have seen that Γ_{rel} (eq. [12]) and Γ_c (eqs. [36], [63], [69]) may be comparable in the deceleration zone at $\sim 10^{14} - 10^{15}$ cm. This means that σ does not have to be much greater than unity for the reverse shock to be suppressed in an outflow with an ordered toroidal magnetic field.

It should be emphasized that the wave speed (76) applies to disturbances propagating in a *uniform* magnetofluid. The response of the fluid to compression is altered substantially if the field undergoes high-frequency reversals, over a distance much smaller than $c\Delta t$. Stochasticity in the dynamo operating in the central engine will produce flips in the sign of the field that drives the outflow. Some further tangling of this field can occur as the jet pushes out through the envelope of the Wolf-Rayet star (§2). The weakened magnetic field is swept outward by the jet beyond the stellar photosphere. Starting in a disordered state, the field remains disordered in the bulk frame as long as Γ_{rel} continues to increase linearly with radius. That is, the two non-radial components B'_ϕ and B'_θ are comparable in magnitude and

$$B_\phi'^2 + B_\theta'^2 \sim \frac{1}{\Gamma_{\text{rel}}^2} \left(\frac{r}{R_*} \right)^2 B_r^2. \quad (79)$$

The field becomes predominantly non-radial in the bulk frame after the fluid Lorentz factor stops growing (e.g. after Γ_{rel} saturates at the value [12]).

The deceleration of the outflow involves a compression of the fluid on a scale $\sim c\Delta t$, much larger than the field reversal scale. The reversing field is susceptible to reconnection and tangling upon compression (Thompson 1994). After tangling, the fluid becomes more nearly isotropic and its sound speed closer to $c/\sqrt{3}$. This makes a crucial difference to the propagation of signals in the outflow. In this situation, the equation of state varies smoothly over a macroscopic distance within the magnetofluid. A localized jump in density can therefore appear if the flow speed is higher than $\sim c/\sqrt{3}$ upstream of the contact.

In the GRB emission model discussed in this paper, the plasma is pair-rich and the mean energy per particle is a modest multiple of $m_e c^2$. A fluid approach is therefore appropriate to the dynamics of the electromagnetic field and the entrained particles. This contrasts with a pulsar wind, where the rest energy of the particles comprises a much smaller fraction of the total wind energy. In that case, the mean Larmor radius of the particles in a neutral sheet can approach the sheet thickness, thereby facilitating reconnection. Lyubarsky (2003) has argued that the reversing component of the magnetic field will be erased at the reverse shock in a pulsar wind, so that the shock jump condition is equivalent to that of a flow containing only the mean magnetic field.

We now consider the thickness of such a mock shock, in the case where the sign of the non-radial magnetic field varies stochastically on a scale $\Delta r'_B$ (as the result of a dynamo process in the central engine; §2.1). The mean flux density averaged over a radial scale $\Delta r' \gg \Delta r'_B$ is $\langle B' \rangle \simeq (2L_p/\Gamma_c^2 r^2 c)^{1/2} (\Delta r'/\Delta r'_B)^{-1/2}$. The magnetization parameter associated with the smoothed magnetic field is

$$\langle \sigma \rangle \simeq \frac{\langle B' \rangle^2}{8\pi\rho'c^2} \simeq \left(\frac{\Delta r'}{\Delta r'_B} \right)^{-1}. \quad (80)$$

In this situation, the radially-averaged magnetic field decays much more slowly with smoothing length than it would in a pulsar wind, where the field structure is nearly periodic (e.g. Coroniti 1990). A reduction in σ from a value ~ 1 down to ~ 0.03 takes place over a lengthscale $\Delta r \sim 30 \Delta r_B = 3(\Delta r_B/0.1 \text{ s})$ light seconds. The degree of compression at the reverse shock will therefore depend in a non-trivial way on the dynamo timescale in the engine, relative to the duration of the burst. The case where the reverse shock is spread out over a lengthscale comparable to the thickness of the prompt ejecta shell deserves examination, but will not be addressed in this paper.

This model of a shock in a flow with a reversing magnetic field implies several modifications of the mechanism of first-order shock acceleration that is commonly employed in GRB emission models. First, the heating of even mildly relativistic particles is de-localized. A distribution of particle energies will result from the finite rate of creation of electron-positron pairs per unit volume (§8.1). Second, this means that rapid Compton cooling can significantly suppress the upper bound on the particle energy behind the shock, in comparison with a fast heating mechanism such as shock acceleration or resonant absorption of ion cyclotron waves by positrons. And, third, the heated light charges are not isotropic, being electrostatically accelerated along the background magnetic field (§6).

Even when a standard magnetosonic shock can form, its compression is significantly weaker at large σ than it would

⁶ A number of authors use σ to denote the ratio of Poynting and kinetic energy fluxes in the frame of the star (e.g. Kennel & Coroniti 1984; Drenkhahn & Spruit 2002), but we are more concerned here with the properties of the magnetofluid in the bulk frame.

be in a cold fluid without magnetic field. Strong compression is essential for the formation of a hard particle spectrum by first-order Fermi acceleration (Blandford & Eichler 1987). The Lorentz factor behind a static shock is $\Gamma_{ps} \simeq (2\sigma)^{1/2}$ when the magnetic field runs parallel to the shock. The field is only compressed by a factor $1 + (4\sigma)^{-1}$ (Kennel & Coroniti 1984). The compression ratio is essentially unaltered at small σ – but only if $\sigma \lesssim 0.05$, that is, if the energy carried by the magnetic field is less than $\sim 10\%$ of the kinetic energy of the entrained baryons. In particular, the value of σ estimated in eq. (2) is large enough that the magnetic field will have a significant softening effect on the particle spectrum generated by shock acceleration.

Calculations of the synchrotron emission from shock-accelerated pairs (Mészáros & Rees 1997; Kobayashi et al. 2005, and references therein) will, therefore, require significant modification if the magnetic field carries 10 percent or more of the energy flux. In the rest of the paper, we will generally refer to the reverse shock without qualifiers, but it should be understood that it is likely to behave quite differently than a standard shock in an ideal magnetofluid.

5.2. Shocked and Pair-Enriched Wolf-Rayet Wind

The medium in between the contact discontinuity and the forward shock contains a relatively weak magnetic field compared with the relativistic outflow. The field that is swept up from the Wolf-Rayet wind is predominantly toroidal and carries a fraction

$$\varepsilon_{B,w} = \frac{B_w^2}{8\pi\rho_w V_w^2} \quad (81)$$

of the kinetic energy density in the wind. The progenitors of GRBs must differ in some key respect from the large majority of Wolf-Rayet stars. Rapid rotation has been invoked (Woosley 1993). If the entire star rotated rapidly, then a relatively strong magnetic field would be advected into the wind. In the regime where the magnetic stresses themselves play a negligible role in driving the wind, one has $\varepsilon_{B,w} \simeq B_*^2 R_*^2 V_{rot,*}^2 / M_* V_w^3 = 10^{-2} B_{*4}^2 (R_* 10/2)^2 V_{rot,*7}^2 M_{*5}^{-1} V_{w8}^{-3}$. Here $B_* = B_{*4} \times 10^4$ G is the surface magnetic field and $V_{rot,*} = V_{rot,*7} \times 10^7$ cm s⁻¹ is the surface rotation speed of the Wolf-Rayet progenitor. (The chosen normalization of B_* corresponds to a net flux $\simeq 10^{25}$ G-cm², comparable to that threading an ordinary radio pulsar but a few orders of magnitude less than what is ultimately needed to drive a Poynting-dominated jet with a luminosity of $\sim 10^{51}$ ergs s⁻¹.)

During the last stages of prompt deceleration, the external medium develops a relativistic motion (59) with respect to the ejecta shell. The magnetic field upstream of the forward shock can be obtained by noting that both the toroidal flux density and the baryon density are compressed by the same factor (eq. [27]),

$$B'_w = \frac{n'_b}{\rho_w/m_p} B_w = \Gamma_c B_w. \quad (82)$$

This field is further compressed behind the forward shock by a factor up to 3 (when $\Gamma_{\pm} \gg 1$).

Slow cooling of the shocked ions would prevent much additional compression of the fluid behind the forward shock. We argue in §8.2 that resonant absorption of ion cyclotron waves by positrons (Hoshino et al. 1992) is not likely to prevent effective thermalization of the protons behind the shock, due to the relatively small fraction of the kinetic energy carried by the positrons.

The energy density behind the forward shock is

$$U'_w = \Gamma_{\pm} (\Gamma_c \rho_w c^2) = \left(\frac{\Gamma_c^2}{2\Gamma_{amb}} \right) \rho_w c^2 \quad (83)$$

and so the fraction of the energy density carried by the immediate post-shock field is

$$\varepsilon'_B = \frac{(3B'_w)^2/8\pi}{U'_w} = 18\Gamma_{amb}\varepsilon_{B,w} \left(\frac{V_w}{c} \right)^2 = 2 \times 10^{-4} \Gamma_{amb} \varepsilon_{B,w} V_{w8}^2. \quad (84)$$

We have found $\Gamma_{amb} \sim 2$ during the final stages of the prompt deceleration. The linearly compressed magnetic field can therefore attain a pressure in excess of 10^{-5} of the thermal pressure behind the forward shock. This is close to some estimates of the magnetic energy density from the observed optical of some GRBs (e.g. Panaitescu & Kumar 2004, and references therein).

The structure of the magnetic field in the Wolf-Rayet wind can be contrasted with that expected in the relativistic outflow. The Wolf-Rayet wind takes a year or so to flow out to the radius $R_{decel+} \sim 10^{15}$ cm (eq. [38]). Even if the progenitor supports an active dynamo, it will be located deep in the star. The magnetic field anchored at the base of the Wolf-Rayet wind is therefore likely to be fairly constant over the time the wind expands to the deceleration zone of the relativistic GRB ejecta.

It has been noted that the Weibel instability will be excited behind a relativistic shock wave that is moving into a weakly magnetized medium (Kazimura et al. 1998; Medvedev & Loeb 1999). This electromagnetic instability is generated by the two counterstreaming populations of electrons (and positrons) behind the shock, and creates strong current fluctuations on the plasma scale $\sim c/\omega_{pe}$. The instability can be modified or suppressed by a strong seed magnetic field $B'_w = \Gamma_c B_w$ if the associated electron gyrofrequency $\omega_{ce} = eB'_w/m_e c \gamma_e$ is larger than the plasma frequency $\omega_{pe} = (4\pi n'_{\pm} e^2/m_e \gamma_e)^{1/2}$ (Hededal & Nishikawa 2005). Taking $\gamma_e = \Gamma_{\pm} = \Gamma_c/2\Gamma_{amb}$ one finds

$$\frac{\omega_{ce}}{\omega_{pe}} = \left[\frac{B_w^2}{4\pi(\Gamma_c/2\Gamma_{amb})n'_{\pm} m_e c^2} \right]^{1/2} = \left(\frac{4\Gamma_{amb}\varepsilon_{B,w}}{\mathcal{M}_{\pm} - 1} \right)^{1/2} \left(\frac{V_w}{c} \right). \quad (85)$$

Substituting $(\mathcal{M}_{\pm} - 1) \sim n'_{\pm} m_e / (\Gamma_c \rho_w) \sim 0.2$ (the pairs carry 20 percent of the particle inertia) and $\Gamma_{amb} \sim 2$, this expression becomes

$$\frac{\omega_{ce}}{\omega_{pe}} \simeq 0.02 \varepsilon_{B,w}^{1/2} V_{w8}. \quad (86)$$

The pre-existing magnetic field is therefore not strong enough to suppress the Weibel instability.

Nonetheless, the small grow scale $\sim c/\omega_{pe}$ of the Weibel instability suggests that both the mean value and the r.m.s. value of the magnetic field will relax to very small values downstream of the shock, leaving the flux that is swept up from the Wolf-Rayet wind. Particle-in-cell simulations of the aftermath of the Weibel instability (Medvedev et al. 2005) have demonstrated that the coherence length of the magnetic field will grow with time; but these simulations cover only a limited dynamic range. On very long wavelengths, the smoothing out of the magnetic field is limited by the speed $V_A = B'/\sqrt{4\pi\rho'}$ with which the field can move the entrained charged particles (Gruzinov 2001). To estimate the limiting magnetic field strength, we suppose that the field has reached equipartition with the kinetic energy density of the pairs on the plasma scale

$$\ell_p \sim \left(\frac{\gamma_e m_e c^2}{4\pi e^2 n'_{\pm}} \right)^{1/2}, \quad (87)$$

namely

$$B'(\ell_p) \sim B'_{\text{eq}} = (8\pi\gamma_e n'_{\pm} m_e c^2)^{1/2}. \quad (88)$$

The conservation of magnetic flux implies that the smoothed field \bar{B}' is

$$\left[\frac{\bar{B}'(L)}{B'_{\text{eq}}} \right]^2 \simeq \left(\frac{\ell_p}{L} \right)^2 \simeq \frac{\alpha_{\text{em}} \gamma_e}{\sigma_T n_{\pm} L} \left(\frac{\hbar}{m_e c L} \right). \quad (89)$$

on a scale $L > \ell_p$. The associated Alfvén speed is $V_A(L) = \bar{B}'(L)/(4\pi\rho')^{1/2}$. Setting $L/V_A(L)$ equal to the post-shock flow time $\sim r/\Gamma c$ (as measured in the bulk frame) gives

$$\begin{aligned} \left[\frac{\bar{B}'(L)}{B'_{\text{eq}}} \right]^2 &\simeq \frac{\Gamma_{\pm} m_e c^2}{(\mathcal{M}_{\pm} - 1)^{1/2} e B'_{\text{eq}} (r/\Gamma c)} \\ &= 5 \times 10^{-13} \frac{(\Gamma_c/50)^3}{r_{15} (\mathcal{M}_{\pm} - 1)^{1/2}} \left(\frac{\Gamma_{\text{amb}}}{2} \right)^{-1} \left(\frac{\Gamma_c B'_{\text{eq}}}{10^5 \text{ G}} \right)^{-1}. \end{aligned} \quad (90)$$

This shows that the smoothed field that is left behind from the Weibel instability is weaker than the field that is swept up from the Wolf-Rayet wind (eq. [84]), even if the rate of smoothing is only $\sim 10^{-4}$ of the maximal rate V_A/L .

5.3. Feedback of Particle Cooling on Magnetic Reconnection

The type of dissipation that is triggered by magnetic reconnection requires careful clarification. In the equatorial region of a pulsar wind, it has been suggested that the reversing magnetic field will largely cancel out (Coroniti 1990). In this manner, the fluctuating component of the non-radial field may be erased whilst preserving the mean field (Rees & Gunn 1974; Lyubarsky 2003). The alternative, which we favor in a relativistic outflow with a much larger particle density, is that reconnection changes the *topology* of the magnetic field lines, so that the non-radial field is partly converted to radial field. In an expanding outflow, this allows the magnetic energy to decrease more rapidly than it otherwise would (Thompson 1994).

A minimal particle density $n_{e\text{min}} = |J_r|/ec$ is required to supply the radial electric current in an outflow carrying a toroidal magnetic field,

$$|J_r| = \frac{c}{4\pi r} \left| \frac{\partial B_{\phi}}{\partial \theta} \right| \sim \frac{(L_{\text{rel}} c)^{1/2}}{4\pi r^2}. \quad (91)$$

The actual pair density in a pulsar wind may exceed $n_{e\text{min}}$ by 4-5 orders of magnitude (e.g. Hibschan & Arons 2001). In a gamma-ray burst outflow there is generally a radius at which the Thomson depth is unity, outside of which the electrons (and pairs) are largely frozen into the flow. At this photosphere (radius $R_{\tau=1}$) one has $n_e = (\sigma_T R_{\tau=1}/2\Gamma^2)^{-1}$, and

$$\begin{aligned} \frac{n_e}{n_{e\text{min}}} &\sim \frac{8\pi e [\Gamma(R_{\tau=1})]^2 R_{\tau=1}}{\sigma_T (L_{\text{rel}}/c)^{1/2}} \\ &= 2 \times 10^6 \frac{[\Gamma(R_{\tau=1})]^2}{L_{\text{rel},51}^{1/2}} \left(\frac{R_{\tau=1}}{2 \times 10^{10} \text{ cm}} \right). \end{aligned} \quad (92)$$

In a gamma-ray burst outflow, one can also expect B_{ϕ} to switch sign on a scale $\Delta r_B \ll r$, due to the intrinsic stochasticity of the dynamo in the central engine (§5.1). The current then has a dominant component $|J_{\theta}'| \sim c B'_{\phi}/4\pi \Delta r'_B = c B_{\phi}/4\pi \Gamma^2 \Delta r_B$ in the bulk frame. Comparing $|J_{\theta}'|$ with $|J_r'| = |J_r|/\Gamma$, one sees that the minimum charge density needed to support the current

increases by a factor $\sim r/\Gamma \Delta r_B$. For realistic values of Δr_B , this factor is $\sim 3 \times 10^3 r_{15} \Gamma_2^{-1} [(\Delta r_B/c)/0.1 \text{ s}]^{-1}$, which is significantly smaller than the pre-factor in eq. (92). The charges advected by the outflow are therefore capable of maintaining the non-radial current out to a radius where photon collisions will raise the pair density above the freezeout value (§7.2).

The importance of pair creation has sometimes been forgotten when considering *macroscopic* breakdowns of MHD in gamma-ray burst outflows. For example, strong wave acceleration at the forward shock (Smolsky & Usov 1996) will be suppressed by pair creation outside the forward shock; and similarly long-wavelength electromagnetic disturbances (Lyutikov & Blackman 2001) will behave in an essentially hydromagnetic manner. The electromagnetic field cannot develop an essentially electric character ($E^2 > B^2$) because the entrained electric charges would have to move at a velocity exceeding the speed of light. Nonetheless, a localized breakdown of the MHD approximation is possible where the magnetic field in the outflow has discontinuities.

We now consider the effect that radiative cooling has on the speed with which magnetic flux can be advected toward a neutral sheet (given that such a field configuration is present in a GRB outflow). A pure electron-positron plasma trapped in a neutral sheet can cool rapidly, which has the effect of reducing the volume integral of the particle pressure across the sheet and greatly increasing the compressibility of the medium. By contrast, ions will cool very slowly by incoherent synchrotron or inverse-Compton processes in the emission region of a gamma-ray burst. The ions can therefore supply a significant back pressure (Fig. 3).

The relativistic expansion of the outflow has an important influence on the geometry of the reconnecting magnetic field. In contrast with the Solar magnetosphere, the magnetic field lines are nearly homogeneous away from the neutral sheet, and extend far beyond the causal scale $r/\Gamma c$. As a result, one expects multiple X-type points to form along the sheet (Thompson 1994; Lyubarsky 2003). The rate of particle cooling implies a characteristic thickness Δ for the layer within which the magnetic field becomes disordered.

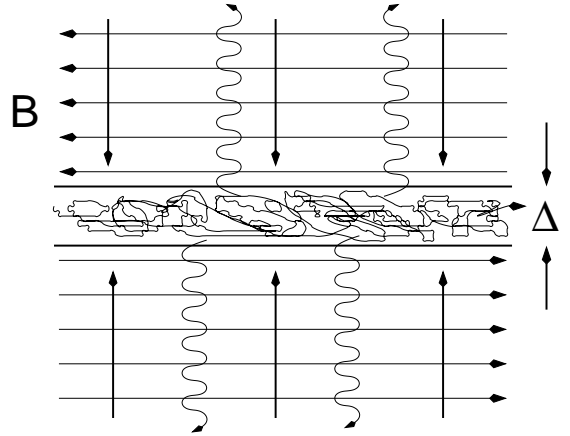


FIG. 3.— Distribution of magnetic field lines around an idealized neutral sheet. The magnetic field is turbulent within the sheet, but all three components of the spatially-averaged field vanish at the mid-plane. When the entrained charges cool rapidly, it is possible for the oppositely directed field lines to reconnect and cancel out, without any sideways fluid motion. The thickness Δ of the sheet is determined self-consistently by the balance between the Poynting flux toward the sheet, and the outward radiative flux. However, a small contamination by slowly cooling ions will induce a significant back pressure which chokes off the transport of magnetic flux toward the neutral sheet.

In what follows, we assume that the magnetic field becomes strongly turbulent within this layer, and that the energy in the fluctuating component of the field is transferred to the particles by a Kolmogorov-type cascade on a timescale $\sim \Delta/c$. As a result, the magnetic field has annihilated in a layer of thickness $\sim ct'$ after the lapse of a time $t' < r/c\Gamma$. The buildup of particles in the sheet forces a decrease in the magnetization parameter⁷,

$$\sigma_{\pm} \sim \sigma_{\pm}^0 \left(\frac{\Delta}{ct'} \right). \quad (93)$$

Here σ_{\pm}^0 is the ambient value, as determined self-consistently by the gamma-ray spectrum. Balancing the advection time Δ/c with the synchrotron cooling time $\sim (r/c\Gamma)(\ell'_B\sigma_{\pm})^{-1}$, where

$$\ell'_B = \frac{\sigma_{\text{T}}(B')^2}{8\pi m_e c^2} \frac{r}{\Gamma_c}, \quad (94)$$

gives

$$\frac{\Delta^2}{(r/\Gamma)(ct')} \sim \frac{1}{\ell'_B \sigma_{\pm}^0}, \quad (95)$$

and

$$\sigma_{\pm} \sim \frac{(\sigma_{\pm}^0)^{1/2}}{(\ell'_B)^{1/2}} \left(\frac{ct'}{r/\Gamma} \right)^{-1/2}. \quad (96)$$

The scattering depth across the sheet is smaller than the total depth of the outflow ($\tau_{\text{T}} \sim \ell'_B/\sigma_{\pm}^0$) by a factor $\Gamma ct'/r$,

$$\tau_{\text{T}}(\Delta) \sim \frac{\ell'_B}{\sigma_{\pm}^0} \left(\frac{ct'}{r/\Gamma} \right). \quad (97)$$

The optical depth to annihilation (over a timescale t') is

$$\tau_{\text{ann}}(t) = \frac{\langle \sigma_{\text{ann}} v \rangle}{\sigma_{\text{T}} c} \frac{\tau_{\text{T}}(\Delta)}{\Delta/ct'} \sim \frac{(\ell'_B)^2}{\sigma_{\pm}^0} \left(\frac{ct'}{r/\Gamma} \right)^2. \quad (98)$$

Here we have made use of $\langle \sigma_{\text{ann}} v \rangle \sim \sigma_{\text{T}} c / \sigma_{\pm}$ for relativistic pairs of energy $\sim \sigma_{\pm} m_e c^2$. One sees that the annihilation of the collected pairs can be neglected as long as $\sigma_{\pm}^0 \gg (\ell'_B)^2$.

Now consider the effects of a small contamination by ions, with a magnetization parameter $\sigma_p = B'^2/4\pi n'_p m_p c^2 \gg 1$. The ions collect in the neutral sheet. Reconnection can be choked off if the ions acquire a significant fraction of the wave pressure. Cooling of the ions by an incoherent process like synchrotron emission is very slow, and can be neglected as long as $\sigma_p < (m_p/m_e)^3 \ell'_B$. The dominant heating mechanism of the pairs is likely to be electrostatic when $\sigma_{\pm}^0 \gtrsim 1$ (§6). The ions will be accelerated to relativistic energies by the same electric field if $\sigma_{\pm} \gtrsim m_p/m_e$ in the neutral sheet, but will absorb a significant fraction of the wave energy only if the numbers of ions and positrons are comparable, i.e., only if $\sigma_p^0 \gtrsim (m_p/m_e)\sigma_{\pm}^0$. It should be noted that requiring $\sigma_{\pm} \gtrsim m_p/m_e$ translates into a stringent constraint on the magnetization of the pairs outside the sheet, $\sigma_{\pm}^0 \gtrsim (m_p/m_e)^2 \ell'_B$ (from eq. [96]). More effective ion heating would result from resonant absorption of high-frequency fast waves (e.g. Yan & Lazarian 2002).

Finally, it should be noted that two-dimensional models of reconnection at a neutral sheet oversimplify the field geometry that is expected in a GRB outflow. If the magnetic field starts in a disordered state, then the field at the boundary of a fluid element in the jet will typically be inclined by a large angle with respect to the field in a neighboring fluid element. (In other words, the two non-radial components B'_ϕ and B'_θ are comparable in magnitude, in a spherical coordinate system aligned with

the jet axis.) Near the boundary between two fluid elements, this means that one tangential component of the field will keep a constant sign and will not vanish in the current sheet at the boundary. The uniform advection of magnetic flux toward the fluid boundary will therefore be suppressed by the pressure of this component of the field.

5.4. Rayleigh-Taylor Instability

We now consider the Rayleigh-Taylor stability of the contact discontinuity that sits at the front of the relativistic ejecta shell. We consider two separate cases: where the inertia of the material that is swept up in front of the contact is dominated by the Wolf-Rayet wind (§3.1), and where it is dominated by a ‘breakout shell’ that is collected during the emergence of the jet from the outer layers of the star (§4). We then consider the influence of a magnetic field on the instability.

The effective gravity felt by material near the contact discontinuity is

$$g' = \frac{d^2 r'}{(dt')^2} = -c^2 \frac{d\Gamma_c}{dr}, \quad (99)$$

where dr' is the radial displacement in the bulk frame. This is directed outward when the effect of the breakout shell is negligible and the dynamics of the contact is dominated by the interaction with the Wolf-Rayet wind. As radiative pre-acceleration is turning off, the Lorentz factor of the contact decreases with radius, as $\Gamma_c \propto r^{-1/4}$. The rest-frame time coordinate is $t' = \int (dr/\Gamma_c c) \simeq \frac{4}{3} r/\Gamma_c c$, and so

$$g' = +\frac{c}{5t'}. \quad (100)$$

On the other hand, the Lorentz factor is still growing close to the central engine, $\Gamma_c \propto r^{1/3}$, where the breakout shell dominates the inertia of the contact. The effective gravity is inward in this regime, and also somewhat stronger,

$$g' = -\frac{c}{2t'}. \quad (101)$$

Here we have made use of $t' \simeq \frac{3}{2} r/\Gamma_c c$.

The forward shock is moderately relativistic near the end of the prompt deceleration phase (eq. [59]). The pressure P'_+ on the front side of the contact discontinuity is dominated by slow-cooling ions of an energy $\Gamma_{\pm} \sim 10$. The gravitating mass density ρ'_+ can be expressed in terms of P'_+ and the energy density $e'_+ \simeq 3P'_+$ by

$$\rho'_+ \simeq \frac{1}{c^2} (e'_+ + P'_+) \simeq \frac{4P'_+}{c^2}. \quad (102)$$

On the back side of the contact, the particles (mainly pairs) are only mildly relativistic when the effects of Compton cooling are taken into account. Their pressure is $P'_- < \frac{1}{3} \rho'_- c^2$ in that case. The two sides of the contact will be in approximate pressure equilibrium, $P'_- = P'_+$, and so one deduces that the fluid behind the contact is denser, $\rho'_- > \rho'_+$. The effective gravity is outward during the last stages of pair-loading in the external medium, and so one expects the contact to be Rayleigh-Taylor unstable.

The fluid on either side of the contact suffers from a strong corrugation instability when its thickness $\Delta r'$ is much smaller than r/Γ_c in the bulk frame. This instability is demonstrated by Vishniac (1983) in the case of a thin cooling shell in a non-relativistic blast wave, but the derivation is not altered in the relativistic case when $\Delta r' \ll r/\Gamma_c$. In this regime, the growth

⁷ Throughout this paper, we define the magnetization parameter in terms of the *rest* energy density of the particles in the bulk frame, $\sigma_{\pm} = B'^2/4\pi n'_{\pm} m_e c^2$.

rate is determined by the net acceleration of the shell material (see eqs. [2.19]-[2.21] of Vishniac 1983).

The peak growth rate is $\gamma' \sim (g'k_{\parallel})^{1/2} \sim (2\pi g'/\Delta r')^{1/2}$ at a wavenumber $k_{\parallel} \sim 2\pi/\Delta r'$ parallel to the contact. When the contact is decelerating, the ratio of flow time to growth time is $\gamma'/t' \sim (2\pi/5)^{1/2}(\Delta r'/ct')^{-1/2}$. This shows that the growing Rayleigh-Taylor fingers will induce only a limited amount of mixing when both fluid shells (on either side of the contact) have a thickness $\Delta r' \sim ct'$. The corrugation instability of an *adiabatic* relativistic shell has been analyzed by Wang, Loeb, and Waxman (2002), who find no growing modes. But growing modes do definitely exist in the thin-shell limit.

The breakout shell, in particular, suffers from a strong corrugation instability. The direction of gravity and the density contrast are $g' < 0$, $\rho'_+ > \rho'_-$ in this case, since the shell material is cooled by adiabatic expansion. The shell also becomes relatively thin as it is pushed outward. The pressure inside the shell decreases with radius as $P' \sim L_{\text{rel}}/4\pi\Gamma_c^2 r^2 c \propto r^{-8/3}$, given the scaling $\Gamma_c \propto r^{1/3}$ (eq. 63). Before the shell becomes optically thin, P' is dominated by the entrained photons. The pressure therefore scales with the shell thickness $\Delta r'$ as $P' \propto (\Delta r' r^2)^{-4/3}$ under adiabatic expansion, and the aspect ratio decreases as $\Delta r'/ct' \propto r^{-2/3}$. The shell suffers from a strong corrugation instability even before it becomes optically thin to scattering (at radius [66]).

The details of the Rayleigh-Taylor instability change when the magnetic field dominates the pressure behind the contact. If the field were predominantly toroidal and of a constant sign (running parallel to the contact), then a Rayleigh-Taylor instability would be suppressed. This can be seen from the dispersion relation (Chandrasekhar 1981)

$$\omega'^2 = g'k_{\parallel} \left(\frac{\rho'_+ - \rho'_-}{\rho'_+ + \rho'_-} \right) + 2V_A'^2 k_{\parallel}^2 \left(\frac{\rho'_-}{\rho'_+ + \rho'_-} \right) \quad (103)$$

which is the sum of the usual Rayleigh-Taylor piece and a second positive piece representing the restoring force of the bent magnetic field lines behind the contact. The growth rate $\gamma' = \text{Im}\omega'$ takes the maximum value

$$\gamma'_{\text{max}} = \left| \left(\frac{g'}{2^{3/2}V_A'} \right) \frac{\rho'_+ - \rho'_-}{(\rho'_-)^{1/2}(\rho'_+ + \rho'_-)^{1/2}} \right| \quad (104)$$

at a wavevector

$$k_{\parallel \text{max}} = \left| \left(\frac{g'}{4V_A'^2} \right) \frac{\rho'_+ - \rho'_-}{\rho'_-} \right|. \quad (105)$$

Effective growth of the Rayleigh-Taylor mode requires $\gamma'/t' \gg 1$. When the contact is decelerating (g' is given by eq. [100]), this is possible if $V_{A-}/c \ll 0.1 |(\rho'_+ - \rho'_-)/\rho'_-|$. The particles behind the contact are mildly relativistic in this situation, and so a large density ratio $\rho'_- \gg \rho'_+$ is inconsistent with pressure equilibrium across the contact. We conclude that a modest magnetic field, which supplies $\sim 10^{-2}$ of the pressure behind the contact, can suppress the Rayleigh-Taylor instability.

On the other hand, a reversing magnetic field is susceptible to reconnection and tangling after it passes through the reverse shock wave. After the field has broken up into small-scale loops, it then behaves more like an isotropic fluid on larger scales. The stress-tensor of the magnetofluid must still be somewhat anisotropic, with a non-radial component that is larger than $2^{1/2}$ times the radial component, $B_{\phi}'^2 + B_{\theta}'^2 = 2(1+\varepsilon)B_r'^2$. We can define an average pressure $P'_- = (B_{\phi}'^2 + B_{\theta}'^2 - B_r'^2)/8\pi$ normal to the contact. The equation of state of the magnetofluid

is then

$$e'_- = \frac{B_{\phi}'^2}{8\pi} + \frac{B_r'^2}{8\pi} + \frac{B_{\theta}'^2}{8\pi} = \frac{3+2\varepsilon}{1+2\varepsilon}P'_-; \quad \rho'_- \simeq \frac{1}{c^2}(e'_- + P'_-). \quad (106)$$

Equating the pressures on either side of the contact and relating them to the densities through equations (102), (106), gives

$$\frac{\rho'_+}{\rho'_-} \simeq \frac{1+2\varepsilon}{1+\varepsilon}. \quad (107)$$

This expression assumes that ε is larger than $1/\gamma$ of the relativistic particles forward of the contact, so that $\rho'_+ \simeq 4P'_+/c^2$. In this case, the anisotropic magnetic field is effectively the *lighter* fluid. The Rayleigh-Taylor mode is therefore stabilized while the contact is decelerating.

6. DAMPING OF ALFVÉN TURBULENCE IN A MAGNETICALLY DOMINATED MEDIUM

Long-wavelength magnetohydrodynamic turbulence is a generic outcome of various instabilities in a GRB outflow, which include the tangling of the stretched non-radial field lines by reconnection (Thompson 1994) and kink instabilities in a jet (Lyutikov & Blandford 2003). The outflow retains enough charges outside its photosphere to enforce the MHD condition on very small scales compared with the causal scale (§5.3). We now examine how energy is transferred from waves to particles, and thence to the photons, when the magnetic energy density approaches or exceeds the rest energy density of the entrained charges.

We should emphasize that we are examining the regime where the energy density in the background magnetic field is much larger than the energy density in high-frequency torsional waves. The conservation of Kolmogorov energy flux, from some forcing scale (eq. [126]) to higher frequencies, implies that the r.m.s. wave amplitude decrease with frequency as $(\delta B^2)_{\omega}^{1/2}/B_0 \propto \omega^{-1/2}$. Models of ‘jitter’ radiation (Medvedev 2000) focus on the opposite limit where the magnetic field has only weak long-range order, and the gyroradius of a particle is much larger than the coherence length of the field.

Our focus here is on the torsional MHD waves which are excited when a reversing magnetic field in the outflow is forced to reconnect. These waves transport energy along the background magnetic field. The excited modes have a characteristic wavevector $k_{\perp 0} \sim 1/\Delta r'_B$ perpendicular to the background magnetic field. Here $\Delta r'_B$ is the reversal scale of the magnetic field (due to the stochasticity of the dynamo operating in the central engine; §2). The component of the wavevector parallel to the background field is $k_{\parallel 0} \sim (V_{\text{rec}}/c)k_{\perp 0}$, where V_{rec} is the speed of transverse motions excited by reconnection. The excited turbulence will therefore be anisotropic even at the outer scale $L_0 \sim 1/k_{\parallel 0}$. In what follows, this forcing scale will be normalized to the causal scale of the outflow,

$$L_0 = \varepsilon_0 \frac{r}{\Gamma_c}. \quad (108)$$

The amplitude of the turbulence at the forcing scale is δB_0 . Notice that

$$\varepsilon_0 \sim \left(\frac{V_{\text{rec}}}{c} \right)^{-1} \left(\frac{\Delta r'_B}{r/\Gamma_c} \right) = 0.3 \frac{\Gamma_c^2}{r_{15}} \left(\frac{V_{\text{rec}}/c}{0.1} \right)^{-1} \left(\frac{\Delta r'_B/c}{0.1 \text{ s}} \right), \quad (109)$$

is characteristically ~ 0.1 if the magnetic field reverses on a timescale of ~ 0.1 s. In this section, we work consistently in the bulk frame, and so we drop the $'$ on all quantities for notational convenience.

Torsional MHD waves can be damped directly by bulk Compton drag (Thompson 1994); or indirectly when non-linear couplings between oppositely propagating waves create higher wavenumber modes (Goldreich & Sridhar 1995). The current density increases with wavenumber in such a cascade, and an upper bound to the frequency of the waves is obtained by balancing this fluctuating current with the maximum conduction current available from the embedded charges (Thompson & Blaes 1998; Lyutikov & Thompson 2005). Damping of the wave motions occurs primarily through electrostatic acceleration of these charges along the background magnetic field. The accelerated charges cool primarily by inverse-Compton scattering the ambient photon field.

In a fluid with $\tau_{\pm} \lesssim 1$, bulk Compton drag is most effective at the outer scale L_0 of the turbulent spectrum. The drag timescale is

$$t_{\text{drag}} \sim \frac{(\delta B)^2 / 8\pi}{\sigma_T n_e c (\delta V_e / c)^2 U_\gamma}. \quad (110)$$

Here $\delta V_e / c \sim \delta B / B$ is the velocity with which the electrons are advected past the ambient photon gas by the MHD wave motions; and U_γ is the energy density in the photons. Normalizing eq. (110) to the flow time in the bulk frame, and re-expressing the magnetization parameter of the pairs in terms of the bulk frame compactness ℓ_B and scattering depth τ_{\pm} ,

$$\sigma_{\pm} = \frac{\ell_B}{\tau_{\pm}} \sim 3 - 10, \quad (111)$$

one has

$$\frac{t_{\text{drag}}}{r / \Gamma_c c} \sim \frac{\sigma_{\pm}}{\ell_\gamma} \sim \frac{1}{\tau_{\pm}} \left(\frac{\ell_B}{\ell_\gamma} \right). \quad (112)$$

We see that t_{drag} is comparable to the flow time if $\tau_{\pm} \sim 1$ and most of the energy in the magnetic field has already been transferred to the photons.

The timescale for 3-mode wave interactions can, however, be significantly shorter than the flow time. In the remainder of this section, we examine in more detail how energy is transferred to the electrons and positrons through the formation of a spectrum of high-frequency waves, and how the heated particles cool.

6.1. Electrostatic Acceleration vs. Resonant Cyclotron Heating of Particles

A turbulent spectrum of torsional MHD waves is created through non-linear couplings between the waves on the outer scale L_0 . Both compressive (fast) and torsional (Alfvénic) waves are created in the fluid, but the torsional waves have stronger couplings with each other than do fast modes of a similar frequency (Troischt & Thompson 2004). Alfvén turbulence has a strong tendency to anisotropy, the wavepackets becoming elongated along the magnetic field at high frequencies (Higdon 1984; Goldreich & Sridhar 1995). This property is preserved in the relativistic regime (Thompson & Blaes 1998; Cho 1995).

The energy that cascades from the outer scale $L_0 = \varepsilon_0 (r / \Gamma_c)$ (eq. [109]) can be written as

$$E_{\text{cas}} = \varepsilon_{\text{cas}} \frac{B^2}{8\pi} \quad (113)$$

per unit volume. The coefficient ε_{cas} depends on the strength of the turbulence. It takes the maximum value $\varepsilon_{\text{cas}} \sim \varepsilon_0^{-1} (\delta B_0 / B)^2$ when the coupling between colliding wavepackets is strong on the timescale $\sim L_0 / c$. The three-mode coupling is strong when

$$\frac{\Delta(\delta B)}{\delta B} \sim \frac{k_{\perp}}{k_{\parallel}} \frac{\delta B}{B} \sim 1 \quad (114)$$

(Goldreich & Sridhar 1995). Here k_{\parallel}^{-1} is the length of a wavepacket parallel to the background magnetic field, and k_{\perp}^{-1} is the transverse size. We can then set a lower bound on this coupling parameter from the requirement that a cascade have time to develop on the (bulk frame) timescale r / Γ_c . When the parameter is small, the effects of subsequent collisions will accumulate as a random walk. A wavepacket of length $\sim L_0$ accumulates a distortion $[\Delta(\delta B) / \delta B]^2 \sim \varepsilon_0^{-1} (k_{\perp} \delta B / k_{\parallel} B)_0^2$ in a time $r / \Gamma_c c$. This distortion is of the order of unity if $(k_{\perp} \delta B / k_{\parallel} B)_0 \gtrsim \varepsilon_0^{1/2}$. Taking $(k_{\perp} / k_{\parallel})_0 \sim (V_{\text{rec}} / c)^{-1}$, and ε_0 from eq. (109), one sees that a significant fraction of the total magnetic field energy will transfer to high-frequency torsional waves if

$$\left(\frac{\delta B_0}{B} \right)^4 \gtrsim 3 \times 10^{-3} \frac{\Gamma_c^2}{r_{15}^2} \left(\frac{V_{\text{rec}} / c}{0.1} \right) \left(\frac{\Delta r_B / c}{0.1 \text{ s}} \right). \quad (115)$$

This inequality is satisfied if $\delta B_0 / B \gtrsim 0.2$.

If coupling parameter (114) is smaller than unity at the forcing scale, it grows with wavenumber and the cascade quickly enters the ‘critically-balanced’ regime where $k_{\perp} \delta B / k_{\parallel} B \sim 1$ (Goldreich & Sridhar 1995; Cho 2005). One then is led to a simple result that has considerable importance for the radiative emission from the turbulent medium (Thompson & Blaes 1998; Lyutikov & Thompson 2005): the turbulent spectrum must be cut off at a frequency that lies well below the gyrofrequency of the electrons and positrons.

A torsional wave transports charge along the background magnetic field at a rate $\delta J = ck_{\perp} \delta B / 4\pi$. Balancing this against the maximum conduction current that can be supplied by the ambient electrons and positrons, one has

$$en_{\pm} \sim \frac{k_{\perp} \delta B}{4\pi} \sim \frac{k_{\parallel} B}{4\pi}. \quad (116)$$

At higher current densities, a displacement current develops through the Maxwell equation

$$\frac{\partial E_{\parallel}}{\partial t} = ck_{\perp} \delta B - 4\pi en_{\pm} v_{\pm} \simeq ck_{\perp} \delta B - 4\pi en_{\pm} c. \quad (117)$$

Only a small imbalance on the right hand side is sufficient to generate an accelerating electric field that deposits energy in the particles.

The charge-starvation scale (116) is therefore

$$k_{\parallel \text{starve}} = \frac{4\pi en_{\pm}}{B} \simeq (2\sigma_{\pm})^{-1} \frac{eB}{m_e c^2}. \quad (118)$$

Referenced to the outer scale L_0 , this is

$$k_{\parallel \text{starve}} L_0 \sim \frac{\tau_{\pm}}{\alpha_{\text{em}} (B / B_{\text{QED}})}. \quad (119)$$

Here $\tau_{\pm} = \sigma_T n_{\pm} L_0$ is the scattering depth of the pairs across a distance L_0 , $\alpha_{\text{em}} = 1/137$ is the fine structure constant, and $B_{\text{QED}} = m_e c^3 / e\hbar = 4.41 \times 10^{13} \text{ G}$ is the QED magnetic field. The field in the dissipation zone⁸ is weaker than B_{QED} by more than 10 orders of magnitude (eq. [74]). One therefore has $k_{\parallel \text{starve}} \sim 10^{12} \tau_{\pm} L_0^{-1}$. One sees that torsional wave turbulence can be supported in a GRB outflow over a very wide range of frequencies.

In general, we will be considering the case where the rest energy density in electrons and positrons smaller than the energy density of the background magnetic field,

$$\sigma_{\pm}^{-1} \equiv \frac{n_{\pm} m_e c^2}{B^2 / 8\pi} \sim \frac{\tau_{\pm}}{\ell_B} \sim 0.1 - 0.3. \quad (120)$$

⁸ Measured in the bulk frame of the outflow.

In this regime, the velocity of a torsional wave (the ‘Alfvén’ velocity V_A) is generally close to the speed of light. However, V_A is significantly smaller than c when the wave is so strongly sheared that $k_\perp \gtrsim \omega_{pe}/c$. The cold plasma dispersion relation reads

$$\omega \simeq V_A k_\parallel, \quad (121)$$

at low frequencies $\omega \ll \omega_{pe} = (4\pi n_\pm e^2/m_e)^{1/2}$. The Alfvén speed is

$$\frac{V_A}{c} = \left(1 + \frac{1}{2\sigma}\right)^{-1/2} \left(1 + \frac{k_\perp^2 c^2}{\omega_{pe}^2}\right)^{-1/2}, \quad (122)$$

including the effects of particle inertia and a strong gradient perpendicular to the background magnetic field. Here $\sigma^{-1} = \sigma_\pm^{-1} + \sigma_p^{-1}$ is the total magnetization parameter, where

$$\sigma_p \equiv \frac{B^2}{8\pi n_p m_p c^2}. \quad (123)$$

refers to the ions. (The derivation of equation [122] is similar to that given by Arons & Barnard 1986 for sheared Alfvén waves in the infinite- B limit.)

In this regime, the energy in the wave is divided nearly equally between the transverse fluctuation in the electromagnetic field, and a *longitudinal* oscillation of the electrons and positrons. Namely,

$$\frac{\langle \frac{1}{2} n_\pm m_e v_{\pm\parallel}^2 \rangle}{\langle \delta B^2 / 8\pi \rangle} \simeq \frac{k_\perp^2 c^2}{\omega_{pe}^2} \quad (124)$$

and

$$\frac{\langle \delta E^2 \rangle}{\langle \delta B^2 \rangle} = \left(1 + \frac{k_\perp^2 c^2}{\omega_{pe}^2}\right) \left(1 + \frac{1}{2\sigma}\right)^{-1}. \quad (125)$$

At a perpendicular wavenumber $k_\perp \gtrsim V_e/\omega_{pe}$, the phase speed of the mode along the magnetic field drops below the speed of light, and the mode is Landau damped on the longitudinal motion of the electrons.

When the ions are warm, the excited modes are electron-supported at perpendicular wavenumbers larger than the inverse ion gyroscale, $k_\perp \gg eB/m_p c V_p$. It should be emphasized that the dispersion relation of these electron-supported modes is not the usual whistler dispersion relation if the kinetic energy density of the ions is smaller than the magnetic energy density, $\frac{1}{2} m_i n_i V_i^2 \ll B^2/8\pi$. The dispersion relation is instead Alfvén-like, and differs from (121), (122) only in the absence of the factor $(1 + \sigma^{-1})^{-1/2}$. Another difference with non-relativistic fluids is that modes of both (circular) polarizations are supported, and so we conjecture that the mode-mode interactions are similar to those of lower-frequency magnetohydrodynamic waves. (More generally, the electron-supported modes will have an Alfvén-like dispersion relation over some range of wavenumbers $k_\perp \lesssim \omega_{pe}/c$ as long as $n_e m_e c^2 \ll B^2/8\pi$. Our considerations are therefore relevant to a non-relativistic medium in which ρc^2 exceeds $B^2/8\pi$, but not by a factor exceeding $\sim m_p/m_e$.)

We will generally be interested in the case where there is a constant energy flux through a critically-balanced spectrum of torsional waves,

$$\frac{dE_{\text{cas}}}{dt} = \frac{V_A}{L_0} \left(\frac{\delta B_0^2}{8\pi}\right) = k_\parallel V_A \left(\frac{\delta B^2}{8\pi}\right). \quad (126)$$

If the coupling parameter (114) is unity at the outer scale $k_\parallel \sim L_0^{-1}$, one has $k_\perp L_0 = (\delta B_0/B)^{-1} (k_\parallel L_0)^{3/2}$ (Goldreich & Sridhar

1995). The scale $k_\perp \sim \omega_{pe}/c$ is therefore reached at a parallel wavelength

$$\frac{k_{\parallel \text{shear}}}{k_{\parallel \text{starve}}} \sim \frac{(\alpha_{\text{em}} \sigma_\pm)^{1/3}}{\tau_\pm^{1/3} (L_0)} \left(\frac{B}{B_{\text{QED}}}\right)^{1/3} \left(\frac{\delta B_0}{B}\right)^{2/3}. \quad (127)$$

Note that the dependence of V_A on the total magnetization parameter σ cancels here. Equation (127) can be re-written as

$$k_{\parallel \text{shear}} L_0 \sim \frac{\sigma_\pm^{1/3} \tau_\pm^{2/3} (L_0)}{\alpha_{\text{em}}^{2/3}} \left(\frac{B}{B_{\text{QED}}}\right)^{-2/3} \left(\frac{\delta B_0}{B}\right)^{2/3} \quad (128)$$

using eq. (119). This transition occurs at a wavenumber

$$k_{\parallel \text{shear}} \sim 10^{-4} k_{\parallel \text{starve}} \quad (129)$$

when $\tau_\pm \sim 1$, $\sigma_\pm \sim 10$, $\delta B_0/B \sim 1$, and the magnetic field is given by eq. (74).

A torsional wave of frequency ω will resonate with the gyromotion of an electron (Lorentz factor γ_e and speed β_e parallel to the background magnetic field) only if

$$\gamma_e (\omega - \beta_e c k_{\parallel \text{starve}}) = \pm \frac{eB}{m_e c}. \quad (130)$$

We have found that $V_A \ll c$ at such high frequencies, and so the resonant energy is

$$\gamma_e |\beta_e| \sim 2\sigma_\pm. \quad (131)$$

If all the charges obtained this Lorentz factor and did not lose energy to radiation, then the kinetic energy density in particles would be comparable to the energy in the *background* magnetic field,

$$\langle (\gamma_e^2 - 1)^{1/2} \rangle m_e c^2 n_\pm \sim \frac{B^2}{8\pi}. \quad (132)$$

This shows that resonant heating of the particles will be prevented if one of two conditions are satisfied:

1. The particles cool significantly in the time required for the MHD wave energy to cascade to small scales;
2. The net wave energy deposited in particles is small compared with the background field energy, $(\delta B)^2 \ll B^2$.

6.2. Heating of Ions by Alfvén Waves

It is possible in principle for *resonant* heating of the ions to limit the range of wavenumbers over which left-handed torsional waves can be supported. This effect can be neglected if the wave frequency at the scale (118) is smaller than the ion gyrofrequency,

$$(k_\parallel V_A)_{k_{\parallel \text{starve}}} \lesssim \frac{eB}{m_p c} = 2\sigma_\pm \left(\frac{m_e}{m_p}\right) k_{\parallel \text{starve}} c. \quad (133)$$

We take the ions to be protons for simplicity. In fact some significant admixture of heavier ions with a charge/mass ratio $\simeq \frac{1}{2}$ is expected in most circumstances. This additional component is mainly helium if the baryons are derived from neutronized material in the central engine (e.g. Beloborodov 2003); but could be carbon and oxygen if there is mixing between a relativistic jet and the outer layers of a Wolf-Rayet star.

To evaluate this expression, it suffices to note that $V_A \propto k_\perp^{-1}$ when $k_\perp \gtrsim \omega_{pe}/c$ (eq. [122]). We assume that the cascade remains critically balanced (i.e., set the coupling parameter $k_\perp \delta B / k_\parallel B \sim 1$), and that the Kolmogorov energy flux (126) is conserved. Then we find $\delta B \sim \text{constant}$ and $k_\parallel \propto k_\perp$ when $k_\perp \gtrsim \omega_{pe}/c$. The left-hand side of eq. (133) is therefore equal to its value at the transition scale $k_{\parallel \text{shear}}^{-1}$. Defining

$$k_{\parallel \text{ion}} = \frac{eB}{m_p c^2} \quad (134)$$

we have

$$\frac{k_{\parallel \text{shear}}}{k_{\parallel \text{ion}}} \sim \frac{\alpha_{\text{em}}^{1/3} (m_p/m_e)}{\tau_{\text{T}}^{1/3} (L_0) \sigma_{\pm}^{2/3}} \times \left(\frac{B}{B_{\text{QED}}} \right)^{1/3} \left(\frac{\delta B_0}{B} \right)^{2/3}. \quad (135)$$

This expression simplifies in a non-relativistic medium where pairs are absent. After expressing the free-electron density in terms of the magnetization parameter $\sigma_e = B^2/8\pi n_e m_e c^2 = (m_p/2m_e)(V_A/c)^2$, one has

$$\frac{k_{\parallel \text{shear}}}{k_{\parallel \text{ion}}} \sim \frac{\alpha_{\text{em}}^{1/3} (m_p/m_e)^{1/3}}{\tau_{\text{T}}^{1/3} (V_A/c)^{1/3}} \left(\frac{B}{B_{\text{QED}}} \right)^{1/3} \left(\frac{\delta B_0}{B} \right)^{2/3}. \quad (136)$$

We reach the interesting conclusion that *the electrons and positrons will experience non-resonant, electrostatic heating even in a fluid where $\rho c^2 > B^2/8\pi$* (but not by a factor exceeding $\sim m_p/m_e$). Non-resonant heating occurs generically if the magnetic field carries even a modest fraction of the outflow luminosity.

6.2.1. Implications for Black Hole Coronae

We now consider the implications of these results for the damping of magnetohydrodynamic turbulence in black hole coronae. An additional damping mechanism, Compton drag by the ambient radiation field, is available to MHD waves in a black hole accretion disk. We argue that, in this case, the dominant damping mechanism remains the turbulent cascade. For the turbulent layer at the base of the black hole corona, we take $V_A/c \sim 0.1$ and $B \sim 7 \times 10^6 (M_{\text{BH}}/10 M_{\odot})^{-1/2}$ G at $r \sim 10 GM_{\text{BH}}/c^2$ (the magnetic field which supplies the accretion torque: eq. 5.9.10, Novikov & Thorne 1973). This gives

$$\frac{k_{\parallel \text{shear}}}{k_{\parallel \text{ion}}} \sim 0.02 \tau_{\text{T}}^{-1/3} \left(\frac{M_{\text{BH}}}{10 M_{\odot}} \right)^{-1/6} \left(\frac{\delta B_0}{B} \right)^{2/3}. \quad (137)$$

Thus, electrostatic heating becomes effective before resonant absorption on the ions (see also Thompson & Blaes 1998). (A relatively small proportion of the cascade energy can be transferred to the ions by Landau damping on the gyration motion of the ions⁹ at an intermediate wavenumber $k_{\perp} \sim eB/m_p c V_p$: Quataert & Gruzinov 1999).

Now let us examine the Compton drag of the X-ray (and UV) radiation field acting on the bulk magnetohydrodynamic motions. The drag timescale is $t_{\text{drag}} \sim 3m_p c/4\sigma_{\text{T}} U_{\gamma}$ in a non-relativistic medium whose inertia is dominated by the ions. Comparing t_{drag} with the non-linear damping timescale $t_{\text{NL}} = 1/k_{\parallel} V_A$ gives

$$\frac{t_{\text{drag}}}{t_{\text{NL}}} \sim \frac{3(c/V_A)}{2\tau_{\text{T}}(\lambda_{\parallel})} \left(\frac{B^2}{8\pi U_{\gamma}} \right), \quad (138)$$

where we have defined $\tau_{\text{T}}(\lambda_{\parallel}) = n_e \sigma_{\text{T}} k_{\parallel}^{-1}$. It has been suggested that the X-ray photons emerging from an optically thick, radiation-dominated disk could be upscattered into a non-thermal tail by these bulk Alfvén motions even close to the disk mid-plane, where the scattering depth $\tau_{\text{T}} \gg 1$ (Socrates, Davis, & Blaes 2004). Setting aside the question of whether the radiation density will be as high as the thermally unstable Shakura-Sunyaev disk solution would imply, we note that the formation of a non-thermal X-ray continuum requires a significant fraction of the energy flux to be carried by the magnetic field. That is, one requires

$$\frac{B^2}{8\pi} V_A \gtrsim \frac{c}{3\tau_{\text{T}}} U_{\gamma} \quad (139)$$

⁹ I thank Yoram Lithwick for a discussion of this point.

¹⁰ Of photons with rest frame energies $E_{\gamma} \lesssim m_e c^2 / \gamma_e$.

at a vertical Thomson depth $\tau_{\text{T}} > 1$. Substituting this expression into eq. (138) gives

$$\frac{t_{\text{drag}}}{t_{\text{NL}}} \gtrsim \frac{1}{2\tau_{\text{T}}(\lambda_{\parallel}) \tau_{\text{T}}} \left(\frac{V_A}{c} \right)^{-2}. \quad (140)$$

To evaluate this expression, note that

$$\frac{1}{\tau_{\text{T}}} \left(\frac{V_A}{c} \right)^{-2} = \frac{4\pi m_p c^2}{\sigma_{\text{T}} B^2 h} \sim 1 \times 10^2 \left(\frac{h}{3GM_{\text{BH}}/c^2} \right)^{-1} \quad (141)$$

where h is the vertical scale height of the dissipating layer. This shows that bulk Compton drag is likely to be less effective than 3-wave couplings at damping MHD turbulence at the base of a black hole corona. We emphasize that the net effect is still to deposit the wave energy directly in the electrons, but by the mechanism of electrostatic heating.

6.3. Compton Cooling

We showed in the preceding section that electrostatic heating of the light charges in a turbulent magnetoplasma can occur gradually, through many small impulses. Heating can, therefore, be compensated by an incoherent cooling process. In this section, we compare the relative importance of inverse-Compton and synchrotron cooling.

Compton drag will damp the motion of the charges on a timescale

$$t_{\text{IC}} = \frac{3m_e c}{4\sigma_{\text{T}} \gamma_e U_{\gamma}} = \left(\frac{3}{4\gamma_e \ell_{\gamma}} \right) \frac{r}{\Gamma_c c} \quad (142)$$

where U_{γ} is the ambient radiation energy density and

$$\ell_{\gamma} = \frac{\sigma_{\text{T}} U_{\gamma} r}{m_e c^2 \Gamma_c} \quad (143)$$

is the corresponding compactness in the bulk frame.¹⁰ The energy equation

$$\frac{\partial \gamma_e}{\partial t} = \left(\varepsilon_{\text{cas}} \sigma_{\pm} - \frac{4\gamma_e^2 \beta_e^2}{3} \ell_{\gamma} \right) \frac{\Gamma_c c}{r}. \quad (144)$$

has the equilibrium solution

$$\langle \gamma_e^2 \beta_e^2 \rangle^{1/2} = \left(\frac{3\varepsilon_{\text{cas}} \sigma_{\pm}}{4\ell_{\gamma}} \right)^{1/2} = \left(\frac{3\varepsilon_{\text{cas}} B^2}{4\tau_{\pm} 8\pi U_{\gamma}} \right)^{1/2}. \quad (145)$$

The corresponding Compton parameter can be expressed in terms of the Thomson depth $\tau_{\pm} = n_{\pm} \sigma_{\text{T}} r / \Gamma_c$ as

$$y_{\text{C}} = \frac{4}{3} \langle \gamma_e^2 \beta_e^2 \rangle \tau_{\pm} = \varepsilon_{\text{cas}} \frac{B^2}{8\pi U_{\gamma}}. \quad (146)$$

This parameter can be large early on in the process of turbulent damping, but must quickly saturate at a value $y_{\text{C}} \lesssim 1$, which a significant fraction of the available magnetic energy density has been transferred to the radiation field (Thompson 1994). The heated particles can sustain relativistic energies only if $\tau_{\pm} \lesssim 1$.

Modulations in the volumetric heating rate will occur over a range of lengthscales and timescales in the fluid. The above estimate of the equilibrium Lorentz factor does not apply when the cascade timescale becomes shorter than the inverse Compton time-scale. We examine this distinct regime of ‘flash’ heating in §6.4.

Let us now estimate the relative importance of synchrotron cooling. When $\tau_{\pm} \gtrsim 1$, the electrons and positrons are maintained at a sub-relativistic temperature. Direct cyclo-synchrotron emission is suppressed by the large optical depth at the cyclotron resonance,

$$\tau_{\text{cyc}} \sim \frac{\pi^2 e n_e (r/\Gamma_c)}{B} \sim \frac{\tau_{\pm}}{\alpha_{\text{em}}(B/B_{\text{QED}})}. \quad (147)$$

Even when the torsional wave spectrum is cut off at a frequency much lower than the electron gyrofrequency $eB/m_e c \gamma_e$, the light charges will still acquire momentum perpendicular to the magnetic field by upscattering ambient photons. An electron moving relativistically along the magnetic field receives a transverse momentum

$$p_{\perp} = \sin \theta' \frac{E'_{\gamma}}{c}, \quad (148)$$

when it scatters a photon into a direction θ' measured with respect to the field. Here $E'_{\gamma} \simeq \gamma_e E_{\gamma} (1 - \cos \theta) \lesssim m_e c^2$ is the photon energy in the electron rest frame, and θ its angle of propagation in the fluid frame. The perpendicular momentum gained per scattering is obtained by averaging over θ and θ' , using the differential cross section $d\sigma_{\text{T}}/d\Omega' = (3\sigma_{\text{T}}/16\pi)(1 + \cos^2 \theta')$ and assuming an isotropic photon distribution in the fluid frame. One finds

$$\langle p_{\perp}^2 \rangle = \frac{4}{5} \left(\gamma_e \frac{E_{\gamma}}{c} \right)^2 \quad (149)$$

at fixed energy E_{γ} . The effects of successive scatterings accumulate as a random walk, giving

$$\langle p_{\perp}^2 \rangle = \frac{4}{5} \sigma_{\text{T}} \left(\frac{r}{\Gamma_c} \right) \int dE_{\gamma} \frac{dn_{\gamma}}{dE_{\gamma}} \left(\frac{\gamma_e E_{\gamma}}{c} \right)^2 = \frac{4\gamma_e^2 \ell_{\gamma}}{5} \left(\frac{\langle E_{\gamma}^2 \rangle m_e}{\langle E_{\gamma} \rangle} \right) \quad (150)$$

over a timescale $r/\Gamma_c c$.

The synchrotron cooling rate can now be calculated as

$$\dot{E}_{\text{synch}} = 2 \left(\frac{p_{\perp}}{m_e c} \right)^2 \sigma_{\text{T}} \frac{B^2}{8\pi}. \quad (151)$$

Comparing with the inverse-Compton power gives

$$\frac{\dot{E}_{\text{synch}}}{\dot{E}_{\text{IC}}} = \frac{3}{2} \left(\frac{p_{\perp}}{\gamma_e m_e c} \right)^2 \frac{B^2}{8\pi U_{\gamma}} \sim \left(\frac{\langle E_{\gamma}^2 \rangle}{\langle E_{\gamma} \rangle m_e c^2} \right) \ell_B. \quad (152)$$

In this expression the radiative compactness ℓ_{γ} (eq. 143) has been rescaled to the total magnetic energy density, $\ell_B = \ell_{\gamma} (B^2/8\pi U_{\gamma})$. The inverse-Compton emission from an ensemble of charges of energy γ_e is beamed into an angle

$$\delta\theta \sim \frac{\langle p_{\perp}^2 \rangle^{1/2}}{\gamma_e m_e c}. \quad (153)$$

The anisotropy of the electron distribution, and the relative output in synchrotron and inverse-Compton radiation, depends on the spectral distribution of the ambient radiation field. When the radiation field has a Wien distribution with a bulk-frame temperature T_r , then

$$\frac{\langle E_{\gamma}^2 \rangle}{\langle E_{\gamma} \rangle m_e c^2} = \frac{4k_{\text{B}} T_r}{m_e c^2} = \frac{3}{\Gamma_c} \cdot \frac{k_{\text{B}} T_{r,\text{obs}}}{m_e c^2}. \quad (154)$$

If the observed temperature $T_{r,\text{obs}}$ is typical of the spectral peak of gamma-ray bursts, $k_{\text{B}} T_{r,\text{obs}} = \frac{4}{3} \Gamma_c k_{\text{B}} T_r \lesssim m_e c^2$, then the bulk-frame temperature will be far below $m_e c^2/k_{\text{B}}$. In this case, the equilibrium pitch angle of the radiating electrons is small,

$$\frac{\langle p_{\perp}^2 \rangle}{(\gamma_e m_e c)^2} \sim \frac{2\ell_{\gamma}}{\Gamma_c} \cdot \frac{k_{\text{B}} T_{r,\text{obs}}}{m_e c^2}. \quad (155)$$

The synchrotron power is also small relative to the inverse-Compton power as long as $\ell_B \lesssim \Gamma_c$ (which is indeed the case when the deceleration is tied to the end of pre-acceleration; eq. [46]).

Similar conclusions are reached when the target radiation field has a high-energy tail. The scattering is in the Thomson regime as long as $E_{\gamma} \lesssim m_e c^2/\gamma_e$. At higher energies the cross section is suppressed by a factor $\sim \frac{3}{4} (m_e c^2/E'_{\gamma}) \ln(E'_{\gamma}/m_e c^2)$. When the spectrum above the observed peak energy E_{peak} is a power law with energy index $\beta = -1$ up to a maximum energy $E_{\text{max}} > \Gamma_c (m_e c^2/\gamma_e)$, the average in eq. (150) becomes

$$\frac{\langle E_{\gamma}^2 \rangle}{\langle E_{\gamma} \rangle} \rightarrow \frac{m_e c^2}{\gamma_e} \frac{1 + (3/8) \ln^2(\gamma_e E_{\text{max}}/\Gamma_c m_e c^2)}{\ln(\Gamma_c m_e c^2/\gamma_e E_{\text{peak}})} \sim \frac{m_e c^2}{\gamma_e \ln \Gamma_c}, \quad (156)$$

where the last equality holds for $\gamma_e \sim 1$. The pitch angle of the electrons saturates at

$$\frac{\langle p_{\perp}^2 \rangle}{(\gamma_e m_e c)^2} \sim \frac{\ell_{\gamma}}{\gamma_e \ln \Gamma_c} \quad (\beta = -1), \quad (157)$$

and the ratio of synchrotron power to inverse-Compton power at

$$\frac{\dot{E}_{\text{synch}}}{\dot{E}_{\text{IC}}} \sim \frac{\ell_B}{\gamma_e \ln \Gamma_c} \quad (\beta = -1). \quad (158)$$

The above expressions for the r.m.s. pitch angle apply to a charge that is heated continuously over the expansion time $\sim r/\Gamma_c c$. The pitch angle is smaller if a charge is accelerated suddenly along the magnetic field, and then cools passively on a timescale $\sim (\ell_{\gamma} \gamma_e)^{-1} r/\Gamma_c c$. Since $\langle p_{\perp}^2 \rangle$ grows linearly with time, one has

$$\frac{\dot{E}_{\text{synch}}}{\dot{E}_{\text{IC}}} \sim \frac{\ell_B}{\ell_{\gamma}} \frac{\langle p_{\perp}^2 \rangle}{(\gamma_e m_e c)^2} \sim \frac{\ell_B}{\ell_{\gamma} \gamma_e^2 \ln \Gamma_c} \quad (\beta = -1). \quad (159)$$

The r.m.s. pitch angle of the cooling particle never grows larger than $1/\gamma_e$, and the emission cone of an ensemble of particles is comparable in width to that of a single particle.

These expressions are easily generalized to softer gamma-ray spectra, with an energy index $-2 \lesssim \beta \lesssim -1$. One finds

$$\frac{\dot{E}_{\text{synch}}}{\dot{E}_{\text{IC}}} \sim \frac{\ell_B}{\ell_{\gamma}} \frac{\langle p_{\perp}^2 \rangle}{(\gamma_e m_e c)^2} \sim \frac{\ell_B}{\gamma_e} \left| \frac{1+\beta}{2+\beta} \right| \left(\frac{\Gamma_c m_e c^2}{\gamma_e E_{\text{peak}}} \right)^{1+\beta} \quad (160)$$

in the case of continuous heating; and

$$\frac{\dot{E}_{\text{synch}}}{\dot{E}_{\text{IC}}} \sim \frac{\ell_B}{\ell_{\gamma} \gamma_e^2} \left| \frac{1+\beta}{2+\beta} \right| \left(\frac{\Gamma_c m_e c^2}{\gamma_e E_{\text{peak}}} \right)^{1+\beta} \quad (161)$$

in the case of sudden heating followed by passive Compton cooling.

6.4. Flash Electron/Positron Heating

We have argued that the relativistic outflow is likely to contain a variable magnetic field, which switches sign on a length-scale that is small compared with $c\Delta t$ (but still much larger than the size of the neutronized torus that feeds the central black hole). As a result, it is plausible that stochastic bursts of dissipation (driven by magnetic reconnection) occur on timescales that are small compared with Δt (that is, on lengthscales that are small compared with r/Γ_c in the frame of the contact). This means that a fraction $(\delta B_0/B)^2$ of the energy of the shock relativistic outflow can be transferred *locally* to the electrons and positrons quickly enough that they reach the equilibrium energy

$$\langle \gamma_e \rangle = \sigma_{\pm} \left(\frac{\delta B_0}{B} \right)^2 \quad (162)$$

before they are able to cool. This sets an upper bound on the size L_0 of the heated region. One requires that $L_0/c \lesssim t_{\text{cool}}(\langle \gamma_e \rangle) = 3m_e c / 4 \langle \gamma_e \rangle \sigma_T U_\gamma$, or equivalently that

$$\frac{L_0}{r/\Gamma_c} \lesssim \frac{1}{\langle \gamma_e \rangle \ell_\gamma} = \frac{\tau_\pm}{\ell_B \ell_\gamma} \left(\frac{\delta B_0}{B} \right)^{-2}. \quad (163)$$

Here we have related the magnetization parameter of the pairs to the scattering optical depth via $\sigma_\pm = \ell_B / \tau_\pm$.

7. BEAMING OF THE INVERSE-COMPTON RADIATION IN A TURBULENT MAGNETOFLUID

We have found that a relativistic shell of ejecta begins to dissipate strongly when the compactness of the radiation streaming across the forward shock has dropped below a characteristic value (§3.1). This results in a characteristic radiative compactness ℓ' within the moving shell (eq. [46]), and a characteristic optical depth to scattering between the reverse and forward shocks (the sum of eqs. [54] and [177]). Because the dissipation is concentrated in a narrow range of radius, one obtains an explanation for the weak evolution of the temporal power spectrum that is typically seen within a gamma-ray burst.

If the gamma-ray emission is triggered by the interaction with the external medium, then the observation of many well-separated subpulses in some gamma-ray bursts forces a significant constraint on the emission mechanism: the gamma-rays must be beamed in the bulk frame (in the frame of the contact discontinuity). By contrast, high-frequency variability from internal shocks is smoothed out due to the curvature of the ejecta shell, unless the internal shocks are occurring well inside the radius where the reverse shock passes through the ejecta shell (Sari & Piran 1997). Emission on a timescale $\delta t \ll r/2c\Gamma_c^2$ must be localized to a small fraction $\sim (2\Gamma_c^2 c \delta t / r)^2$ of the surface area of the shell that is visible to the observer. The emission occurs at a radius $r \sim 2\Gamma_c^2 c \Delta t$ when it is triggered by the interaction with the external medium. This means that $\sim (\Delta t / \delta t)^2$ independent regions of the shell contribute to each time interval δt , and only a fraction of them must be visible to the observer in a highly variable burst.

What is the cause of this beaming? Reconnection in a high- σ magnetofluid can, in principle, create bulk motions as fast as

$$\gamma_{\text{bulk}} \lesssim \frac{1}{(1 - V_A^2/c^2)^{1/2}} = (1 + 2\sigma)^{1/2} \quad (164)$$

where $V_A^2 = (B')^2 / 4\pi\rho'$ (Blackman & Field 1994) and $\sigma^{-1} = \sigma_p^{-1} + \sigma_\pm^{-1}$. So one could ascribe the gamma-ray variability to stochastic variations in the direction of bulk motion (Lyutikov & Blandford 2003). It is not clear, however, that significant elements of the fluid will be able to accelerate to relativistic speeds, as they evidently do in the outer magnetosphere of a Soft Gamma Repeater during a giant flare (e.g. Thompson & Duncan 2001). In contrast with an isolated neutron star, whose magnetic dipole field pressure drops off rapidly with radius (as $\sim r^{-6}$), one expects the pressure to equilibrate rapidly after the relativistic outflow has passed through the reverse shock. An element of magnetofluid may therefore feel a strong drag force off the ambient fluid as it attempts to move relativistically.

A quite different beaming mechanism is afforded by our model of decaying Alfvénic turbulence (§6). The energy of the waves is extracted by electrostatically accelerating electrons and positrons along the magnetic field. As a result, the radiation of these charges is collimated along the local direction of the field lines (Fig. 4).

The beaming pattern depends in a subtle way on how the charges are heated. The charges start out with small perpendicular motion in the case of flash heating (where energy is transferred from the torsional waves on a timescale much shorter than the cooling time; §6.4). Their radiation is therefore beamed into a solid angle $\sim \pi/\gamma_e^2$. Repeated inverse-Compton scatterings impart some gyration motion. By the time a charge has lost half of its initial kinetic energy, the pitch angle has increased to $\langle p_\perp^2 \rangle^{1/2} / \gamma_e m_e c \sim 1/\gamma_e (\ln \Gamma_c)^{1/2}$ (in the case of hard high-energy photon spectrum; eq. [157]). Here $\gamma_e \sim \sigma_\pm (\delta B'_0 / B')^2$ depends on the fraction of the magnetic energy that is transferred quickly to the charges (eq. [162]). The beaming pattern of a large collection of charges does not change significantly from that of a single charge.

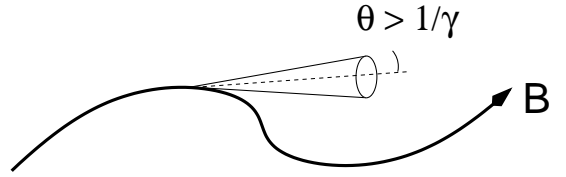


FIG. 4.— Torsional MHD waves in a magnetofluid transfer energy to the light charges by forming a high-frequency spectrum of current fluctuations, and an accelerating electric field. The charges cool primarily by inverse-Compton scattering ambient photons along the local direction of the magnetic field. The observed duration of a gamma-ray spike decreases with energy (eqs. [170], [169]). The scaling with energy depends on whether cooling is faster than the shift in beaming direction that is caused by the long-wavelength undulations of the magnetic field.

The heating may, alternatively, be slow enough to be balanced by inverse-Compton drag. The electrons and positrons will then maintain a pitch angle (157) – but at a somewhat smaller Lorentz factor, $\langle \gamma_e^2 \rangle^{1/2} \sim (3\sigma_\pm / 4\ell'_\gamma)^{1/2}$ (eq. [145]). The radiation of many charges is now beamed into a larger solid angle $\pi\theta'^2 \sim \pi \langle p_\perp^2 \rangle / (\gamma_e m_e c)^2 \sim \pi \ell'_\gamma / \gamma_e \ln \Gamma_c$. One sees that beamed radiation is a direct consequence of the damping of Alfvénic turbulence.

The beaming pattern of the gamma-rays, as seen by the observer, is sensitive to the presence of slow undulations of the contact, through an angle larger than the beaming angle $\delta\theta'$. The inverse-Compton radiation is beamed in the directions parallel and anti-parallel to the magnetic field. An observer situated in the rest frame of the central engine will see the seed thermal photons emitted within an angle $\sim 1/\Gamma_c$ of the radial direction. The inverse-Compton photons will, by contrast, be visible only in two spots of angle diameter $\sim \delta\theta' / \Gamma_c$ that are displaced by an angle $\sim 1/2\Gamma_c$ from the center of the visible patch of the ejecta shell.

7.1. Correlation between Variability Timescale and Photon Energy

We now consider the temporal pattern of the beamed radiation that is emitted by the heated pairs. A torsional wave of an amplitude ξ and a period $P' = 2\pi/(k_\parallel c)$ imparts a tilt $\delta B' / B' = k_\parallel \xi$ to the magnetic field. This tilt varies with time, and so the wave motion forces the radiation beam to sweep past an observer on the timescale

$$\delta t'_B \sim \frac{\delta\theta'}{\partial(k_\parallel \xi) / \partial t'} = \frac{\delta\theta' P'}{2\pi(\delta B' / B')} \propto k_\parallel^{-1/2} \quad (165)$$

(in the bulk frame). The fluctuation timescale is shorter in the observer's frame, $\delta t_B = \delta t'_B / \Gamma_c$.

This expression for $\delta t'_B$ holds when $\delta B' / B' \gtrsim \delta \theta'$, which is possible only over a certain range of wavenumbers in a critically balanced Alfvénic cascade. The conservation of energy flux (eq. [126]) implies that $\delta B' / B' \propto k_{\parallel}^{-1/2}$. The minimum fluctuation timescale is

$$\frac{\delta t_B}{\Delta t} \sim \frac{\varepsilon_0}{2\pi} \left(\frac{\delta \theta'}{\delta B'_0 / B'} \right)^2, \quad (166)$$

given a wave amplitude $\delta B'_0$ at an outer scale $L_0 = \varepsilon_0 (\Gamma_c c \Delta t)$ in the bulk frame.

Two other timescales for variability are relevant here when the particles undergo flash heating. The motion of the charges along the magnetic field is damped on the timescale

$$\frac{\delta t_{\text{cool}}}{\Delta t} \sim \frac{1}{\gamma_e \ell'_\gamma} \quad (167)$$

(as seen by an observer who is at rest with respect to the central engine). Finally, the beaming angle $\delta \theta'$ broadens in response to repeated Compton scatterings. In particular, the r.m.s. pitch angle becomes comparable to $\sim 1/\gamma_e$ on a timescale

$$\frac{\delta t_\theta}{\Delta t} \sim \frac{\ln \Gamma_c}{\gamma_e \ell'_\gamma}. \quad (168)$$

(This expression assumes a hard photon spectrum, $\beta = -1$, and is easily generalized to softer spectra using eq. [160].)

All of these timescales are potentially resolvable in a gamma-ray burst light curve. By contrast, if the emission mechanism were synchrotron radiation, then the cooling time would be far too short to agree with the observed width of the gamma-ray sub-pulses. One requires a Lorentz factor $\gamma_e \gtrsim 10^4$ to generate photons with an observed energy of 100 keV or greater (eq. [74]). The corresponding synchrotron cooling time is $\Delta t / \ell'_\gamma \gamma_e \lesssim 10^{-4} \Delta t$.

Each of these variability timescales become shorter as the energy of the inverse-Compton photon increases. When photons from the advected thermal peak are the principal seeds, one has $E_\gamma \sim \gamma_e^2 E_{\text{peak}}$ and

$$\delta t_{\text{cool}}, \delta t_\theta \propto E_\gamma^{-1/2}; \quad (169)$$

$$\begin{aligned} \delta t_B \propto \delta \theta' &\propto E_\gamma^{-1/4} && \text{(continuous heating);} \\ \delta t_B \propto \delta \theta' &\propto E_\gamma^{-1/2} && \text{(flash heating).} \end{aligned} \quad (170)$$

Which of these scalings is most applicable depends on the speed of Compton cooling relative to the change in beaming direction that is driven by long-wavelength undulations of the magnetic field. It is interesting to recall, in this regard, that some gamma-ray bursts are composed of spikes which show noticeable asymmetry between rise and decay - the so-called FRED behavior (e.g. Fenimore et al. 1996). Other bursts are highly variable but composed of spikes with no clear asymmetry between rise and decay. We associate this second type of variability with fluctuations in beaming direction on a timescale that is shorter than the cooling time. FRED pulses demonstrate the scaling between width and frequency that is characteristic of cooling, $\delta t \propto E_\gamma^{-1/2}$ (eq. [170]; e.g. Fenimore et al. 1995; Norris et al. 1996). An analysis which separates out the two types of variability has not yet been done, but would be illuminating.

¹¹ We ignore spectral evolution for the purpose of this comparison.

7.2. Pair Creation: Effects of Beamed Emission and Inertia of the Breakout Shell

The ejecta are photon rich during the deceleration process. The number of photons emitted per unit area inside radius r is

$$N_\gamma = \frac{L_\gamma}{\langle E_\gamma \rangle} \left(\frac{r}{2\Gamma_c^2 c} \right). \quad (171)$$

This can be normalized to the electron column by¹¹

$$\frac{\sigma_T N_\gamma}{\tau_\pm} = \frac{\ell_+}{\varepsilon_+ \tau_\pm} \left(\frac{\langle E_\gamma \rangle}{m_e c^2} \right)^{-1}. \quad (172)$$

Substituting eqs. (30), (34), and (36) gives

$$\begin{aligned} \frac{\sigma_T N_\gamma}{\tau_\pm} &= \frac{\ell_{\text{crit}} \tilde{\Gamma}_{\text{eq}}^{1/2}}{2^{3/2} \varepsilon_+ \tau_\pm} \left(\frac{\langle E_\gamma \rangle}{m_e c^2} \right)^{-1} \left(\frac{r}{R_{\text{decel-}}} \right)^{-1/2} \\ &\simeq 10^3 \tau_\pm^{-1} \left(\frac{\langle E_\gamma \rangle}{m_e c^2} \right)^{-1} \left(\frac{r}{R_{\text{decel-}}} \right)^{-1/2}. \end{aligned} \quad (173)$$

The shocked outflow will, itself, have a modest optical depth to scattering (eq. [54]). The larger contribution to the optical depth τ_\pm comes from gamma-ray collisions within the shell. An estimate can be obtained directly from the observed gamma-ray spectrum, under the assumption that the high-energy power-law extends up to the pair-creation threshold $\sim m_e c^2$ in the emitting frame (e.g. Baring & Harding 1997). The standard estimate assumes *isotropic emission* of the gamma-rays in the bulk frame.

Given an observed peak energy E_{peak} , the density of photons of energy $m_e c^2$ in the bulk frame is

$$n'_\gamma(m_e c^2) \sim \frac{L_\gamma}{4\pi r^2 \Gamma_c E_{\text{peak}} c \ln(m_e c^2 / E_{\text{peak}})} \left(\frac{\Gamma_c m_e c^2}{E_{\text{peak}}} \right)^{-1}. \quad (174)$$

We specialize here to a hard power-law with a photon energy index -1 extending from energy E_{peak} up to a bulk frame energy $\sim m_e c^2$. The density (174) can be re-expressed as

$$\sigma_T n'_\gamma(m_e c^2) \frac{r}{\Gamma_c} \simeq \frac{\ell'_\gamma}{\ln(m_e c^2 / E_{\text{peak}})}, \quad (175)$$

where ℓ'_γ is the bulk frame compactness of the photons, defined analogously to eq.(43),

$$\ell'_\gamma = \frac{\sigma_T L_{\text{rel}}}{4\pi \Gamma_c^3 m_e c^3 r}. \quad (176)$$

The density of created pairs is $n'_\pm \simeq 2\varepsilon_{\gamma\gamma} \sigma_T [n'_\gamma(m_e c^2)]^2 (r/\Gamma_c)$, where $\varepsilon_{\gamma\gamma}$ normalizes the frequency-averaged photon collision cross section to σ_T , and is $\varepsilon_{\gamma\gamma} \simeq 0.1$ for a $\beta = -1$ photon energy index (Svensson 1987). The scattering depth in the region of shocked relativistic material behind the contact is then

$$\tau_\pm(r < R_c) = \varepsilon_{\gamma\gamma} \frac{2(\ell'_\gamma)^2}{\ln^2(\Gamma_c m_e c^2 / E_{\text{peak}})} \simeq 0.9 L_{\text{rel}51}^{-1/2} \dot{M}_{w-5}^{5/6} V_{w8}^{-5/6} \Delta t_1^{-1/3}. \quad (177)$$

Here we have substituted eq. (45) using $\varepsilon_+ = 0.25$ at the radius where half the ejecta are shocked.

There is, however, considerable reason to doubt this assumption of isotropic emission. Some bursts show strong variability, which in the framework advanced in this paper demands that this emission be beamed in the bulk frame (§7). In such a situation, the production rate of pairs rises considerably. Suppose, for example, that the emission is collimated within cones of angular width $2\delta\theta' \sim 2/\gamma_e$ that run anti-parallel (in the bulk

frame). We fix the net emissivity per unit volume. The intensity of gamma-ray photons in the oncoming beam increases by a factor $2\pi/\pi(\delta\theta')^2 \sim 2\gamma_e^2$. In addition, the threshold condition for pair creation by the two colliding photons,

$$E_{\gamma 1} E_{\gamma 2} (1 - \cos\theta_{12}) > 2(m_e c^2)^2, \quad (178)$$

is more easily satisfied. If the photons are moving anti-parallel, $\theta_{12} \simeq \pi$, then the threshold energy for pair creation is reduced by a factor $\sim 1/\sqrt{2}$ compared with the r.m.s. value in an isotropic photon gas. Assuming the same spectrum as in eq. (174), the pair creation rate therefore increases by a factor ~ 2 .

The breakout shell also has a strong effect on the compactness of the shocked fluid. Inward from the point where Γ_c reaches its peak value, the compactness rises rapidly toward small r , $\ell'(r) \propto r^{-2}$ (eq. [72]). The proportion of the relativistic ejecta which has been shocked decreases only slowly inward, as $\Delta r \propto r^{1/3}$. The optical depth in pairs is proportional to $(\ell')^2$. Combining these scalings, one sees that τ_{\pm} is an extremely strong function of the thickness of the shocked relativistic shell,

$$\tau_{\pm} \propto (\Delta r)^{-12}. \quad (179)$$

In addition, the relativistic jet material can develop a mildly relativistic motion with respect to the fragmenting breakout shell. This reduces the energy threshold for pair creation by allowing some of the gamma-ray photons to side-scatter off the denser shell material.

We conclude that a substantial fraction of the relativistic outflow will dissipate at optical depths $\tau_{\pm} \gtrsim 1$, when the effects of beaming and the breakout shell are taken into account.

8. IMPLICATIONS FOR THE SPECTRA OF GAMMA-RAY BURSTS

We have explored in some detail the physics of a relativistic outflow, composed of a gas of seed thermal photons and a stochastically reversing magnetic field, which is launched into the dense wind of a Wolf-Rayet star. In this section, we outline the implications of our results for the non-thermal spectra of gamma-ray bursts. We first address the origin of the high-energy non-thermal continuum that is a defining feature of GRBs. Second, we show how the observations of gamma-rays at energies $\gtrsim 10^2$ times the peak energy provide a valuable diagnostic of the physics of pair-loading, the density of the ambient medium, and the compactness of the zone in which the ejecta decelerate. Third, we address the spectral transition that occurs between the end of the prompt GRB phase and the beginning of the afterglow emission (a good example being GRB 980923: Giblin et al. 1999). We then explain how prompt optical synchrotron emission may be suppressed (without self-absorption) in a turbulent magnetoplasma. Finally, we connect our model with a previous suggestion (Thompson 1994) that thermal radiation generated close to the central engine is the dominant source of inverse-Compton seeds for the non-thermal radiation of GRBs. The physical mechanisms that we have examined in this paper can also be applied to spectrally harder classes of bursts – the short GRBs (Kouveliotou et al. 1993) and the giant flares of the SGRs (e.g. Hurley et al. 2005). In these types of bursts, one requires that the outflow go into (nearly) free expansion much closer to the engine than it does in the Wolf-Rayet/jet model.

Two general lessons emerge here. First, a close correspondence between the peak of the seed thermal spectrum and the peak of the final GRB spectrum arises much more easily if the

heating of the pairs is spatially and temporally distributed, instead of being localized at a strong shock wave (or a few such shock waves within each causal patch of the outflow). Even in a situation where the magnetic energy density greatly exceeds the rest energy density of the radiating particles, rapid Compton cooling allows the mean particle Lorentz factor to remain close to $m_e c^2$ in the fluid rest frame.

Second, single-box models of the radiation spectrum can provide some subtle insights into the interplay between different radiative processes (e.g. Pe'er & Waxman 2004b), but ultimately the GRB emission problem is one of radiative transport. The prompt GRB emission continues only as long as the thermal seed photons continue to overlap with the dissipating magnetized shell. The prompt 100 MeV component of the GRB spectrum is a byproduct of the dissipative processes occurring two distinct regions: the inverse-Compton emission behind the contact discontinuity; and the side-scattering of these gamma-rays in the Wolf-Rayet wind. The fluid that passes through the reverse shock builds up pairs by collisions between gamma-rays, but this pair creation is extended in time. As a result, the mean energy per particle has a strong negative gradient away from the reverse shock. A high-energy spectral tail is the byproduct of this inhomogeneous distribution of particle energies.

8.1. Power-Law Spectral Tails above the Peak Frequency

The spectra of gamma-ray bursts are characteristically non-thermal, and in many cases appear to have a power-law shape above the peak energy E_{peak} . BATSE burst data do not characteristically cover a wide energy range above the peak energy; but some Ginga bursts with lower peak energies have high-energy power-law tails that cover more than two orders of magnitude in frequency (Strohmayer et al. 1998).

Compton upscattering of the seed thermal photons will preserve the relation between peak energy and isotropic luminosity if i) the optical depth through the dissipating shell is $\tau_{\pm} \gtrsim 1$; and ii) the particle heating is distributed broadly through the fluid. We have seen that the thermal photons follow the Amati et al. (2002) relation – both in slope and normalization – if they are generated in the turbulent core of the jet near the photosphere of the Wolf-Rayet star (eq. [8]). And the scattering depth can attain values near unity in an outflow of isotropic luminosity $10^{51} L_{\text{rel}51}$ ergs s^{-1} and duration $10 \Delta t_1$ s, moving in a Wolf-Rayet wind with mass-loss rate $10^{-5} \dot{M}_{w-5} M_{\odot} \text{ yr}^{-1}$ (eq. [177]). This requires a hard photon spectrum (energy index $\beta = -1$), which is consistent with a significant majority of BATSE bursts (Band et al. 1993) and essentially all of the sample of Ginga bursts analyzed by Strohmayer et al. (1998) (excepting those with high peak energies in which the high-energy tail was not fully sampled). Even when $\dot{M}_w < 10^{-5} M_{\odot} \text{ yr}^{-1}$, the optical depth can be strongly enhanced by the residual inertia of the breakout shell, and by angular inhomogeneities in the outflow that allow side-scattering of photons off slower, denser material (§7.2).

A net optical depth $\tau_{\pm} \gtrsim 1$ in the dissipation zone is required for several reasons. First, the energy radiated by each charge is inversely proportional to τ_{\pm} . The energy of the inverse-Compton photons scales as τ_{\pm}^{-2} at small optical depths, and so the peak of the inverse-Compton spectrum lies far above the peak of the thermal seed photon spectrum. Second, a hard inverse-Compton tail $dL_{\gamma}/dE_{\gamma} \propto E_{\gamma}^{-1/2}$ is generated below the peak energy if the base of the non-thermal electron spectrum

lies at an energy $\gamma_e \gg 1$. Third, a significant fraction of seed blackbody photons must be scattered, so as to avoid a strong and localized thermal bump in the transmitted spectrum.

A lower bound to the luminosity of the seed photons is obtained by demanding that the first-order inverse-Compton (IC) photons carry a significant fraction of the bolometric output of the burst. As the heated particles cool off, and the energy density of the IC photons may begin to exceed that of the blackbody seeds, in which case the first-order IC photons become the dominant coolant for the heated pairs. Nonetheless, because $\ell' > 1$, it is possible for the particles to be energized repeatedly – followed by cooling off the ambient radiation field – so that the instantaneous energy remains close to $\gamma_e \sim 1$. Starting with a compactness ℓ'_{bb} in seed photons, it is possible to radiate a total energy $\ell' \sim (\ell'_{\text{bb}})^2$ this way. The seed photons must carry a minimal fraction of the outflow energy

$$\frac{\ell'_{\text{bb}}}{\ell'} \gtrsim (\ell')^{-1/2} \quad (180)$$

to avoid the appearance of a prominent $E_\gamma^{1/2}$ tail in the soft gamma-ray spectrum.

The existence of some bursts (or subcomponents of bursts) with very soft high-energy spectra (Pendleton et al. 1997) is, of course, fully consistent with this model. The thermal seed photons will not be significantly reprocessed if the Wolf-Rayet wind has a mass-loss rate much less than $\sim 10^{-5} M_\odot \text{ yr}^{-1}$. At the same time, one can expect that the optical depth will continue to drop as the ejecta expand, so that the later parts of a burst will have a tendency to be spectrally softer. So there is a general expectation that NHE *sub*-components of bursts will be concentrated toward the end of the burst. A good example is GRB 920622B (Fig. 2a in Pendleton et al. 1997).

There is, nonetheless, a basic tension in this model between maintaining the $E_{\text{peak}} - L_{\text{iso}}$ relation, and allowing rapid variability in a burst light curve. It should be emphasized that beaming of the inverse-Compton photons will be maintained when $\tau_\pm \gtrsim 1$, because the motion of the electrons and positrons is collimated along the direction of the magnetic field. Nonetheless, strong beaming cannot be maintained below the thermal peak energy at $\tau_\pm \gtrsim 1$, because the Compton parameter $y_C = \frac{4}{3} \tau_\pm \langle \beta_e^2 \rangle$ is limited to a value $y_C \lesssim 1$. The relative absence of bursts with smooth light curves at the highest measured fluxes (Norris et al. 2005) may be connected to the modest decrease in τ_\pm that is expected at higher luminosities, $\tau_\pm \propto L_{\text{rel}}^{-1/2}$. The hypothesis that greater variability corresponds to lower optical depths is testable: more variable bursts should be spectrally harder, on the average, than the Amati et al. (2002) relation would imply.

A hard gamma-ray spectrum depends on the presence of inhomogeneities in the outflow. We now consider three possibilities that are suggested by this model.

8.1.1. First-order Fermi Acceleration of Pairs at a Mildly Relativistic Reverse Shock, followed by Inverse-Compton Cooling

A non-thermal positron tail extending upward from a minimum energy $\gamma_e \sim 1$, and having a significant optical depth $\tau_\pm \gtrsim 1$, would generate a hard, high-energy tail to the gamma-ray spectrum by cooling off the seed thermal photons (Thompson 1997). The asymptotic Lorentz factor that the jet material attains after escaping the Wolf-Rayet star (eq. [12]) is barely a factor 2 larger than the equilibrium Lorentz factor of the contact

during the deceleration phase (eq. [39]). This means that the reverse shock wave is mildly relativistic, and the mean energy of the thermal pairs behind the shock is indeed $(1-2)m_e c^2$. However, our deceleration model suggests that the optical depth of the pairs crossing the reverse shock, and the energy they carry, are too small to produce the desired effect.

Collisions between gamma-rays that flow upstream across the reverse shock will generate a somewhat smaller depth, $\tau_\pm = 0.1 \tau_{\pm-1}$, than they do in the downstream fluid. (This optical depth is sensitive to the amount of cooling and compression that occurs downstream of the shock. The bulk motion of the fluid and the beaming of the emission downstream of the reverse shock both have the effect of suppressing the pair creation rate upstream.) This means that the pairs carry only a fraction

$$\varepsilon_\pm \sim \frac{\tau_\pm}{\ell'} \sim 10^{-2} \tau_{\pm-1} \quad (181)$$

of the outflow energy when they hit the reverse shock.

The proportion of the outflow energy carried by the ions, $\varepsilon_b = \Gamma_{b \text{ crit}} / \Gamma_b$, can easily be larger than ε_\pm , even though the number of positrons exceeds the number of ions by a factor $\sim (m_p/m_e)\varepsilon_\pm/\varepsilon_b$. Particle-in-cell simulations of pair-dominated shocks show that the shocked positrons can acquire a non-thermal tail by absorbing the cyclotron waves emitted by the ions (Hoshino et al. 1992). However, the ions are only mildly relativistic behind the reverse shock, and so the frequency of the ion ring is too low to resonate with the gyromotion of the positrons. (While Fermi-acceleration of the ions is possible, such a non-thermal ion tail would presumably be a much weaker emitter of ion cyclotron waves.)

Two other problems with this mechanism present themselves. First, rapid variability in the gamma-ray emission is not possible at a reverse shock that is triggered by the deceleration off the ambient medium (Sari & Piran 1997). And, second, non-thermal positrons of an energy $\gamma_e \sim 10^2 \varepsilon_B'^{-1/2}$ will emit synchrotron photons in the optical band (§8.4). The observed upper bound of $\sim 10^{-4} - 10^{-3}$ to the fraction of the bolometric output that is carried in the optical-IR band (Akerlof et al. 1999; Vestrand et al. 2005) then requires that $\varepsilon_B' \lesssim 10^{-4}$ upstream of the reverse shock.

For all of these reasons, we turn to other mechanisms for energizing pairs behind the reverse shock, that are special to strongly magnetized plasmas.

8.1.2. Gradient in Electron Energy due to Gradual Pair Loading

The scattering depth builds up after the relativistic outflow passes through the reverse shock. The minimal optical depth of the entrained electrons and ions is less than $(m_e/m_p)\ell' \lesssim 10^{-2}$; the optical depth in pairs is roughly an order of magnitude larger.

There is, therefore, a *distribution* of magnetization parameters σ_\pm in the fluid between the reverse shock and the contact. As pairs are created by photon collisions, the shocked magnetofluid will also be heated continuously (by reconnection of the reversing magnetic field; §6.4). This leads to a steady decrease in the mean energy (eqs. [145], [162]) of the heated electrons and positrons (Fig. 5).

The energy of the inverse-Compton photons decreases in parallel with (162). To illustrate the effect, we take the pair density to increase as a power of time, $\sigma_\pm \propto B^2/n_\pm \propto t^{-\alpha}$, and the wave energy density to decrease as $\delta B_0^2 \propto t^{-\beta}$. One then

has $\gamma_e \propto t^{-(\alpha+\beta)}$ during repeated episodes of flash heating, followed by Compton cooling. The scaling is slightly different, $\gamma_e \propto t^{-(\alpha+\beta+1)/2}$, if the heating is slow enough to be balanced continuously by Compton cooling. The energy of the Comptonized thermal photons decreases with distance behind the reverse shock, as $E_\gamma \propto t^{-2(\alpha+\beta)}$ (flash heating) and $E_\gamma \propto t^{-(\alpha+\beta+1)}$ (continuous heating). When the pair-creating photons are supplied by the emission at smaller radius, one has $\alpha \simeq 1$. The fluence F_{IC} in high energy photons is proportional to $\delta B_0^2 t$, and so

$$\frac{dF_{\text{IC}}}{d \ln E_\gamma} \propto t^{-\beta+1} \propto E_\gamma^{-\gamma}, \quad (182)$$

where $\gamma = (1-\beta)/2(1+\beta)$ (flash heating) and $\gamma = (1-\beta)/(2+\beta)$ (continuous heating). The same spectrum is obtained, independent of the mode of heating, when the turbulent intensity is independent of distance behind the reverse shock ($\beta = 0$). In this case, the integrated spectrum is hard, $dF_{\text{IC}}/d \ln E_\gamma \propto E_\gamma^{-1/2}$. One also recovers the observed scaling (Fenimore et al. 1995) between peak duration and frequency, $t \propto E_\gamma^{-1/2}$, independent of the mode of heating.

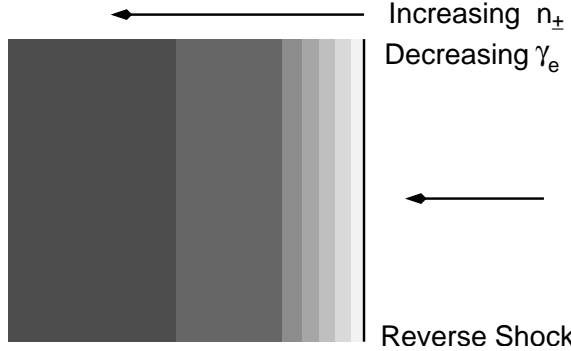


FIG. 5.— The pair density builds up gradually after the magnetofluid passes through the reverse shock wave, due to a finite rate of photon collisions. This leads to a gradual decrease in the mean energy of the charges that are heated electrostatically by decaying, high-frequency MHD turbulence. A high energy gamma-ray spectral tail emerges from the Compton cooling of this extended particle energy spectrum (eq. [182]).

An important feature of this mechanism is that the emission of the soft photons lags behind that of the hard photons: the softer photons are emitted at later times on average as the pair density builds up. The presence of such a hard-soft lag is a well established feature of a subclass of gamma-ray bursts with smooth and easily separable sub-pulses (Norris et al. 2005, and references therein). Its existence therefore provides interesting circumstantial evidence for this type of feedback between pair creation and distributed heating.

8.1.3. Turbulent Cells Driven by Reconnection

The turbulence in the outflow is expected to be strongly intermittent if the magnetic field reverses sign in a stochastic manner. The size $L_0 = \varepsilon_0(r/\Gamma_c)$ of the ‘cells’ can be related to the reversal scale of the field through eq. (109). They are typically smaller than the causal scale r/Γ_c , so that the expansion of the outflow has a small effect on their internal dynamics.

A high-energy gamma-ray tail can be generated in cells with optical depths $\Delta\tau_\pm \gtrsim 0.1$, when the photons are multiply scattered by the bulk turbulent motions (Thompson 1994, 1997). While this mechanism could operate in bursts with smooth light

curves, it is disfavored in highly variable bursts. Strong beaming of the inverse-Compton photons requires relativistic bulk motion in this case, so that the various orders of Compton scattering should be well separated in frequency. A smooth power-law spectrum is not naturally produced unless the dissipation is spread over a wider range of radius.

8.2. Compton Cooling of Pairs behind the Forward Shock

A pair-rich medium sweeps past the forward shock during the prompt deceleration phase. Although the number of positrons in this flow consistently exceeds the number of ions, the proportion of the kinetic energy carried by pairs gradually declines from a value $\mathcal{M}_\pm - 1 \sim 1$ at $r \sim R_{\text{decel-}}$ to $\sim (R_{\text{decel+}}/R_{\text{decel-}})^{-1/2} \sim 0.2$ when the reverse shock has finished passing through the ejecta shell (eq. [52]). The total energy dissipated at radius r scales as $\sim (r/R_{\text{decel+}})^{3/2}$; a fraction $\sim \frac{1}{2}$ of this being dissipated behind the forward shock.

The kinetic energy of the pairs is readily radiated away behind the forward shock: the cooling time is a small fraction $\sim 1/\ell\Gamma_\pm$ of the flow time behind the shock. We have argued that the magnetic field is likely to carry a smaller fraction (84) of the energy behind the forward shock than do the gamma-ray photons. The shocked pairs therefore lose energy by inverse-Compton scattering the gamma-ray photons (Thompson 1997; Beloborodov 2005; Fan, Zhang, & Wei 2005).

The spectral distribution of these inverse-Compton photons provides a direct probe the dynamics of the ejecta shell, and of the coupling between the ions and the lighter charges. First let us consider the case where the ions decouple entirely. The shocked pairs have a mean energy $\Gamma_\pm = \Gamma_c/2\Gamma_{\text{amb}}$, and the characteristic energy of the inverse-Compton photons is

$$E_{\text{IC}} \sim \frac{4}{3}\Gamma_\pm^2 E_{\text{peak}} \sim \frac{4}{3} \left(\frac{r}{R_{\text{decel-}}} \right)^{3/2} E_{\text{peak}}. \quad (183)$$

At the end of the prompt emission phase ($r = R_{\text{decel+}}$), one finds

$$\frac{E_{\text{IC}}(R_{\text{decel+}})}{E_{\text{peak}}} \sim \frac{4}{3} \left(\frac{R_{\text{decel+}}}{R_{\text{decel-}}} \right)^{3/2} = 1 \times 10^2 \varepsilon_+^{-1} L_{\text{rel51}}^{1/2} \dot{M}_{w-5}^{-3/2} V_{w8}^{3/2} \Delta t_1, \quad (184)$$

which is $E_{\text{IC}}/E_{\text{break}} \sim 400 L_{\text{rel51}}^{1/2} \dot{M}_{w-5}^{-3/2}$ for $\varepsilon_+ = \frac{1}{4}$. This means that the inverse-Compton photons have an energy less than $\sim m_e c^2$ in the frame of the contact only if $E_{\text{peak}} \lesssim 50$ keV. It will be recalled that $\Gamma_\pm \propto \Gamma_c^{-3}$, and so

$$E_{\text{IC}} \propto \Gamma_c^{-6}. \quad (185)$$

The energy of the inverse-Compton photons is a strong function of the Lorentz factor of the contact, and a modest increase or decrease in the external inertia will push E_{IC} to higher or lower energies.

The total power in Comptonized photons at energies $E_\gamma \leq E_{\text{IC}}$ is

$$\frac{dL_{\text{IC}}}{d \ln E_\gamma} \simeq L_{\text{rel}} (\mathcal{M}_\pm - 1) \left(\frac{R_{\text{decel+}}}{R_{\text{decel-}}} \right)^{-1/2} \left(\frac{E_\gamma}{E_{\text{IC}}} \right)^{1/2}. \quad (186)$$

Unless the input gamma-ray spectrum is soft at high energies, this inverse-Compton tail will not be visible, due to the combination of small factors $(\mathcal{M}_\pm - 1)(R_{\text{decel+}}/R_{\text{decel-}})^{-1/2}$.

A rapid coupling between the gyromotion of the protons and positrons could cool the protons. The PIC simulations of Hoshino et al. (1992) suggest that the positrons will develop a hard, non-thermal tail (number index $d \ln N_{e^+}/d \ln \gamma \gtrsim -2$) when $m_p n_p \gtrsim m_e n_{e^+}$. However, resonant excitation of the gyromotion of positrons of energy $\sim \gamma_{e^+}$ requires that the proton ring emit a significant power in cyclo-synchrotron waves

at a frequency $n(eB/\Gamma_{\pm}m_p c) = (m_p/m_e)(eB/\gamma_{e^+}m_p c)$. Thermal positrons ($\gamma_{e^+} = \Gamma_{\pm}$) behind the shock will be heated only if $0.3\Gamma_{\pm}^2 \gtrsim (m_p/m_e)\Gamma_{\pm}^{-1}$, i.e., only if $\Gamma_{\pm} \gtrsim 20$ and $n \gtrsim 6 \times 10^3$. In the case where the proton ring has a small thermal spread, which limits the harmonic to a value $n \leq n_{\max} \ll m_p/m_e$, one requires a secondary mechanism for creating non-thermal positrons with an energy $\gamma_{e^+} \gtrsim n_{\max}^{-1}(m_p/m_e)\Gamma_{\pm}$. Unless the non-thermal component of the spectrum is very hard, its energy density is a modest fraction of the thermal positron energy density behind the shock (which itself is $\lesssim 10\%$ of the energy density of the protons). For this reason, it is plausible that the protons will retain a significant fraction of their kinetic energy after thermalizing downstream of the shock. Rapid proton cooling requires a collective process that persists longer than the synchro/Compton cooling time of the absorbing particles.

It is also useful to contrast this calculation with previous estimates, which gives some sense of the subtleties involved. The cooling of synchrotron-emitting particles is dominated by inverse-Compton scattering of the synchrotron photons if the energy density of the cooling particles exceeds the energy density of the magnetic field and the synchrotron radiation is sufficiently soft (e.g. Sari & Esin 2001). It has been suggested that the prompt gamma-ray photons will be inverse-Compton scattered at the forward shock, thereby triggering a pair cascade (Fan et al. 2005). This calculation however neglected pair creation in the external medium and assumed rapid energy equilibration between ions and electrons, thereby yielding $\langle \gamma_e \rangle \sim 10^3$ rather than $\langle \gamma_e \rangle \sim 10$ behind the forward shock. Pair creation in the Wolf-Rayet wind guarantees at least a $\sim 10\%$ conversion efficiency of bulk kinetic energy to inverse-Compton photons at the forward shock. A high-energy particle tail is, of course, probably present at the forward shock; but the lower-energy part of the inverse-Compton spectrum will be dominated by cooling particles that start with an energy $\sim \langle \gamma_e \rangle$.

It has also been noted that electrons emitting optical synchrotron photons could upscatter the gamma-ray peak photons to GeV-TeV energies (Beloborodov 2005). However, Compton cooling of these particles cannot, by itself, explain the low optical efficiency that is observed in GRBs 990123 and 041219a (Akerlof et al. 1999; Vestrand et al. 2005) if the magnetic field is strong in the gamma-ray emitting region (§8.4). One infers, instead, that the particles must be restricted to a more limited range of energy and pitch angle than one would expect from standard shock-acceleration.

Compton GRO detected a very bright burst, GRB 941017, whose bolometric output was dominated by a high-energy component with an energy index $\beta \simeq 0$ above 1–10 MeV (González et al. 2003). This high-energy emission probably involved the inverse-Compton scattering of the prompt burst photons by energetic electrons and positrons. This spectrum was harder than eq. (186), and is more consistent with continuously heated particles. For this reason, and because of the relatively low normalization of (186), we favor emission from pairs that are heated by a reconnecting magnetic field behind the reverse shock. A more detailed discussion of this event is given in §8.6.

8.3. Harder Classes of Gamma-Ray Bursts

Even when an extended Wolf-Rayet envelope is absent, one still obtains a characteristic temperature for thermalization at the base of the outflow. The free expansion phase begins at a

smaller radius. In a rapidly rotating source, this thermalization radius can be normalized to the light cylinder, $R_{\text{bb}} \sim cP/2\pi = 5 \times 10^6 (P/\text{msec})$ cm; whereas in a Soft Gamma Repeater flare it can be normalized to the radius of the star. The blackbody temperature is then higher than we deduced for a thermalization radius of $R_* = 2 \times 10^{10}$ cm (eq. [8]); it works out to

$$kT'_{\text{bb}} = 0.5 \frac{(\epsilon_{\text{bb}} L_{50})^{1/4}}{\Gamma(R_{\text{bb}})^{1/2} P_{\text{msec}}^{1/2}} \left(\frac{\Delta\Omega}{4\pi} \right)^{1/4} \text{ MeV.} \quad (187)$$

The normalization here is well above that relation between E_{peak} and L_{iso} for long bursts with measured redshifts.

The same conclusion holds for two recent short gamma-ray bursts with tentative redshift measurements: GRB 050509b ($z \simeq 0.2$; Bloom et al. 2005), and GRB 050709 ($z \simeq 0.16$; Price, Roth, & Fox 2005). In both cases, the spectrum is therefore consistent a binary neutron star merger as the source of the burst; and, in the case of GRB 050509b, the energetics is marginally consistent with an extragalactic SGR flare. (The accretion-induced collapse of a white dwarf following a binary white dwarf merger could give rise to the birth of a young, active magnetar in a galaxy with a low star formation rate: King, Pringle, & Wickramasinghe 2001; Thompson & Duncan 1995.)

8.4. Suppression of Optical-IR Synchrotron Emission

The presence of the Wolf-Rayet wind forces the relativistic ejecta to decelerate at a radius where electrons of an energy $\gamma_e \sim 10^2$ will radiate in the optical band behind the reverse shock (eq. [75]). Observations of direct optical-IR emission from two gamma-ray bursts (990123: Akerlof et al. 1999; and 041219a: Vestrand et al. 2005; Blake et al. 2005), and upper bounds on other bursts (Akerlof et al. 2000) therefore allow stringent constraints to be placed on the particle distribution in the outflow. The fraction of the bolometric power released in the optical band in these two bursts was $\sim 10^{-4} - 3 \times 10^{-3}$ in different parts of GRB 990123, and $\sim 1 - 3 \times 10^{-4}$ in GRB 041219a. Electrons/positrons of an energy $\gamma_e \sim 10^2$ must, therefore, contribute only modestly to the energy density in the emitting region; or have small pitch angles.

Taking the simplest case of mono-energetic electrons with a fixed pitch angle κ , the absorption coefficient at frequency $\nu' \lesssim 0.3\gamma_e^2(\sin \kappa)\nu'_{Be} = 0.3\gamma_e^2(\sin \kappa)(eB'/2\pi m_e c)$ is

$$\alpha'_{\nu} = \frac{8\pi^2 e n'_{\pm}}{3^{4/3} \Gamma(1/3) (\sin \kappa) B'} \left[\gamma_e \frac{\nu'}{(\sin \kappa) \nu'_{Be}} \right]^{-5/3} \quad (188)$$

in the bulk frame (e.g. Rybicki & Lightman 1979). The optical depth $\tau_{\nu} = \alpha'_{\nu}(r/\Gamma_c) \propto \gamma_e^{-5/3}$, and so there is a critical energy $\gamma_e(\tau_{\nu} = 1)$ above which the medium is optically thin at any given frequency. We normalize this frequency¹² to $\nu' = \Gamma_c^{-1}(1 \text{ eV}/h) \simeq 5 \times 10^{12} (\Gamma_c/50)^{-1}$ Hz in the bulk frame. Relating the pair density n'_{\pm} to the Thomson optical depth τ'_{\pm} , one finds

$$\gamma_e(\tau_{\nu} = 1) = 0.9 \frac{\tau'_{\pm}{}^{3/5} (\sin \kappa)^{2/5}}{\alpha_{\text{em}}^{3/5} (B'/B_{\text{QED}})^{3/5}} \left(\frac{\nu'}{\nu'_{Be}} \right)^{-1}. \quad (189)$$

Setting $B' = B/\Gamma_c = 2 \times 10^3 B_5 (\Gamma_c/50)^{-1}$ G in the gamma-ray emission zone (we expect the magnetic field to have a weak dependence on L_{rel} and \dot{M}_w : eq. [74]) gives

$$\gamma_e(\tau_{\nu} = 1) = 3 \times 10^4 B_5^{2/5} \tau_{\pm}^{3/5} (\sin \kappa)^{2/5} \left(\frac{\Gamma_c}{50} \right)^{3/5}. \quad (190)$$

¹² We are most interested in the case of anisotropic emission, with a small pitch angle $\kappa \ll 1$, along a magnetic field with a non-radial orientation in the bulk frame. The mean frequency of a synchrotron photon therefore transforms as $\nu = \Gamma_c \nu'$ from the bulk frame to the rest frame of the engine.

In practice, the optical depth in such energetic particles is limited to $\tau_{\pm} \sim 1/\gamma_e^2$, and so we have

$$\gamma_e(\tau_{\nu} = 1) = 1 \times 10^2 B_5^{2/11} (\sin \kappa)^{2/11} \left(\frac{\Gamma_c}{50} \right)^{3/11}. \quad (191)$$

Synchrotron radiation in the optical band requires the electrons to be more energetic than $0.3\gamma_e^2(\sin \kappa)h(\Gamma_c\nu'_{Be}) > 1$ eV or, equivalently,

$$\gamma_e \gtrsim \gamma_{e\min} = 50B_5^{-1/2} (\sin \kappa)^{-1/2}. \quad (192)$$

The optical synchrotron emission is self-absorbed if $\gamma_{e\min} < \gamma_e < \gamma_e(\tau_{\nu} = 1)$, and is determined only by the temperature $k_B T'_e \simeq \frac{1}{3}\gamma_e m_e c^2$ of the electrons. The energy density of optical photons in the bulk frame is

$$(\nu U_{\nu}^O)' = \frac{k_B T'_e}{\pi^2} \left(\frac{2\pi\nu'}{c} \right)^3. \quad (193)$$

The isotropic luminosity of the optical photons ($h\nu' = 1$ eV/h) is

$$\begin{aligned} \frac{\nu L_{\nu}^O}{L_{\text{rel}}} \Big|_{R_{\text{decel+}}} &= 4\pi r^2 c \Gamma_c^2 (\nu U_{\nu}^O)' / L_{\text{rel}} \\ &= 1 \times 10^{-2} \left(\frac{\gamma_e}{10^2} \right) L_{\text{rel}51}^{-1/4} \dot{M}_{w-5}^{-1/4} V_w^{1/4} \Delta t_1^{3/2}. \end{aligned} \quad (194)$$

Here we have substituted expressions (38) and (39) for the deceleration radius $R_{\text{decel+}}$ and the Lorentz factor at this radius.

One possible way of avoiding excess optical/IR emission is to inject electrons with random Lorentz factors $\gamma_e \sim 10^4 - 10^5$, so that their synchrotron radiation is in the gamma-ray band (e.g. Rees & Mészáros 1994). The synchrotron output in the optical/IR band is then suppressed by a factor $(\hbar\omega/E_{\text{peak}})^{1/2} \sim 10^{-2} - 10^{-2.5}$. However, such a large mean energy per particle is inconsistent with the level of pair creation that must necessarily occur if decelerating agent is a dense Wolf-Rayet wind or breakout shell (§7.2). In such a compact environment, the mean energy per electron/positron is reduced to $\sigma_{\pm} \sim \ell'_B/\tau_{\pm} \sim 3 - 10$. The cooling spectrum emitted by the particles ($dL/d\ln E_{\gamma} \propto E_{\gamma}^{1/2}$) is also inconsistent with the observed low-energy spectra of GRBs (Ghisellini & Celotti 1999).

The optical synchrotron emission is also suppressed if the high-energy portion of the gamma-ray spectrum arises from inverse-Compton scattering of thermal seed photons, and if shock acceleration is *not* the principal energization mechanism. The inverse-Compton spectrum extends up to an energy $\sim 4\gamma_e^2 k_B T_{\text{bb}}$, which means that a distribution of particle energies up to $\gamma_e \lesssim 10 - 30$ is sufficient to create an extended gamma-ray spectral tail. The maximum energy to which electrons and positrons may be flash heated by decaying MHD turbulence is $\gamma_e \sim \sigma_{\pm}$, which is typically less than $\sim 10^2$ in the prompt deceleration phase. Their synchrotron emission is also suppressed by a factor $\sim 1/\gamma_e^2 \ln \Gamma_c$ compared with the inverse-Compton emission (in the case of a flat particle energy spectrum; eq. [159]).

By contrast, the particle spectrum that is generated by shock acceleration is cut off by synchrotron cooling at a much higher energy, where the synchrotron energy is $\sim \alpha_{\text{em}}^{-1} m_e c^2$. First-order fermi acceleration is therefore disfavored as the mechanism for heating particles behind the reverse shock, given that a GRB radiates only $\lesssim 10^{-3}$ of its bolometric output in the optical-IR band. The same conclusion applies to other acceleration mechanisms which operate on a short timescale, including the resonant absorption of ion cyclotron waves by positrons (Hoshino et al. 1992).

8.5. Transition of Prompt Gamma-Ray Burst to Afterglow

In the model advanced in this paper, the prompt gamma-ray emission continues as long as the shell of seed thermal photons overlaps the shell of turbulent magnetofluid. We now examine the transition from the prompt burst emission to the afterglow. A good example is GRB 980923 (Giblin et al. 1999). At such a transition, the prompt emission is often much more variable than the afterglow.

Several factors point to the region between the reverse shock and the contact as the source of the prompt gamma-ray emission. First, strong variability in the burst emission requires beaming of the radiation in the bulk frame (§7). Second, the radiative efficiency is larger when the pairs contribute a larger fraction of the particle inertia, which is the case behind the contact (compare eqs. [54] and [177]). And, third, the magnetic field is expected to be stronger between the reverse shock and the contact (§5.2).

The Wolf-Rayet wind remains pair-loaded and mildly relativistic beyond the point at which the reverse shock has completed its passage through the ejecta shell. We have found that it is still being pushed to $\Gamma_{\text{amb}} \sim 2\dot{M}_{w-5}^{2/3} \Delta t_1^{-2/3}$ at the radius $R_{\text{reel+}}$ (eqs. [38] and [40]), independent of L_{rel} . Beyond this point, Γ_{amb} decreases inversely with radius. One infers that the ambient medium becomes fully quiescent only after the seed thermal photons have decoupled from the forward shock. The time since the burst scales as $r/\Gamma_c^2 \propto r^{3/2}$, and so one expects an observable transition in the brightness of the X-ray synchrotron emission from the forward shock around a time $t \sim 30(1+z)\dot{M}_{w-5}$ s following a burst. Beyond this point, a much larger fraction of the energy density behind the forward shock is in slowly cooling ions than during the prompt burst phase. It should be emphasized that there is no clear connection between the amplitude of the prompt gamma-ray emission and the immediate post-flare synchrotron emission in this model.

A rapid decline in the X-ray flux has been observed following several Swift bursts, the most plausible explanation for which is off-axis emission from the prompt emission phase (Tagliaferri et al. 2005). Since the overlap of the prompt MeV photons with the forward shock will not cut off sharply (we expect $\tau_T \sim 1$ at the end of the prompt emission phase), this would require strong dissipation of the non-radial magnetic field behind the reverse shock, if the ejecta shell were spherical.

The contact discontinuity is, however, expected to be strongly nonspherical (§7.2). We have argued that Rayleigh-Taylor modes are excited in the cooling breakout shell over a wide range of angular scales. Relativistic ejecta penetrating through holes in the breakout shell will form ‘subjets’ that are boosted with respect to the shell material. The size of the holes decreases with the radius at which they are created, and the final generation of holes is created on an angular scale $\lesssim \Gamma_c^{-1}$. One may therefore expect a few subjets to be present within each causal patch of area $(r/\Gamma_c)^2$ (cf. Kumar and Piran 2000).

We note that some bursts show very smooth pulses which decay exponentially. These events appear to be dimmer on average, and are rare amongst the brightest bursts (Norris et al. 2005). Some possibly involve a different emission geometry, such as the breakout of a mildly relativistic shock from the surface of the Wolf-Rayet star (Tan et al. 2001) that is powered by a buried jet. It should also be noted that the optical depth in pairs grows toward lower values of the isotropic luminosity

L_{rel} and higher Wolf-Rayet mass loss rates \dot{M}_w , because the relativistic outflow is stopped more rapidly: $\tau_{\pm} \propto L_{\text{rel}}^{-1/2} \dot{M}_w^{5/6}$ (eq. [177]). Variability in the burst light curve would be washed out when $\tau_{\pm} \gg 1$.

There are suggestions from the analysis of broadband afterglow emission that the mass density in the ambient wind material is as low as $\dot{M}_{w-5}/V_{w8} \sim 10^{-3} - 10^{-2}$ in a few bursts (Kumar & Panaitescu 2003; Chevalier et al. 2004). In this case, one can still define a radius at which the photon shell will decouple from the relativistic ejecta (in the absence of a breakout shell). Taking the Lorentz factor of the ejecta to be $\Gamma_{\text{rel}} = \Gamma_{b \text{ crit}}$ (eq. [12]) gives the decoupling radius

$$\begin{aligned} R_{\text{overlap}} &= 2\Gamma_{\text{rel}}^2 c \Delta t \\ &= 3 \times 10^{15} \frac{\varepsilon_{\text{bb}}^{1/2} L_{\text{rel}51}^{3/4} \Delta t_1^{5/4}}{(1 - \varepsilon_{\text{bb}})^{3/4}} \left(\frac{R_{\star}}{2 \times 10^{10} \text{ cm}} \right)^{-1/2} \text{ cm}. \end{aligned} \quad (195)$$

In this expression, we have made use of the relation $L_{\text{iso}} = L_{\text{rel}}/(1 - \varepsilon_{\text{bb}})$. The compactness in the bulk frame is

$$\begin{aligned} \ell' &\simeq \frac{\sigma_{\text{T}} L_{\text{rel}} \Delta t}{4\pi \Gamma_{\text{rel}} R_{\text{overlap}}^2 m_e c^2} \\ &= 1.0 \frac{(1 - \varepsilon_{\text{bb}})^{15/8}}{\varepsilon_{\text{bb}}^{5/4} L_{\text{rel}51}^{7/8} \Delta t_1^{13/8}} \left(\frac{R_{\star}}{2 \times 10^{10} \text{ cm}} \right)^{5/4}. \end{aligned} \quad (196)$$

Note that a much lower compactness would be obtained if the ejecta began to expand freely from a smaller radius $\sim 10^7 - 10^8$ cm (rather than the photosphere R_{\star} of the Wolf-Rayet star). It should also be emphasized that ℓ' is sensitive to the asymptotic Lorentz factor of the ejecta shell, $\ell' \propto \Gamma_{\text{rel}}^{-5}$. This means that, if the reverse shock is sub-relativistic, then the photon shell will decouple from the ejecta shell before the reverse shock has completed its passage through the ejecta shell. However, a sub-relativistic reverse shock implies that $\Gamma_{\text{rel}} \lesssim 50 L_{\text{rel}51}^{1/4} \Delta t_1^{-1/6}$ (eq. [39]), in which case $\ell' \gtrsim 6 L_{\text{rel}51}^{-1/4} \Delta t_1^{-1/6}$ at the radius of decoupling. The portion of the magnetized shell which dissipates in the presence of the thermal photon bath will, therefore, do so at a large compactness.

8.6. The Peculiar (?) Burst 941017

The hard, high-energy spectral component that was observed in GRB 941017 (González et al. 2003) has interesting implications for the mechanism of particle heating. The energy index was observed to flatten from $\beta \simeq -\frac{1}{2}$ to $\beta \simeq 0$ at high energies. The high-energy component decayed more slowly, and so the transition energy between the two power-law components also decreased with time, from ~ 10 MeV down to ~ 300 keV. The burst had a very long duration, $T_{90} \simeq 10^2$ s, and its fluence was one of the dozen highest measured by BATSE. The source was, therefore, probably located at a cosmological redshift $z < 1$. It is not clear how atypical this high-energy emission is, given the brightness of GRB 941017 and the relative difficulty of detecting it in lower-fluence bursts. The presence of strong high-energy emission in bursts with relatively soft 1-10 MeV spectra would significantly boost the pair creation rate and the optical depth in the emitting plasma.

Inverse-Compton scattering of the ~ 0.5 MeV peak photons is the most obvious source of the high-energy component. If the

cooling particles are isotropically distributed, then the $\beta = 0$ index is inconsistent with passive Compton cooling ($\beta = -\frac{1}{2}$) and so the particles must be continuously heated (Stern & Poutanen 2004). The slope of the rising spectrum would then mirror that of the spectrum below E_{peak} ; indeed $\beta \simeq 0$ is the most commonly measured low-energy spectral slope in GRBs.

This line of reasoning allows one to place some significant constraints on the mechanism of particle heating. In particular, one can show that the heated particles must occupy a small fraction of the volume of the ejecta, during the peak of the burst emission. Given that the dominant contribution to the bolometric output of GRB 941017 is at high energies, each electron or positron must, on average, radiate a total energy $\sim \sigma_{\pm} m_e c^2$ in inverse-Compton photons. Note that the value of the magnetization parameter σ_{\pm} in the high-energy emission zone may be significantly larger than the average value within the ejecta (§8.1.2). The cooling time at a random Lorentz factor $\gamma_e \gtrsim 30$ is much shorter than the burst duration, $t_{\text{cool}}/\Delta t \sim 1/\ell' \gamma_e$ (as measured by the observer). This means that each particle must perform its emission duties over a very short timescale, $t_{\text{emission}}/\Delta t \sim (\sigma_{\pm}/\gamma_e) t_{\text{cool}} \sim \sigma_{\pm}/\ell' \gamma_e^2 \lesssim 10^{-4} \sigma_{\pm}$. Energy must, therefore, be transferred to the particles over a short, but not microscopic timescale. For example, shock acceleration does not satisfy this constraint, because the residency time of a particle of energy $\gamma_e \sim 30$ near the shock is orders of magnitude shorter than t_{cool} . One infers that the outflow must have small-scale structure, on a scale $\lesssim 10^{-4} \sigma_{\pm} c \Delta t \sim (0.01 \text{ s}) \sigma_{\pm} c$, which allows dissipation to take place so rapidly. Indeed, reconnection of a reversing magnetic field in the outflow will have the desired effect (§5.1; 8.1.2).

Could the $\beta = 0$ spectrum be a signature of slow Compton cooling of the emitting particles? This requires the compactness to be tuned to a value somewhat smaller than $\sim \gamma_e^{-1} \lesssim 0.03$. During the peak of the burst emission, we deduce $\ell' \simeq 5 L_{\text{rel}51}^{-1/4} \dot{M}_{w-5}^{5/12} V_{w8}^{-5/12}$ from eq. (46), which indicates that the external wind inertia must be exceedingly small for this explanation to hold. It is, nonetheless, clear that the compactness of the ~ 1 MeV photons must drop rapidly toward the end of the burst. The increasing dominance of the high-energy component is therefore consistent with a drop in τ_{\pm} and an increase in the cooling time (at fixed γ_e) at the reverse shock.

Synchrotron self-Compton emission by $\gamma_e \sim 3 \times 10^4$ electrons at the forward shock is another possible high-energy emission mechanism (Granot & Guetta 2003; Pe'er & Waxman 2004a), which was motivated by the delayed onset of the high-energy component in GRB 941017 and the apparent need for slow cooling to explain the hard $\beta = 0$ spectrum. We note that for the parameters $\varepsilon_B \lesssim 10^{-4}$ and $\Gamma_c \sim 300$ adopted in this model, Compton cooling by the MeV photons will, in fact, dominate¹³ cooling by optical synchrotron photons as long as the gamma-ray photons overlap the forward shock (Beloborodov 2005).

9. CONCLUSIONS

We have examined, in some detail, the hypothesis that long gamma-ray bursts are emitted by relativistic material that breaks out from the photosphere of a Wolf-Rayet star, and then propagates through the surrounding dense wind. We have started with a key simplifying assumption, that there are only two major sites of dissipation in the outflow: where the relativistic jet breaks out of the Wolf-Rayet star (at $R_{\star} \sim 2 \times 10^{10}$

¹³ Including the Klein-Nishina suppression of the scattering cross section.

cm); and the much larger zone where the reverse shock makes significant backward motion through the ejecta shell (at a distance $10^{14} - 10^{15}$ cm). The key components of the relativistic outflow are a non-radial magnetic field and a thermal bath of hard X-ray photons. The magnetic field changes sign many times, due to the stochasticity of the dynamo operating in the central engine. The photons are created in the turbulent jet core as it is heated by Kelvin-Helmholtz instabilities during the passage of the jet through the envelope of the Wolf-Rayet star. The kinetic energy of the entrained baryons can be comparable to the energy carried by these other two components, but does not have to be.

Our analysis has covered the deceleration of the ejecta shell, as influenced by pair-creation in the ambient wind material; the entrainment of a thin shell of stellar material by the jet head; and the structure and composition of the fluid on either side of the contact discontinuity. We have described a mechanism by which turbulent motions in an expanding, relativistic magnetofluid will transfer energy to electrons and positrons, and then (by Compton scattering) to an ambient radiation field. This inverse-Compton radiation is *beamed* along the magnetic field in the bulk frame, thereby providing an explanation for the rapid variability of many gamma-ray bursts, without resort to an ill-defined source of internal variability in the outflow. The ultimate source of seed photons is the relativistic jet itself (and not in its sub-relativistic cocoon) as it suffers Kelvin-Helmholtz instabilities during its emergence from the Wolf-Rayet star.

The normalization and slope of the Amati et al. (2002) relation between peak energy and isotropic energy of long gamma-ray bursts is reproduced, essentially without free parameters. This relation is *predicted* to flatten from $E_{\text{peak}} \sim L_{\text{iso}}^{1/2}$ to $E_{\text{peak}} \sim L_{\text{iso}}^{1/4}$ below a luminosity $L_{\text{iso}} \sim 3 \times 10^{50}$ ergs s^{-1} . This transition corresponds to a wide jet opening angle, $\theta \gtrsim 1/\sqrt{3}$, at the surface of the Wolf-Rayet star.

One also obtains an explanation for why the short gamma-ray burst GRB 050509b (Bloom et al. 2005) did not follow this relation: the relatively hard spectrum of this burst reflected a smaller radius at which the ejecta went into free expansion, and at which the temperature of the seed black body photons was frozen. The bright initial spikes of the SGR flares are another example of energetic bursts which deviate from the Amati et al. relation, and are consistent with a smaller thermalization radius of 10-100 km (Hurley et al. 2005; Palmer et al. 2005).

We close with a summary list of some additional conclusions.

9.1. Additional Conclusions

1. The passage of the reverse shock wave through the ejecta shell occurs when the compactness of the radiation field near the contact discontinuity has dropped to a characteristic value $\ell' \sim 10$. At this point, the gamma-ray flux across the forward shock is no longer sufficient to push the ambient medium up to a speed comparable to that of the contact discontinuity. There is no detachment of the pair-loaded wind material from the ejecta shell.
2. The prompt gamma-ray emission takes place in a medium with an optical depth ~ 1 in electron-positron pairs. Pairs generated by side-scattering of gamma-ray photons in the Wolf-Rayet wind are the dominant source of scattering particles in between the forward shock and the contact. Pairs are created at a somewhat higher rate

by collisions between photons in the turbulent region between the reverse shock and the contact. This shocked material becomes optically thin only outside $\sim 10^{15}$ cm from the central engine.

3. The shocked Wolf-Rayet wind and the shocked relativistic outflow are themselves subject only to a weak Rayleigh-Taylor instability at their mutual contact discontinuity. However, the shell of matter that is entrained by the jet head during the final breakout from the star is much denser. This breakout shell will gradually accelerate as it intercepts relativistic ejecta from behind, and will suffer from a strong corrugation instability as it cools. The radiation that is trapped by the breakout shell has a temperature of ~ 2 keV when the shell becomes optically thin.
4. The interaction of the relativistic ejecta with the fragmenting breakout shell offers a hybrid mechanism for triggering dissipation and gamma-ray emission. In this case, the breakout shell does not form a truly 'external' medium, since its structure depends on its interaction with the relativistic wind material at a smaller radius. It is especially important when the mass-loss rate in the Wolf-Rayet wind preceding the burst is much less than $10^{-5} M_{\odot} \text{ yr}^{-1}$. The role of the corrugation instability in generating long null regions in gamma-ray bursts should be investigated.
5. Electrons and positrons in the outflow are electrostatically heated in regions of strong MHD turbulence. The Kolmogorov energy flux in torsional waves is damped at a smaller frequency than the ion gyrofrequency. We find that similar conclusion applies to the magnetic corona of a black hole, and to any magnetofluid in which $B^2/8\pi$ is larger than the rest energy density in electrons (pairs).
6. The radiation emitted by charges in a turbulent magnetofluid is beamed along the background magnetic field. The damping of MHD turbulence in a medium with $(B')^2/8\pi \gg n_{\pm} m_e c^2$ leads to electrostatic acceleration of charges along the magnetic field. Indeed, when the gamma-ray emission is triggered by the deceleration of the relativistic ejecta, one requires beaming in the bulk frame to explain the fast variability observed that is observed in many bursts.
7. The outflow is photon rich ($n_{\gamma}/n_{\pm} \sim 10^2 - 10^3$) and the photons are the dominant coolant of the electrons and positrons – even if the magnetic field has a higher energy density. Numerical simulations (e.g. Pe'er, Mészáros, & Rees 2005) which do not account for the anisotropy or spatial inhomogeneity of the electron distribution will lead to qualitatively different results.
8. The observed correlation $\delta t \propto E_{\gamma}^{-1/2}$ between photon energy and the width of gamma-ray pulses arises naturally from inverse-Compton cooling of pairs that have been flash-heated up to a limiting Lorentz factor $\langle \gamma_e \rangle \sim \ell'_B (\delta B'/B')^2 / \tau_{\pm} \gtrsim 1$. Some substructure in GRBs does not show clear asymmetries between rise and decay; we ascribe it to variations in the direction of beaming associated with wave excitations of the background magnetic field.

9. The electrons/positrons that are heated by decaying MHD turbulence behind the reverse shock have a negative gradient in energy away from the shock. There is, correspondingly, a gradient in the energy of the inverse-Compton photons. The harder spectra that are often observed at the beginning of GRB sub-pulses could be explained by this effect.
10. Synchrotron emission in the optical range is suppressed because the heated electrons and positrons have small pitch angles. The inverse-Compton emission of MeV-GeV gamma-rays only requires particle energies up to $\gamma_e \sim 30 - 10^2$, which is smaller than the energy that is needed for optical synchrotron emission ($\gamma_e \sim 50(\sin\kappa)^{-1/2}$) when the small pitch angle is taken into account.
11. The magnetization is very different in the fluids that have passed through the forward and reverse shocks: the magnetic field probably contributes a much smaller fraction of the pressure in front of the contact. The Weibel instability generates a very small-scale magnetic field. This field has a tendency to smooth out and increase its scale downstream of the shock (Medvedev et al. 2005). However, if the rate of smoothing is at least $\sim 10^{-4}$ of the maximal rate allowed by causality, then the r.m.s. smoothed field will be weaker than the field which is swept up from the Wolf-Rayet wind and linearly compressed behind the forward shock.
12. The thermal photons advected out from the sub-photospheric region of the Wolf-Rayet star have a finite duration, and a transition from prompt burst to afterglow can be explained by a drop in the thermal photon density. A modest anisotropy in the gamma-ray emission on an angular scale $\sim \Gamma_c^{-1}$, due to corrugation instabilities of the breakout shell, could also influence the shape of the transition to the afterglow regime.
13. The gamma-rays themselves are the dominant coolant at the forward shock. As pre-acceleration turns off, the medium ahead of the shock develops relativistic motion with respect to the contact discontinuity (a differential Lorentz factor ~ 20). The pairs which pass across the forward shock emit inverse-Compton gamma-rays with an energy $\frac{4}{3}\Gamma_{\pm}^2 \sim 500$ times the peak energy of the burst. This emission is, however, too spectrally soft and too weak to explain the rising high-energy component of GRB 941017. We argue that the high-energy emission in GRB 941017 requires rapid (but not too rapid) heating of the particles behind the reverse shock, most probably triggered by magnetic reconnection.
14. The global MHD instabilities identified by Lyutikov and Blandford (2003) are effective at tangling the magnetic field while the jet is still working its way through the envelope of the Wolf-Rayet star. They are probably less important in the prompt emission zone at $\sim 10^{14} - 10^{15}$ cm. The Lorentz factor of the contact is still large at this stage, $\Gamma_c \sim 50$, and much larger than the inverse of the jet opening angle. Smaller angular structures in the outflow will be created by the corrugation instability of the breakout shell; but the growing mode

will have a fairly large angular scale close to the star, $\theta \sim \Gamma_c^{-1} \propto (r/R_*)^{-1/3}$, where the Lorentz factor of the contact is still modest. The angular scale decreases as the breakout shell is accelerated outward, but at the end of the prompt deceleration phase the contact is moving nearly as fast as the ejecta.

We close this paper with a question: What is the main outstanding theoretical problem relating to the prompt emission of gamma-ray bursts? This question is far from being rhetorical: the proper design of numerical experiments to study the 3-dimensional behavior of plasmas – especially in the extreme regimes that are encountered in GRB outflows – requires a basic understanding of the dominant physical effects that are likely to be encountered.

Most recent research would seem to point to the following answer: one must understand the structure and intermittency of the outflow from a stellar-mass black hole that is surrounded by a neutronized torus. However, this problem is vast, as it encompasses the mass flow in the torus; the Blandford-Znajek process operating in the black hole magnetosphere; the acceleration and collimation of the outflow near the engine; the interaction of this jet with the envelope of the Wolf-Rayet star; nuclear processes occurring over a wide range of radii; and the various instabilities that occur in the jet outside the star. In this picture, the emission problem *cannot* simply be reduced to the problem of understanding particle acceleration and radiation at a mildly relativistic shock wave, since the details of the microphysics depend strongly on where the shock occurs in the outflow, the strength of the magnetic field, and the feedback of radiation processes on the particle composition and energy distribution.

We are suggesting here that, in fact, the theoretical problem is a bit more tractable. Because the non-thermal emission is triggered by the interaction with the external wind and the material of the breakout shell, one can focus down on a small part of the outflow, and in particular on the problem of how long-wavelength magnetohydrodynamic turbulence is damped in a fluid satisfying the following conditions: approximate equipartition between thermal radiation and magnetic field; $B^2/8\pi \gtrsim n_{\pm}m_e c^2$; and compactness $\ell \sim 10$. Because the dissipation zone has been localized to a well-defined region, one can now begin to examine the radial structure of the outflow in a constrained way, and to understand the origin of distinct emission components such as was observed in GRB 941017 (González et al. 2003).

From this perspective, the classical gamma-ray bursts have a greater affinity with the giant flares of the Soft Gamma Repeaters that has been generally assumed in the recent literature. Much of the early confusion about whether gamma-ray bursts originate in the magnetospheres of Galactic neutron stars, or in relativistic fireballs at cosmological distances, turns out to be connected to a similarity in the mechanism underlying these spectacular releases of radiant energy.

The author would like to thank Maxim Lyutikov for several discussions of particle heating during the early stages of this work, Yoram Lithwick for discussions of MHD turbulence, and Chris Matzner for discussions of shock breakout. This work was supported by the NSERC of Canada.

REFERENCES

- Akerlof, C., et al. 1999, *Nature*, 398, 400
Akerlof, C., et al. 2000, *ApJ*, 532, L25
Amati, L., et al. 2002, *A&A*, 390, 81
Arons, J., & Barnard, J. J. 1986, *ApJ*, 302, 120
Band, D., et al. 1993, *ApJ*, 413, 281
Baring, M. G., & Harding, A. K. 1997, *ApJ*, 491, 663
Begelman, M. C., & Li, Z. 1994, *ApJ*, 426, 269
Beloborodov, A. M., Stern, B. E., & Svensson, R. 1998, *ApJ*, 508, L25
Beloborodov, A. M. 2002, *ApJ*, 565, 808
Beloborodov, A. M. 2003, *ApJ*, 588, 931
Beloborodov, A. M. 2005, *ApJ*, 618, L13
Blackman, E. G., & Field, G. B. 1994, *Physical Review Letters*, 72, 494
Blake, C. H., et al. 2005, *Nature*, 435, 181
Blandford, R., & Eichler, D. 1987, *Phys. Rep.*, 154, 1
Bloom, J. S., Frail, D. A., & Kulkarni, S. R. 2003, *ApJ*, 594, 674
Bloom, J.S., et al. 2005, preprint ([astro-ph/0505480](http://arxiv.org/abs/astro-ph/0505480))
Blustin, A. J., et al. 2006, *ApJ*, 637, 901
Cavallo, G., & Rees, M. J. 1978, *MNRAS*, 183, 359
Chandrasekhar, S.A. 1981, *Hydrodynamic and Hydromagnetic Stability* (Dover: New York)
Chevalier, R. A., Li, Z., & Fransson, C. 2004, *ApJ*, 606, 369
Chiang, J., & Dermer, C. D. 1999, *ApJ*, 512, 699
Cho, J. 2005, *ApJ*, 621, 324
Coroniti, F. V. 1990, *ApJ*, 349, 538
Drenkhahn, G., & Spruit, H. C. 2002, *A&A*, 391, 1141
Duncan, R. C. 2001, *AIP Conf. Proc.* 586: 20th Texas Symposium on relativistic astrophysics, 586, 495
Eichler, D., Livio, M., Piran, T., & Schramm, D. N. 1989, *Nature*, 340, 126
Fan, Y. Z., Zhang, B., & Wei, D. M. 2005, *ApJ*, in press ([astro-ph/0504039](http://arxiv.org/abs/astro-ph/0504039))
Fenimore, E. E., in 't Zand, J. J. M., Norris, J. P., Bonnell, J. T., & Nemiroff, R. J. 1995, *ApJ*, 448, L101
Fenimore, E. E., Madras, C. D., & Nayakshin, S. 1996, *ApJ*, 473, 998
Frail, D. A., et al. 2001, *ApJ*, 562, L55
Galama, T. J., et al. 1998, *ApJ*, 497, L13
Ghirlanda, G., Ghisellini, G., Firmani, C., Celotti, A., & Bosnjak, Z. 2005, *MNRAS*, 360, L45
Ghisellini, G., & Celotti, A. 1999, *ApJ*, 511, L93
Ghisellini, G., Lazzati, D., Celotti, A., & Rees, M. J. 2000, *MNRAS*, 316, L45
Goldreich, P., & Sridhar, S. 1995, *ApJ*, 438, 763
Goodman, J. 1986, *ApJ*, 308, L47
González, M. M., Dingus, B. L., Kaneko, Y., Preece, R. D., Dermer, C. D., & Briggs, M. S. 2003, *Nature*, 424, 749
Granot, J., & Guetta, D. 2003, *ApJ*, 598, L11
Hededal, C. B., & Nishikawa, K. 2005, *ApJ*, 623, L89
Hibschman, J. A., & Arons, J. 2001, *ApJ*, 560, 871
Higdon, J. C. 1984, *ApJ*, 285, 109
Hoshino, M., Arons, J., Gallant, Y. A., & Langdon, A. B. 1992, *ApJ*, 390, 454
Hurley, K., et al. 2005, *Nature*, 434, 1098
Kazimura, Y., Sakai, J. I., Neubert, T., & Bulanov, S. V. 1998, *ApJ*, 498, L183
Kennel, C. F., & Coroniti, F. V. 1984, *ApJ*, 283, 694
King, A. R., Pringle, J. E., & Wickramasinghe, D. T. 2001, *MNRAS*, 320, L45
Kobayashi, S., Zhang, B., Mészáros, P., & Burrows, D.N. 2005, preprint ([astro-ph/0506157](http://arxiv.org/abs/astro-ph/0506157))
Kouveliotou, C., Meegan, C. A., Fishman, G. J., Bhat, N. P., Briggs, M. S., Koshut, T. M., Paciesas, W. S., & Pendleton, G. N. 1993, *ApJ*, 413, L101
Kumar, P., & Piran, T. 2000, *ApJ*, 535, 152
Kumar, P., & Panaitescu, A. 2003, *MNRAS*, 346, 905
Lamb, D. Q., Donaghy, T. Q., & Graziani, C. 2005, *ApJ*, 620, 355
Lyubarsky, Y., & Kirk, J. G. 2001, *ApJ*, 547, 437
Lyutikov, M., & Blackman, E. G. 2001, *MNRAS*, 321, 177
Lyutikov, M., & Blandford, R. D. 2003, [astro-ph/0305410](http://arxiv.org/abs/astro-ph/0305410), unpublished.
Lyutikov, M. & Thompson C., *ApJ*, in press (Sept 10)
Matzner, C. D. 2003, *MNRAS*, 345, 575
McKinney, J. C. 2005, preprint ([astro-ph/0506368](http://arxiv.org/abs/astro-ph/0506368))
McKinney, J. C. 2005, preprint ([astro-ph/0506369](http://arxiv.org/abs/astro-ph/0506369))
McKinney, J. C., & Gammie, C. F. 2004, *ApJ*, 611, 977
Medvedev, M. V. 2000, *ApJ*, 540, 704
Medvedev, M. V., & Loeb, A. 1999, *ApJ*, 526, 697
Medvedev, M. V., Fiore, M., Fonseca, R. A., Silva, L. O., & Mori, W. B. 2005, *ApJ*, 618, L75
Mészáros, P., & Rees, M. J. 1993, *ApJ*, 405, 278
Mészáros, P., Rees, M. J., & Papathanassiou, H. 1994, *ApJ*, 432, 181
Mészáros, P., & Rees, M. J. 1997, *ApJ*, 476, 232
Mészáros, P., & Rees, M. J. 2000, *ApJ*, 530, 292
Mészáros, P., Ramirez-Ruiz, E., Rees, M. J., & Zhang, B. 2002, *ApJ*, 578, 812
Nakar, E., & Piran, T. 2004, *MNRAS*, 353, 647
Narayan, R., Piran, T., & Kumar, P. 2001, *ApJ*, 557, 949
Norris, J. P., Nemiroff, R. J., Bonnell, J. T., Scargle, J. D., Kouveliotou, C., Paciesas, W. S., Meegan, C. A., & Fishman, G. J. 1996, *ApJ*, 459, 393
Norris, J. P., Bonnell, J. T., Kazanas, D., Scargle, J. D., Hakkila, J., & Giblin, T. W. 2005, *ApJ*, 627, 324
Novikov, I.D., & Thorne, K.S. 1973, in *Black Holes*, eds. C. DeWitt and B.S. DeWitt (Gordon and Breach, New York), p. 343
Nugis, T., & Lamers, H. J. G. L. M. 2000, *A&A*, 360, 227
Paciesas, W. S., et al. 1999, *ApJS*, 122, 465
Paczyński, B. 1998, *ApJ*, 494, L45
Palmer, D. M., et al. 2005, *Nature*, 434, 1107
Panaitescu, A. 2005, *MNRAS*, 363, 1409
Panaitescu, A., & Kumar, P. 2000, *ApJ*, 543, 66
Panaitescu, A., & Kumar, P. 2001, *ApJ*, 554, 667
Panaitescu, A., & Kumar, P. 2002, *ApJ*, 571, 779
Panaitescu, A., & Kumar, P. 2004, *MNRAS*, 353, 511
Pe'er, A., & Waxman, E. 2004, *ApJ*, 603, L1
Pe'er, A., & Waxman, E. 2004, *ApJ*, 613, 448
Pe'er, A., Mészáros, P., & Rees, M.J. 2005, preprint ([astro-ph/0504346](http://arxiv.org/abs/astro-ph/0504346))
Price, P.A., Roth, K., & Fox, D. W. 2005, *GCN* 3605
Quataert, E., & Gruzinov, A. 1999, *ApJ*, 520, 248
Ramirez-Ruiz, E., & Fenimore, E. E. 2000, *ApJ*, 539, 712
Ramirez-Ruiz, E., MacFadyen, A. I., & Lazzati, D. 2002, *MNRAS*, 331, 197
Rees, M. J., & Mészáros, P. 1994, *ApJ*, 430, L93
Rees, M. J., & Meszaros, P. 1998, *ApJ*, 496, L1
Rees, M. J., & Mészáros, P. 2005, *ApJ*, in press ([astro-ph/0412702](http://arxiv.org/abs/astro-ph/0412702))
Rybicki, G. B., & Lightman, A. P. 1979, *New York, Wiley-Interscience*, 1979. 393 p.,
Sari, R., & Piran, T. 1997, *ApJ*, 485, 270
Sari, R., & Esin, A. A. 2001, *ApJ*, 548, 787
Sari, R., & Piran, T. 1995, *ApJ*, 455, L143
Sari, R., & Piran, T. 1999, *ApJ*, 520, 641
Shapiro, S. L., Lightman, A. P., & Eardley, D. M. 1976, *ApJ*, 204, 187
Shemi, A., & Piran, T. 1990, *ApJ*, 365, L55
Sikora, M., Begelman, M. C., Madejski, G. M., & Lasota, J.-P. 2005, preprint ([astro-ph/0502115](http://arxiv.org/abs/astro-ph/0502115))
Skilling, J. 1975, *MNRAS*, 172, 557
Smolsky, M. V., & Usov, V. V. 1996, *ApJ*, 461, 858
Socrates, A., Davis, S. W., & Blaes, O. 2004, *ApJ*, 601, 405
Somov, B. V. 1992, *Physical Processes in Solar Flares* (Kluwer: Dordrecht)
Stanek, K. Z., et al. 2003, *ApJ*, 591, L17
Stern, B. E., & Poutanen, J. 2004, *MNRAS*, 352, L35
Strohmer, T. E., Fenimore, E. E., Murakami, T., & Yoshida, A. 1998, *ApJ*, 500, 873
Svensson, R. 1987, *MNRAS*, 227, 403
Tagliaferri, G., et al. 2005, preprint ([astro-ph/0506355](http://arxiv.org/abs/astro-ph/0506355))
Tan, J. C., Matzner, C. D., & McKee, C. F. 2001, *ApJ*, 551, 946
Thompson, C. 1994, *MNRAS*, 270, 480
Thompson, C., & Duncan, R. C. 1995, *ASP Conf. Ser.* 72: Millisecond Pulsars. A Decade of Surprise, 72, 301
Thompson, C. 1997, in *Relativistic Jets in AGNs*, eds. M. Ostrowski, M. Sikora, G. Madejski, & M. Begelman, pp. 63-84
Thompson, C., & Blaes, O. 1998, *Phys. Rev. D*, 57, 3219
Thompson, C., & Madau, P. 2000, *ApJ*, 538, 105
Thompson, C., & Duncan, R. C. 2001, *ApJ*, 561, 980
Troischt, P., & Thompson, C. 2004, *Phys. Rev. D*, 70, 124030
Usov, V. V. 1994, *MNRAS*, 267, 1035
Vestrand, W. T., et al. 2005, *Nature*, 435, 178
Vishniac, E. T. 1983, *ApJ*, 274, 152
Wang, X., Loeb, A., & Waxman, E. 2002, *ApJ*, 568, 830
Waxman, E., & Mészáros, P. 2003, *ApJ*, 584, 390
Woosley, S. E. 1993, *ApJ*, 405, 273
Woosley, S. E., & Weaver, T. A. 1995, *ApJS*, 101, 181
Yost, S. A., Harrison, F. A., Sari, R., & Frail, D. A. 2003, *ApJ*, 597, 459
Zhang, B., & Kobayashi, S. 2005, *ApJ*, 628, 315